DEVELOPMENT AND CHARACTERIZATION OF A MAGNESIUM/POLYMER COMPOSITE FOR GUIDED BONE REGENERATION

by

Andrew James Brown

Bachelor of Science, University of Pittsburgh, 2009

Submitted to the Graduate Faculty of

Swanson School of Engineering in partial fulfillment

of the requirements for the degree of

Doctor of Philosophy

University of Pittsburgh

2016

UNIVERSITY OF PITTSBURGH

SWANSON SCHOOL OF ENGINEERING

This dissertation was presented

by

Andrew James Brown

It was defended on

December 9, 2015

and approved by

Aaron Barchowsky, Ph.D., Professor, Department of Environmental and Occupational Health

BJ Costello, D.M.D., M.D., Associate Professor, Department of Oral and Maxillofacial Surgery

Juan Taboas, Ph.D., Assistant Professor, Department of Oral Biology

Yadong Wang, Ph.D., Professor, Department of Bioengineering

Dissertation Director: Charles Sfeir, D.D.S, Ph.D., Associate Professor, Department of Oral Biology

DEVELOPMENT AND CHARACTERIZATION OF A MAGNESIUM/POLYMER COMPOSITE FOR GUIDED BONE REGENERATION

Andrew James Brown, Ph.D.

University of Pittsburgh, 2016

Every year in the United States, 2 million implant supported dental prostheses are placed in order to restore the functionality and cosmetic appearance of missing teeth. In over half of these cases, a bone grafting procedure must be performed to build the bony foundation necessary for implant survival. Unfortunately, the current gold-standard bone graft substitutes impart limited osteoconductivity and exhibit long degradation times leading to unpredictable outcomes. Thus, there exists a significant need for degradable dental bone graft substitutes capable of enhancing the bone regeneration process.

The overall goal of this work was to design guided bone regeneration devices that address the limitations of current bone graft substitutes and barrier membranes. First, bone graft substitutes were synthesized from metallic magnesium (Mg) particles and poly-(lactic-co-glycolic acid) (PLGA) and subsequently characterized. These Mg/PLGA scaffolds were found to release magnesium at a controllable rate that ameliorated the acidic degradation profile of PLGA and enhanced bone marrow stromal cell proliferation *in vitro*. Next, we evaluated the Mg/PLGA scaffolds in a canine socket preservation model and found that the scaffolds increased bone height and bone volume regenerated relative to controls.

Other groups have demonstrated enhanced osteogenic activity surrounding magnesium implants in orthopedic applications. However, the cellular mechanisms underlying these observations have not been well defined. Our next objective was to assess these cellular mechanisms *in vitro,* following exposure of bone marrow stromal cells (BMSCs) to varying concentrations of magnesium ion, simulating device degradation. We found that certain magnesium concentrations enhanced cell proliferation and matrix mineralization and impacted gene pathways associated with increased osteogenic activity.

Finally, we designed and evaluated a Mg/PLGA barrier membrane and magnesium micromesh in a canine vertical ridge augmentation model which showed promise for a fully degradable and osteoconductive magnesium-based guided bone regeneration therapy. This work established the use of degradable magnesium devices for enhancing dental bone regeneration while expanding knowledge of the cellular mechanisms impacted by magnesium's degradation.

TABLE OF CONTENTS

LIST OF TABLES

LIST OF FIGURES

PREFACE

This thesis is the culmination of 6 years of research in the Department of Bioengineering and Center for Craniofacial Regeneration at the University of Pittsburgh. But really it started long before that with another 4 years in the Department of Bioengineering at the University of Pittsburgh and another 19 years of education before that. I would like to thank all of my teachers throughout my career at Villa Maria Elementary, Our Lady of Peace and Cathedral Preparatory Schools, especially Joann Mullen and William Clancey. These teachers provided me with the foundational knowledge and enthusiasm for science, engineering and technology on which I've built my research career. I would also like to thank the faculty of the Swanson School of Engineering, particularly in the Department of Bioengineering, for continuing this tradition. Thank you to my early research mentors at the Musculoskeletal Research Center, Richard Debski, Carrie Voycheck and Steve Abramowitch. They strengthened my ability to design experiments, present, write and think independently.

I owe a great deal of gratitude to my advisor Charles Sfeir for the innumerable things that he has done to allow me to develop as a researcher and the freedom to explore numerous other opportunities during the time in my lab. This opportunity was due in no small part to the Revolutionizing Metallic Biomaterials Engineering Research led by Jag Sankar. I would also like to thank Bill Wagner and Rich Hoff for the support they've provided me throughout my time in the ERC. I'm thankful for the unwavering support of Dr. Borovetz throughout my time in undergrad and during my time with the ERC and especially for accepting me into the PhD program.

None of this work could have been done without the amazing team that Charles has built at the Center for Craniofacial Regeneration. Thank you to Diane Turner, Michele Leahy and Jill

Smith for all the work that they do to keep our lab running. Nicole Myers, Andressa Pen, Sabrina Noorani and Michele Mulkeen had the unglamorous responsibilities of performing much of the histological analyses throughout this thesis and I am endlessly thankful for their help. Thank you also to Sayuri Yoshizawa and Samer Zaky for their mentorship throughout my PhD and to all the other CCR faculty, graduate students and staff for their feedback and support throughout my time here.

This thesis looks nothing like the PhD proposal that I presented to my committee three years ago. I would like to thank my committee members Aaron Barchowsky, BJ Costello, Juan Taboas and Yadong Wang for their patience, guidance, feedback and willingness to support my desire to add, delete and edit entire specific aims at every committee meeting that we held.

A major factor in allowing me to keep my sanity throughout my PhD were all the other activities that I was able to involve myself in throughout my time here. I'd like to thank Rick Schaub and everyone at the UPMC Artificial Heart Program for providing me with an amazing and unique clinical experience over the last 4 years. Thank you to everyone at the Innovation Institute for allowing me to take part in their numerous educational and entrepreneurial programs that have set my career path in the direction that it is currently going. Also, thank you to Don Taylor and the rest of the team at bioStratica for providing me with a new way to utilize all the translational research skills and knowledge that I've built throughout my time at Pitt.

Finally, I'd like to thank all of my friends and family for their support throughout my education and research experiences so far. Thank you particularly to my mom, dad, brother and sister for their support throughout my whole life, particularly in the past few years and their understanding of me not wanting to talk about when I would be done with grad school. A special thanks goes to Amy Chaya who I have spent the last 10 years with in Pitt Bioengineering, at the

MSRC, at CCR and now at bioStratica. Thank you especially to my boyfriend Vince and to Phil, Nora, Chelsea, Britta, Matt and Josh for their friendship and support throughout my PhD and for accompanying me on the numerous escapes to Mad Mex Shadyside that helped make all of this possible.

1.0 INTRODUCTION

Every year in the United States, 2 million implant supported dental prostheses are placed in order to restore the functionality and cosmetic appearance of missing teeth (1). In over half of these cases, a bone grafting procedure must be performed to build the bony foundation necessary for implant survival. The current gold standards for treatment of these bone defects are autogenous and allogenic bone grafts, but there are size limitations and donor site morbidity for autogenous grafts, as well as prolonged recovery due to delayed osteoconductivity for allogenic grafts. In order to improve bone regeneration, degradable magnesium devices are currently being explored for enhanced fracture fixation and bone grafting materials. Mg devices implanted *in vivo* have been shown to be advantageous by exhibiting appropriate mechanical properties, minimizing inflammation and neighboring tissue damage and providing simultaneous promotion of osteoblast proliferation and biodegradation. However, there remains a need for improved dental bone grafting therapies and for a better understanding of the biology underlying magnesium's osteoconductive properties.

1.1 BONE LOSS AND CURRENT TREATMENTS

1.1.1 Conditions and Injuries Leading to Dental and Craniomaxillofacial Bone Loss

Many of the bones within the face suffer from fractures similar to those elsewhere in the body. The pediatric population is particularly susceptible to craniofacial bone fractures due to their greater cranial-mass-to-body ratio and account for up to 15% of all facial fractures (2). These injuries are often sustained in motor vehicle accidents, falls and sports-related accidents. In addition to bone fractures, dentoalveolar trauma represents a majority of craniofacial injuries reported in one study (3). Such trauma manifests itself in crown fracture and tooth subluxation or avulsion which can often result in the loss of one or more teeth. In the US, by age 65, the average person has lost 6 adult teeth due to trauma, disease or poor hygiene and 4% of the adult population has no remaining teeth (4). Significant bone loss can result following the loss of teeth as a result of reduced loading in the underlying bone. Significant bone loss can also occur in the craniofacial region as a result of blast injuries, tumor resections (5, 6) and radiotherapy (7).

1.1.2 Current Bone Grafting Materials for Dental and Craniomaxillofacial Bone Loss

Significant dental bone defects are caused by a wide range of events including open fractures, non-unions, infection, tumor resection and radiotherapy. These severe conditions can lead to a critical loss of bone, for which normal regeneration processes are inadequate at restoring adequate volume for maintaining dental implants. Unfortunately, current therapies for repairing these severe bone defects have limitations and drawbacks including high risk of complications, size constraints, poor quality of life during healing and poor function post-healing (8). Innovations in the development

of synthetic, porous, degradable scaffolds have shown promise in quickly, effectively and cost-effectively regenerating bone compared to autografts, allografts and traditional synthetic bone graft substitutes.

Table 1 Commercially available bone graft substitutes typically used for dental bone grafting procedures

Product Name	Manufacturer	Composition
Biogran	Biomet3i	Bioglass
BioOss	Geistlich	Irradiated bovine bone +/- porcine collagen
Easy-Graft	Guidor/Sunstar	PLGA + HA particles
IngeniOs	Zimmer	Synthetic hydroxyapatite
PerioGlas	NovaBone	Bioglass
PRO-DENSE	Wright Medical	Calcium sulfate + calcium phosphate
Puros	Zimmer	Demineralized human bone allograft
RegenerOss	Biomet3i	Demineralized + mineralized human bone allograft
Vitoss	Stryker	Bioglass
Infuse	Medtronic/BioHorizons	Bovine collagen + rhBMP-2
OP-1	Stryker	Bovine collagen + rhBMP-7

1.1.2.1 Autografts

The current gold-standard treatment for regeneration of large bone defects is the autogenous bone graft. This treatment involves the harvest of “donor” bone tissue from other anatomical sites in the patient. Autografts are osteoinductive due to the presence of bioactive proteins and cells found in the healthy harvested bone (9). This osteoinductivity results in faster healing times and improved outcomes compared to other therapies for large bone defect repair (10). Since the “donor” tissue is harvested from the same patient there is also no risk of disease transmission or graft rejection. The biggest limitation of autogenous bone grafting is the availability of “donor” bone and the

morbidity associated with the harvesting procedure (8, 9, 11). Due to this limitation and the similar success rates of bone graft substitutes, allografts are not typically used for minor dental implant-associated bone grafting (12, 13). However, for more complex dental bone grafting, a combinatorial grafting approach may be pursued which involves the use of bone graft substitutes combined with autogenic bone or bone marrow aspirates (14).

1.1.2.2 Allografts

Allogenic bone grafts address the size restrictions and donor site morbidity drawbacks of autogenic bone grafting. Allogenic bone is obtained from human cadavers by tissue banks and then screened for diseases, processed and resold to healthcare providers. Allogenic bone processing involves removal of cells and other antigenic components of the bone, typically through physical and chemical methods and gamma irradiation. The most common form of allogenic bone is demineralized bone which can be purchased in powder, particle, putty or block formulations (9, 10). While allografts overcome the size limitation and donor site morbidity drawbacks of autografts, they suffer from decreased osteoconductivity due to the extensive processing and sterilization methods necessary to prepare the materials. Allografts also lack pre-vascularization and carry increased infection and graft rejection risks (8, 15). Since allografts come from various individual donors, there are also concerns with batch variability which can result in varied healing rates. In spite of these limitations, demineralized bone autografts are frequently used for dental bone grafting and result in generally good outcomes (12, 14).

1.1.2.3 Synthetic, Growth Factor and Tissue Engineering Approaches

There are a large number of reports in the literature on the use of porous scaffolds for bone tissue engineering, focusing primarily on polymers and ceramics. Many groups have developed porous

scaffolds that are functionalized with growth factors, such as commercially available recombinant human bone morphogenetic protein-2 (rhBMP2) and -7 (rhBMP7) doped collagen scaffolds (16). However, these products are expensive, have limited approved indications for use, require fixation with permanent materials and are associated with serious complications (17, 18). Therapies using magnesium would be less expensive and complex to manufacture, require less rigorous regulatory review, result in fewer complications and be fully degradable while capturing the same market segment.

1.1.2.4 Barrier Membranes are used to Constrain and Protect Bone Grafts

The aforementioned bone grafting materials are frequently used with barrier membranes as part of a guided bone regeneration "GBR" approach (Table 2). These barrier membranes are composed of processed biological or synthetic occlusive sheets that serve to constrain the bone graft material within the regenerating defect and prevent the ingrowth of gingival tissue (19). These barrier membranes can also be used without bone graft substitutes to protect regenerating bone defects from gingival tissue ingrowth as is commonly the case in periodontal applications (20, 21).

Table 2 Commercially available barrier membranes typically used for guided bone regeneration.

Product Name	Manufacturer	Composition
Alloderm	BioHorizons	Decellularized human dermal matrix
Guidor	Guidor Sunstar	Poly-lactic acid
Inion	Inion/Curasan	PLGA
Bio-Gide	Geistlich	Collagen
conFORM/RCM6	ACE Surgical	Collagen
CopiOs	Zimmer/RTI Biologics	Bovine pericardium
OsseoGuard	Biomet3i	Bovine dermal collagen

Barrier membranes can be classified into three groups with distinct applications, advantages and disadvantages. Non-degradable barrier membranes, typically comprised of

expanded poly(tetrafluoroethylene) (ePTFE) are frequently used to protect and maintain slow-to-heal bone defects (22, 23). While they exhibit good biocompatibility, they lack structural reinforcement needed to protect large defects and typically require surgical device removal following bone healing. Thus, titanium alloy reinforced ePTFE were developed to provide a larger degree of mechanical integrity (24, 25). Unfortunately, Ti-reinforced ePTFE membranes also require device removal surgeries and exhibit a high rate of membrane re-exposure due to the presence of rigid metal reinforcements. Finally, degradable barrier membranes are available that eliminate the need for device removal surgery following bone healing and significantly reduce the risk of re-exposure (26-28). These degradable membranes can either be natural (26) or synthetic (28, 29) in nature which allows for a wide range of mechanical/handling and degradation properties. Much of the current research on barrier membranes is focused on cell/material (30), growth factor/material (31, 32) and composite membranes (33-36) to overcome limitations of commercially available devices.

Unfortunately, these degradable membranes do not possess the structural rigidity necessary for maintaining large bone grafting sites. Thus there remains a need for a mechanically reinforced, yet degradable barrier membrane.

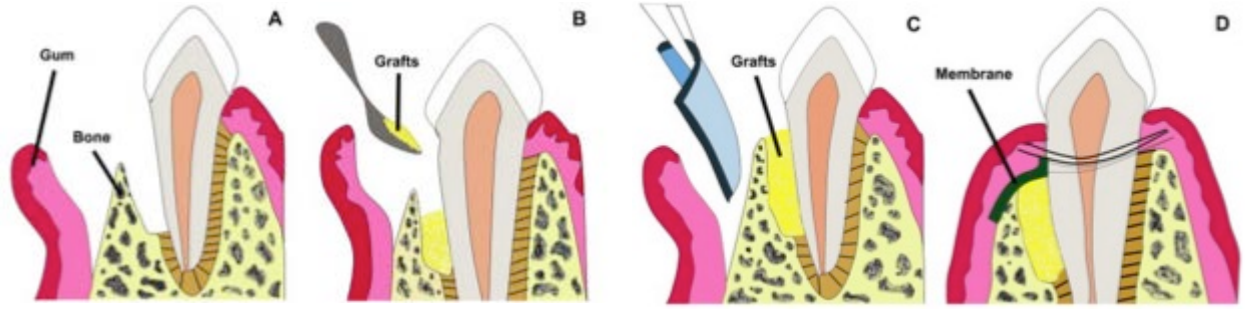

Figure 1 Schematic of guided bone regeneration approach in a periodontal setting using a bone graft material and barrier membrane in an attempt to regenerate a bone defect. Republished from Chen, et. al. (37).

1.1.3 Additional Significant Need for Bone Repair in Orthopedic and Spinal Applications

Musculoskeletal injuries are the most common form of injuries and bone injuries and disorders make up a significant portion of these (38). Over 6.2 million bone fractures occur in the United States each year, 10 million Americans suffer from osteoporosis and 300,000 patients require bone grafting prior to receiving dental implants (39, 40). Treatments of bone injuries and disorders include medication to prevent or treat osteoporosis, conservative casting of long bone fractures, internal fixation of open fractures and elective bone grafting in preparation for dental implants. The burden of these treatments range from outpatient procedures with several hundred dollars in costs to long hospitalizations generating over $25,000 in medical costs (41, 42). Additional burdens are borne by the patients who face pain, limited mobility, as well as potential economic loss due to short and long-term disability. The significant incidence of bone injuries and cost of their subsequent treatments suggest that improving bone repair therapies could result in reduced healthcare costs.

The 6.2 million bone fractures that occur in the United States each year result in an annual medical-cost of over $20 billion (8, 42). The average person has a 29% chance of sustaining a fracture throughout the course of their life with fracture incidence rapidly increasing after 60 years

of age (43). Meling, et al, found that of all fractures requiring in-hospital treatment, 56% of fractures required some form of internal fixation (43), usually with titanium or stainless steel plates and screws (43). These permanent fixation devices frequently remain in the body which can result in local inflammation and metal sensitivities as the device surface wears and the surrounding bone may weaken due to stress shielding (44-46). In pediatric cases or with certain fracture locations, these devices are removed following healing. One study examining ankle fractures found that 72% of patients receiving permanent metallic fixation devices underwent a second removal surgery which increased total treatment cost by an adjusted US$2,400 or 27% compared to degradable fixation devices (47). Neither the removal of these fracture fixation devices nor their remaining in the body following bone healing are particularly desirable outcomes (48), thus new degradable materials have been developed to overcome these drawbacks.

1.2 MAGNESIUM SHOWS PROMISE FOR BONE REPAIR DEVICES

1.2.1 Magnesium Devices' Degradation known to be Biocompatible

Magnesium alloys were first used for biomedical applications over 200 years ago (49, 50); however, their widespread development for orthopedic applications did not accelerate until the manufacturing advancements were made in more recent decades (51-57). Magnesium alloys degrade through surface oxidation in aqueous environments, such as in the body (Eq 1. and 2.) (58). The Mg degradation products are absorbed into the blood and removed by the kidneys. Numerous studies have found that varying alloy synthesis parameters affects degradation rate and osteoconductivity *in vivo* (53, 54, 56, 57, 59-61). While Mg alloys have been found to be

osteoconductive, few studies have examined the development of porous Mg scaffolds for large bone defect regeneration.

$$Mg(s) + 2H_2O \rightarrow Mg(OH)_2(s) + H_2 \quad (1)$$

$$Mg(OH)_2(s) + 2Cl^- \rightarrow MgCl_2(aq) + 2OH^- \quad (2)$$

1.2.2 A Wide Range of Magnesium Devices have been Manufactured and Evaluated

Magnesium alloys have been used for biomedical applications shortly after the discovery of elemental magnesium and the ability to manufacture it over 200 years ago (50). One of the first documentations of human use was reported in 1872 when Mg wires were used as degradable ligatures to control bleeding (49). Mg was explored for use in orthopedic applications due to its similar density and mechanical properties compared to bone (62). Reports on the use of Mg plates and screws for orthopedic reconstruction followed in 1906. Although clinical outcomes were promising, the difficulties of controlling degradation rate and assessing materials prior to human use limited their development (63). Numerous studies were conducted to determine the *in vitro* and *in vivo* responses of various alloys for various applications. However, difficulty characterizing cytotoxicity and osteogenicity *in vitro* meant future assessments of Mg scaffolds would rely primarily on expensive *in vivo* characterization techniques.

1.2.3 Magnesium Based Scaffolds

A wide variety of magnesium scaffolds have been synthesized and characterized. The bulk material for magnesium scaffolds can be synthesized using casting, selective laser sintering and other techniques (64). A basic design change that has been evaluated is the introduction of one or more alloying elements to the bulk Mg. Gu, et al. synthesized nine binary Mg alloys which were

subsequently found to affect mechanical and degradation properties, as well as cytotoxicity (51). After synthesis of the bulk material, numerous processing steps, such as annealing, extruding and surface treatments can be performed to further alter the behavior of the magnesium scaffold. These final processing steps can also include manufacturing of the final scaffold shape, including the introduction of pores to allow cellular infiltration (65). Testing each of these possible design iterations *in vivo* would be cost prohibitive and would lack *in vitro* biocompatability data required for regulatory approval.

It has long been understood that porous biomaterials enable faster cell infiltration and tissue regeneration than their non-porous counterparts. The literature suggests that pore sizes greater than 100um and higher overall porosity best support osteogenesis *in vivo*. (66). While there has been much work reported on porous polymer, hydroxyapatite and natural material orthopedic scaffolds, there are few reports of porous magnesium scaffolds in the literature. Several groups have created porous magnesium scaffolds using pressing, sintering and salt-casting techniques (65, 67-69). These scaffolds exhibited good mechanical properties and porosity, but this synthesis method prevents more complex geometries from being constructed without advanced machining. Cifuentes, et. al., pressed and sintered PLLA/Mg sheets to create non-porous Mg/polymer scaffolds (70). A porous composite Mg powder/polymer scaffold could be synthesized using traditional casting and salt leaching techniques. Creation of these composite scaffolds would harness the osteoconductive properties of Mg, while overcoming limitations of currently available technologies.

1.2.4 Magnesium Device Evaluation is Limited *in vitro*

The healthy human body is capable of removing very high concentrations of Mg and many common alloying elements. Previous *in vitro* examinations of cell viability and proliferation have used conditioned media with alloy degradation products which is not physiologically relevant and fails to take into account temporal aspects of degradation (51, 56, 57). Li, et al allowed cells to attach and proliferate prior to placing a Mg alloy onto the cells (52, 71). This method also does not model the *in vivo* regeneration process where cells would be required to attach and proliferate on a Mg scaffold. Two groups performed cytotoxicity evaluations by seeding cells directly onto magnesium alloys (71, 72). While this model is the most physiologically relevant, this and other proliferation assays performed were rudimentary and destructive, such as cell counting (52, 73) and MTT (51, 53, 56, 57, 72, 74) assays. Recently, several traditional proliferation assays functioning on metabolic cycles, such as MTT were found to be confounded by Mg (75). Limitations of the studies aside, most have found that bone-related cell lines tolerate magnesium and most of its alloying elements well and that for several alloys, cell proliferation was increased. However, the *in vitro* assessments of cytotoxicity reported in the literature are not physiologically relevant, time consuming and sample-destructive.

1.2.5 Magnesium Scaffolds' Performance *in vivo*

Numerous studies have examined the biocompatibility and osteogenicity of Mg scaffolds *in vivo*. Mg scaffolds of varying composition (56, 57, 59-61), porosity (53) and surface treatments (54) have been implanted in animals to assess their osteogenicity in bone defects. These studies have all found that varying Mg scaffold properties affects degradation rate and cellular invasion.

However, all studies have found Mg scaffolds are osteoconductive and allow full regeneration of bone in the defect using histological stains (53, 54, 59, 61) and radiographic methods (54, 61) (Figure 2). Although *in vivo* characterizations of Mg scaffolds for bone regeneration have yielded promising results, a lack of comprehensive *in vitro* assessments present significant regulatory hurdles in the development of subsequent medical devices. Additionally, iterative design changes, such as varying alloying element concentrations or scaffold processing steps would require additional *in vivo* studies to requalify toxicity and osteogenicity properties.

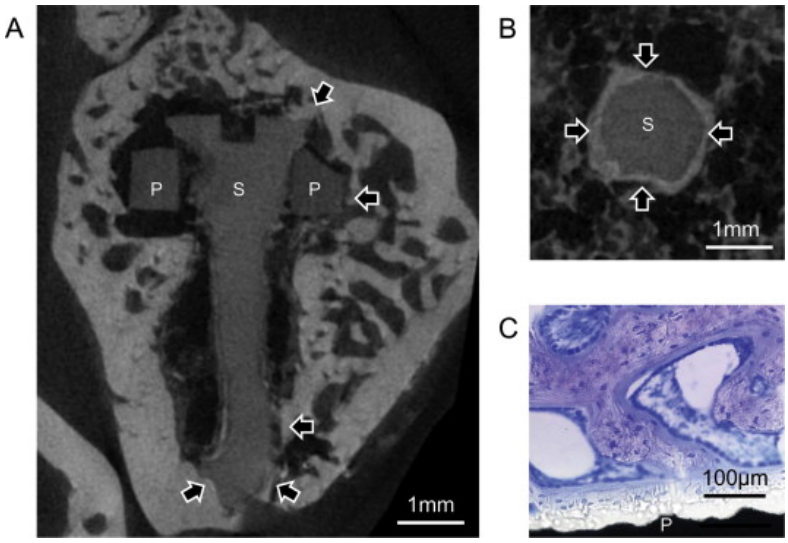

Figure 2 Figure republished from Chaya, et al (76). Significant bone formation was identified surrounding implanted magnesium devices and significant bone/device contact was identified which showed promise for magnesium bone devices. A longitudinal slice of a Mg plate (P) and screw (S) shows areas of bone contact around the screw head, shaft, and plate edge (A). A transverse slice of a Mg screw shaft (S) shows bone contact around the screw perimeter after 16 weeks (B). Toluidine Blue shows bone morphology at bone-plate (P) interface after 8 weeks (C).

1.2.6 Little Understanding of Magnesium's Inflammatory, Angiogenic and Osteogenic Capabilities

Solubilized magnesium ion (Mg^{2+}) is known to be a co-factor for many enzymes, as well as a stabilizer of DNA (77). Since, Mg^{2+} is an important component of the human physiology, it is important to determine the local effect of the resorbed alloys on the cells. Several reports have suggested stimulatory effects on the growth of new bone tissue (74, 78). However, few investigations have identified specific Mg^{2+} effectors relevant to osteogenesis or predictive of Mg alloys' performances *in vivo*. Mg^{2+} has been found to increase expression of vascular endothelial growth factor, proliferation and migration in human umbilical vein endothelial cells suggesting that magnesium could support angiogenesis which may be a source of the enhanced osteogenesis observed *in vivo (79, 80)*. Examining angiogenic and inflammatory markers in tissue surrounding magnesium implants could elucidate the mechanisms that underlie the enhanced bone regeneration seen *in vivo*.

The healthy human body is capable of removing very high concentrations of Mg and many common alloying elements. Previous *in vitro* examinations of cell viability and proliferation have used conditioned media with alloy degradation products which is not physiologically relevant and fails to take into account temporal aspects of degradation (51, 56, 57). Li, et al allowed cells to attach and proliferate prior to placing a Mg alloy onto the cells (52, 71). This method also does not model the *in vivo* regeneration process where cells would be required to attach and proliferate on a Mg scaffold. Two groups performed cytotoxicity evaluations by seeding cells directly onto magnesium alloys (71, 72). While this model is the most physiologically relevant, this and other proliferation assays performed were rudimentary and destructive, such as cell counting (52, 73) and MTT (51, 53, 56, 57, 72, 74) assays. Recently, several traditional proliferation assays

functioning on metabolic cycles, such as MTT were found to be confounded by Mg (75). Limitations of the studies aside, most have found that bone-related cell lines tolerate magnesium and most of its alloying elements well and that for several alloys, cell proliferation was increased. However, the *in vitro* assessments of cytotoxicity reported in the literature are not physiologically relevant, time consuming and sample-destructive.

Magnesium scaffolds for bone regeneration are required to recruit mesenchymal stem cells and support osteogenic differentiation. Most osteogenic gene profiling performed *in vitro* has used quantitative polymerase chain reaction (qPCR) for quantification of specific gene expression following experimental manipulation. In experiments analyzing the osteogenic capacity of Mg scaffolds, matrix production and remodelling was observed to be increased through Col-I, II and IX and MMP-13 expression (73). Additionally, Mg scaffolds were found to increase expression of alkaline phosphatase (71, 74), an established marker of bone formation. Several of the studies examining *in vitro* cytotoxicity assess basic osteogenic markers, such as alkaline phosphatase secretion (53, 71, 74) or mineralization through von Kossa staining (74). These studies use rudimentary and destructive assessment techniques that are not conducive to rapid and comprehensive screening of candidate alloys.

1.3 DEGRADABLE POLYMERS

1.3.1 Degradable Polymers used for Medical Applications

Polymers can be found naturally, many inside the body, or synthesized synthetically and have various chemical, mechanical and degradation properties. Degradable polymers have been used

for a wide range of medical applications, such as drug delivery vehicles, sutures, bone graft substitutes, barrier membranes wound healing bandages and skin grafts, bone cement plugs, suture anchors, hernia repair meshes, clips, pins and fracture fixation plates and screws (81-84) (Table 3). These degradable polymers are frequently classified by their mechanism of degradation. Degradation typically occurs hydrolytically (i.e. the body's hydrate environment cleaves bonds within the polymer) or enzymatically (i.e. enzymes within the body, such as proteases, cleave bonds within the polymer). Hydrolytically degradable polymers are comprised of many synthetic polymer classes of interest for biomedical applications including PLA, PGA, and PCL. These polymers are often co-polymerized to yield PLGA or PLA-PCL blends to tailor polymer product degradation time for varying applications. Enzymatically degradable polymers are comprised of many natural polymer classes used for medical products. Collagen, fibrin, elastin, chitosan, hyaluronic acid and other biologically occurring polymers are frequently harvested from allogenic or xenogenic sources and processed to form gels, sheets and scaffolds for a range of biomedical applications (27, 85, 86). Finally, many combination polymer products exist as a means to leverage multiple polymers' characteristics, such as PEG-PLA(87). All of these polymers tend to be versatile and require extensive optimization and processing in order to be suitable for a particular biomedical application.

Table 3 Commercially available polymer devices relevant to bone regeneration and repair procedures

Product Name	Application	Manufacturer	Composition
Dexon	Suture	Covidien	PGA
Vicryl	Suture	Ethicon	PLGA
Monacryl	Suture	Ethicon	PCL
Lactosorb	Fracture fixation system	Biomet	PLGA
Rapidsorb	Fracture fixation system	Depuy Synthes	PLGA
LEADfix	Membrane fixation pin	Biovision	PLLA
BIOCRYL	ACL interference screw	Depuy Synthes	PLLA + B-TCP

1.3.2 Degradable PLGA-Based Bone Repair Devices

PLLA, PLDLA and PLGA have been extensively studied in bone repair applications and have been used to synthesize commercially available and FDA-approved fracture fixation devices (88). These devices are generally associated with good outcomes, but have been associated with the development of sterile abscesses (82, 89, 90). Researchers hypothesize that the development of these abscesses may be due to a non-specific foreign body reaction in response to the acidic degradation profile these polymers exhibit. This hypothesis is further supported by in vitro cytocompatibility assessments of PLDLA and PLGA extracts which showed that high concentrations of degradation products decreased cell proliferation and viability (91). Animal studies carried out with commercially available LactoSorb PLGA plates and screws have more intensively studied the temporal biological response to device degradation. Eppley, et. al., found that fibrous tissues typically encapsulate the devices at 2 months while an increased macrophage

and fibrovascular presence is observed 6 months post-implant. As the device continues to degrade through one year, the macrophage presence decreases, as there are fewer remaining degradation products, and few inflammatory cells remain (92).

1.3.3 Polymer-Based Composites

Numerous studies have examined polymer/mineral and polymer/ceramic composite scaffolds (93-98). One study examined polymer coating of a bulk Mg alloy (99) and another studied Mg/TCP-doped collagen scaffolds (100). Hydroxyapatite (HA)/PLLA composite scaffolds have also received great attention with several HA/PLLA screws commercially available for clinical use (101, 102). Cifuentes, et. al., examined embedding magnesium within a PLLA matrix, but did not assess in vivo biocompatibility (70). There are no reports of porous Mg/polymer scaffolds, barrier membranes or meshes for bone tissue engineering. Coupling Mg powder with polymers could allow rapid prototyping of complex patient/injury-specific scaffolds for bone regeneration, as has been accomplished with hydroxyapatite powder and polymeric binders (103). Additionally, there is a much larger body of literature regarding functionalization of polymers with growth factors, and drugs than there is for Mg (81, 104). A drawback of some polymers is that their acidic byproducts that can threaten cell attachment and viability, as well as protein delivery (105). Addition of Mg, which produces hydroxide ions during its corrosion (Eq. 2), to these polymers could create a buffering effect to eliminate the drawbacks of acidic polymer products. Finally, polymers are less commonly used for bone healing applications due to their low strength compared to bone and traditional orthopedic metals, such as titanium and stainless steel. Doping polymer scaffolds with Mg could increase their mechanical strength and increase their utility for bone healing applications (70). Composite materials containing both Mg-based powder and polymer

could serve as a whole platform for therapeutics capturing the advantages of both Mg alloy and polymer systems.

1.4 OVERALL RESEARCH GOAL AND SPECIFIC AIMS

The incidence of dental bone grafting procedures and the cost associated with them has made dental bone tissue engineering an attractive field of study. New technologies and therapies are needed to provide low-cost, less-painful and more reliable bone void regeneration. The clinical goal of this research is to develop guided bone regeneration materials capable of providing faster bone regeneration in a fully degradable manner through the combination of magnesium and PLGA. Additionally, through this research we will expand our knowledge on the biological effects of magnesium, specifically in terms of osteogenesis, angiogenesis and inflammatory processes. Our research group hypothesized that successful creation and characterization of a magnesium-based bone grafting platform would demonstrate enhanced osteogenicity both *in vitro* and *in vivo* compared to clinically used gold-standard materials.

1.4.1 Specific Aim 1: Synthesize and Perform Material Characterizations of Magnesium/PLGA Composite Scaffolds

Scaffolds with varying Mg/NaCl ratios will be fabricated using PLGA/DCM solvent casting with negative salt casting technique. Scanning electron microscopy, true and apparent density and mercury intrusion porosity techniques will be used to determine scaffold porosity. Degradation analyses will be performed through pH measurement and inductively coupled plasma atomic

emission spectroscopy measurement of released magnesium. Mechanical properties will be measured with compression testing. Indirect cytocompatibility assessment will be performed based on ISO-10993 with bone marrow stromal cells and an MTT assay. The outcomes of these assays were analyzed to select an optimized Mg/PLGA composition for further study in Specific Aim 2.

We hypothesized that porous Mg/PLGA scaffolds could be successfully manufactured using a solvent casting salt leaching method. Additionally, we hypothesized that the incorporation of metallic magnesium particles into a PLGA scaffold would 1) increase compressive strength and modulus, 2) buffer the acidic byproducts of PLGA degradation, 3) release magnesium throughout degradation and 4) enhance bone marrow stromal cell proliferation compared to PLGA Only scaffolds.

1.4.2 Specific Aim 2: Evaluate the Therapeutic Potential of Magnesium/PLGA Scaffolds in a Canine Socket Preservation Model

Mg/PLGA scaffolds will be used as a bone grafting material and implanted into canine pre-molar sockets following tooth extraction. Following 8wk and 16wk healing periods, mandibles will be explanted, formalin fixed and subjected to microCT analysis in order to quantify bone regeneration and assess scaffold degradation. Following micro-CT, samples will be trimmed, embedded in plastic and sectioned in preparation for histological analysis. Goldner's Trichrome staining will be used to examine general tissue morphology. Alizarin Red and von Kossa staining will be used to identify mineralized tissue within the healing tooth sockets. Chloroacetate esterase staining will be performed in order to identify any neutrophil collections indicative of inflammation in the healing site.

We hypothesized that the Mg/PLGA scaffolds could be successfully implanted into the socket defects and proven safe and effective at regenerating bone in a canine socket preservation model. We also hypothesized that the bone height and bone volume of the Mg/PLGA treated defects would be increased compared to defects left empty.

1.4.3 Specific Aim 3: Evaluate the Osteogenic, Angiogenic and Inflammatory Gene Expression Profile of hBMSCs exposed to Magnesium

Human bone marrow stromal cells will be cultured *in vitro* and exposed to varying concentrations of magnesium sulfate ($MgSO_4$) as a standardized simulation of degrading magnesium implants. The hBMSCs will be maintained in standard maintenance medium or exposed to osteogenic differentiation medium in addition to the $MgSO_4$ supplementation. hBMSC proliferation will be determined using trypan blue exclusion and counting with a hemocytomer, as well as the MTT assay at 1, 3, 5 and 7 days post-plating. Matrix mineralization will be assessed using Alizarin Red staining followed by dye solubilization and quantification following 3 weeks of culture. Also at the 3 week experimental endpoint, RNA and total protein will be extracted from the cell monoloayers and subjected to qPCR and Western blotting, respectively. The findings from qPCR will be input to gene network analysis software to identify proteins of interest for further investigation of Mg-affected pathways.

We hypothesized that increased concentrations of magnesium in cell culture medium would result in increased cell proliferation and matrix mineralization. Additionally, we aimed to identify possible Mg-affected pathways that could explain the increased bone regeneration observed around Mg implants *in vivo*.

1.4.4 Specific Aim 4: Synthesize and Perform a Proof-of-Concept *in vivo* Implantation of a Complete Magnesium-Based Guided Bone Regeneration Platform

Mg/PLGA guided bone regeneration barrier membranes will be synthesized using a solvent-casting approach. Additionally, a magnesium micromesh will be fabricated using a laser-cutting approach. These devices will be implanted in a canine vertical ridge augmentation model using magnesium screws as a grafting material. Following explantation at 12wks post-implantation, explants will be subjected to microCT scanning, formalin fixed and embedded in plastic. Bone height and bone volume regenerated will be calculated using microCT scan analysis. Following plastic embedding, histological analysis will be performed to assess general biocompatibility, osteogenic and inflammatory response.

We hypothesized that a magnesium/PLGA barrier membrane and magnesium micromesh could be synthesized meeting the design criteria of currently used barrier membranes. Additionally, we hypothesized that the barrier membrane, micromesh and magnesium screw could be successfully implanted in our *in vivo* model with no adverse events. We compared the performance of our magnesium-based guided bone regeneration platform to a repair with a commercially available bone graft substitute secured by titanium micromesh.

2.0 SPECIFIC AIM 1: SYNTHESIS AND MATERIAL CHARACTERIZATION OF MAGNESIUM/PLGA SCAFFOLDS

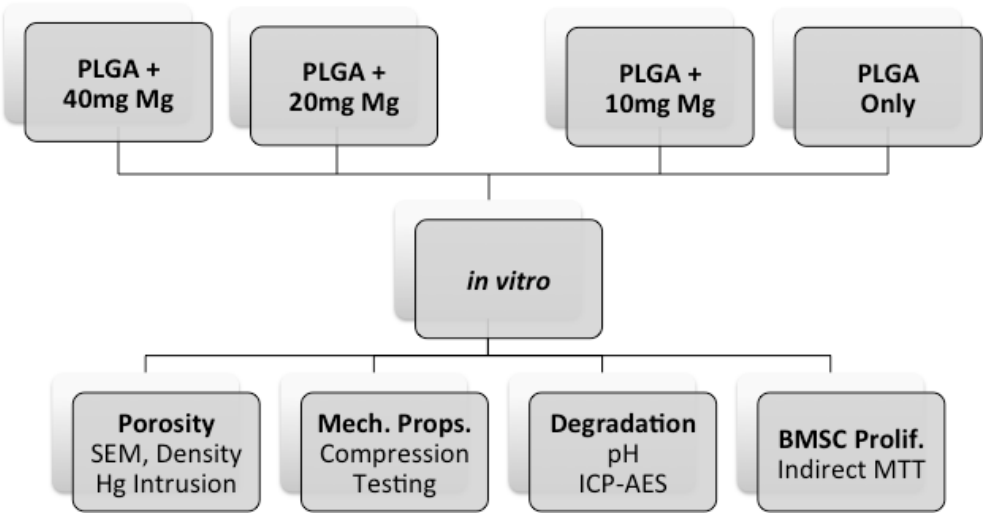

Figure 3 Experimental overview of Specific Aim 1

The first step in achieving the overall research goal of this thesis was to synthesize, optimize and characterize the material properties of the magnesium/PLGA scaffolds (Figure 3). During the preliminary phases of this study, several different polymer components including fibrin, PEG/gelatin, alginate, polycaprolactone (PCL), chitosan and three variations of PLGA were considered based on their manufacturability and adherence to design criteria in Table 4. 502H PLGA was identified as the most promising polymer component due to its widespread clinical use in other devices, mechanical strength, tunable degradation properties and versatility. The synthesis and characterization of these magnesium/PLGA scaffolds was described in: Brown A, Zaky S, Ray H, Sfeir C. Porous magnesium/PLGA composite scaffolds for enhanced bone regeneration following tooth extraction. *Acta Biomaterialia* 11(1): 543-53, 2015. Portions of the manuscript are reproduced here with permission of the publisher.

Table 4 Design criteria guiding evaluation of magnesium/polymer scaffolds

Cell Attachment	Support BMSC Attachment
Cell Proliferation	Increase BMSC Proliferation
Degradation Time	8-12 weeks
Mg Release	Throughout full degradation time
Compressive Modulus	> 50MPa
Compressive Yield Strength	> 2MPa
Pore Size	> 100um

2.1 INTRODUCTION

Magnesium and magnesium alloys have been increasingly researched in the past decade and have been found to be excellent biomaterials for orthopedic applications (58). Magnesium degrades non-toxically in the body, thus allowing full bone regeneration in the implant site (106). Magnesium has also been shown to increase osteoconductivity *in vivo* compared to polymer rods (59). Furthermore, *in vitro* studies found that exposing cells to magnesium increased proliferation and expression of osteogenic markers (73, 107). Overall, magnesium provides many of the osteoinductive effects seen with recombinant growth factors while remaining significantly less expensive and safer.

Composites have been widely used for bone regeneration scaffolds and fixation devices including organic/inorganic composites such as collagen/HA (97) and polymer/mineral composites such as PLGA/B-TCP and PLLA/HA (98). However, little work has focused on composites of polymers and metallic magnesium particles. Magnesium salts, such as $MgCO_3$ and

$Mg(OH)_2$, have been embedded in PLGA microspheres and scaffolds and were found to buffer the acidic pH degradation of the PLGA (108, 109). This was found to increase bioavailability of proteins and drugs encapsulated in the PLGA/Mg microspheres. Other studies have investigated coating bulk magnesium alloys with PLGA, PLLA or PCL in order to control the degradation rate of the alloy (99, 110, 111). These coatings were found to decrease short-term degradation rate, as well as increase cell attachment and viability on the coated-alloy. Cifuentes, et. al., produced non-porous PLLA/Mg cylinders through compression of numerous solvent-casted thin films (70). This process found that inclusion of Mg particles into the PLLA matrix enhanced mechanical strength of the scaffolds. While these studies captured various advantages of combining polymers and several forms of magnesium, none synthesized porous magnesium/PLGA composites for use as bone tissue engineering scaffolds.

The overall goal of this study was to develop and characterize a porous metallic magnesium particle/PLGA scaffold in order to harness the advantages and strengths of both polymers and magnesium. In order to investigate the impact of varying amounts of magnesium on scaffold mechanical, degradation and cytocompatibility properties, we explored a range of Mg/NaCl compositions in PLGA. We hypothesized that the addition of metallic magnesium particles into the PLGA scaffold would 1) increase compressive strength and modulus, 2) buffer the acidic byproducts of PLGA degradation, 3) release magnesium throughout its degradation and 4) enhance bone marrow stromal cell proliferation.

2.2 MATERIALS AND METHODS

2.2.1 Synthesis of Scaffolds

Four compositions of magnesium/PLGA scaffolds were synthesized using a traditional solvent casting, salt leaching technique (112) (Figure 4). The scaffold compositions were chosen such that the mass of PLGA was constant between the four groups while the magnesium mass was varied. In order to produce scaffolds of the same size, variations in the mass of Mg particles was balanced by the addition of sodium chloride particles. First, molds were created by covering one open end of Tygon tubing pieces with aluminum foil (Cole Parmer, Vernon Hills, IL) to produce cylindrical scaffolds in small (3mm Diameter, 8mm Length), medium (7mm D, 6mm L) and large (6mm D, 8mm L) sizes. These geometries were chosen in order to provide the optimal sample dimensions for downstream characterizations discussed below. Next, the molds were filled with pure metallic magnesium particles (>99% purity, <300um particle size, Sigma Aldrich, St. Louis, MO), sodium chloride (Sigma Aldrich), sieved to a particle size of 106um-212um, or a mixture of Mg particles and NaCl according to Table 5 for small scaffolds. Medium scaffold molds were filled in the same manner with twice the masses listed in Table 5 while large scaffolds were filled with four times the masses listed in Table 5.

Table 5 Compositions for small Mg/PLGA scaffolds. Medium scaffolds were synthesized with 2x the masses and large scaffolds with 4x the masses described in the table.

	Mg Mass (mg)	NaCl Mass (mg)	PLGA Mass (mg)
PLGA + 40mg Mg	40	0	40
PLGA + 20mg Mg	20	40	40
PLGA + 10mg Mg	10	60	40
PLGA Only	0	80	40

Once the molds were filled with Mg and/or NaCl, PLGA (50:50, M_w 7,000-17,000, Sigma Aldrich) was dissolved into dichloromethane (DCM, Sigma Aldrich) at a concentration of 40% (w/v) and briefly sonicated. Volumes of 100ul, 200ul or 400ul of the PLGA/DCM mixture were then pipetted into the small, medium and large molds, respectively. The molds were left in a fume hood for 48h to allow DCM evaporation after which the scaffolds were removed from the molds and allowed to vent for an additional 24h.

Salt leaching was performed by placing scaffolds in ddH_2O at a ratio of 5ml/scaffold, 10ml/scaffold and 20ml/scaffold for small, medium and large scaffolds, respectively. The scaffolds in ddH_2O were placed on an orbital shaker and the ddH_2O was replaced three times over the course of 24h. Immediately before and after each ddH_2O change, the scaffolds were vacuumed to -60kPa for 5min to encourage water flow into the scaffolds. After salt leaching was complete, scaffolds were placed in the fume hood to dry for 48h. All scaffolds were weighed before and after salt leaching to confirm full salt washout.

Following salt washout and drying, scaffolds were lyophilized for 48h. Scaffolds for all assays were then placed into sealed tubes and gamma sterilized with a dose of 20,000Gy at a dose

rate of 23.5Gy/min (Mark I 68, JL Shepherd and Associates, San Fernando, CA) prior to use in the characterizations described below.

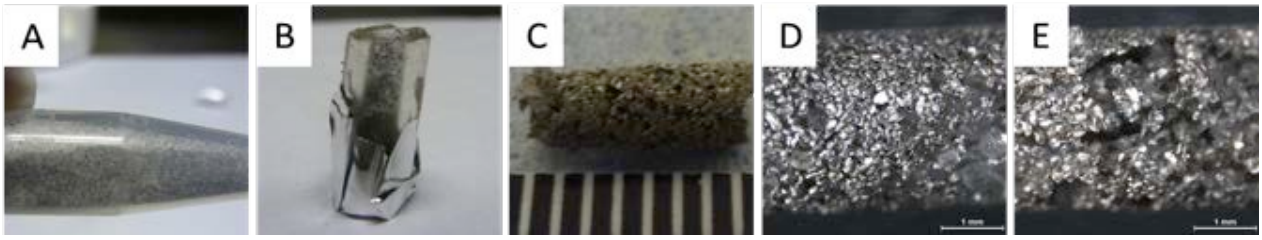

Figure 4 Synthesis Overview of Mg/Polymer Scaffolds. A) 50%/50% Mg / NaCl mixture B) Mg/NaCl mixture in tygon tubing mold C) Scaffold with NaCl after polymerization of PLGA in DCM D) High magnification view of Mg/PLGA scaffold prior to salt washout E) Final Mg/PLGA scaffold after NaCl washout.

2.2.2 Compression Testing

Six medium scaffolds per group were subjected to unconfined compression testing using a materials testing machine (Instron Model #5566, Norwood, MA) outfitted with a 2000N load cell. A 0.2N preload was applied to the sample followed by compression at a crosshead displacement of 0.2mm/min until sample failure or 0.30 strain was reached. Stress and strain were calculated by dividing the load and elongation data by pre-compression cross-sectional area and height, respectively. Maximum stress was defined as the point at which the material exhibited a failure resulting in a decrease in load of greater than 50%, or in the case of failure by barreling, the load at 30% strain. Modulus was defined by measuring the slope of the linear portion of the curve immediately prior to maximum load.

Two univariate one-way ANOVAs with Dunnett's post-hocs were performed to assess differences in maximum stress and modulus between the Mg/PLGA and PLGA Only scaffolds (SPSS, IBM, Armonk, NY).

2.2.3 Porosity Characterization

The porosity of three large scaffolds per group was calculated through the measurement of true and envelope density for three scaffolds per group. The true density of each scaffold was measured using a gas displacement density analyzer (AccuPyc 1340, Micromeritics, Norcross, GA) with 5 purge/measurement cycles at 19.5psig. The same scaffolds were then subjected to envelope density analysis (GeoPyc 1360, Micromeritics) with a consolidation force of 38N. Porosity was calculated by dividing apparent density by true density.

The pore size distribution of one large sized scaffold per group was measured using mercury intrusion porosity (AutoPore IV, Micromeritics). Samples were subjected to mercury intrusion pressures from 0.5-30,000psia correlating to pore sizes of 346-0.005um. Pore size distribution and median pore size for each sample was analyzed.

Scanning electron microscopy (SEM) was also performed to qualitatively examine scaffold porosity and morphology. Small sized scaffolds were briefly dipped in liquid nitrogen and then fractured to provide both an outer and cross-sectional surface for imaging. Scaffolds were sputter coated with gold/palladium to a thickness of 6nm (Cressington #108auto, Watford, England). After sputter coating, scaffolds were mounted in order to image three outer surfaces and three cross-sectional surfaces per group (JEOL #JSM 6335F, Tokyo, Japan).

A one-way ANOVA was performed to assess differences in porosity, as measured using true and apparent density, between the scaffold groups.

2.2.4 Degradation Testing

Four small scaffolds per group were subjected to degradation testing in order to characterize changes in pH and Mg release over the course of 10 weeks. Following gamma sterilization, scaffolds were placed into 12 well tissue culture plates, immersed in 5ml BMSC growth medium (formulated as described below) and placed in a tissue culture incubator. Early timepoint media sampling was performed at 1h, 1d and 3d by extracting 500ul of medium from each sample and immediately replenishing it with 500ul of fresh medium. Following the early timepoints, the full 5ml of medium was extracted and replaced on a weekly basis for a total of 10 weeks.

Immediately upon sampling the medium, the pH was measured using a combination pH electrode (Hanna Instruments #1083B, Smithfield, RI) and pH meter (Beckman #350, Indianapolis, IN).

Media samples were thawed and diluted 20X in HEPES-buffered saline and subjected to inductively coupled plasma atomic emission spectroscopy (Thermo Fisher #iCAP 7200, Waltham, MA) in order to determine concentration of magnesium in the medium. The average of 3 measurements of the Mg2790 line were taken for each sample, multiplied by 20 to obtain undiluted concentration in parts per million then divided by magnesium's molecular weight to obtain concentration in millimolar.

Differences in media pH during the degradation assessment were analyzed using a one-way ANOVA with Dunnett's post-hocs at each timepoint.

2.2.5 Indirect Cytocompatibility

BMSC growth medium was formulated according to Colter, et al, and Sekiya, et al (113, 114). Medium was sterile filtered following the combination of 82.5% alpha minimum essential medium with L-glutamine, without ribonucleosides, without deoxyribonucleosides (Life Technologies, Grand Island, NY), 16.5% fetal bovine serum (premium select, Atlanta Biologicals, Atlanta, GA), 1% penicillin G (10,000 units/ml, Lonza, Basel, Switzerland) and streptomycin sulfate (10,000ug/ml) and 1% L-glutamine (200mM, Life Technologies). The pH of BMSC growth medium as-formulated was 7.5-7.6 at 37degC and 5% CO_2.

Cytocompatibility testing of the Mg/PLGA scaffolds was performed using an indirect method adapted from ISO 10993:5, 10993:12 and Fischer, et al (115). Extracts were obtained by immersing small scaffolds (10 per group) in BMSC growth medium at a ratio of 200mg scaffold / 1000ul extraction medium and then allowing the scaffolds to degrade for 72h at 37degC on an orbital shaker. After 72h, the individual medium extracts from each group of scaffolds were pooled and 2X, 4X and 10X dilutions with fresh medium were created.

Bone marrow stromal cells for the indirect cytocompatibility assay were obtained from the Institute for Regenerative Medicine at Scott & White and cultured based on Colter, et al, and Sekiya, et al (113, 114). A vial containing one million P1 BMSCs were plated in growth medium in a 10cm dish and allowed to recover overnight. BMSCs were passaged by re-plating at a density of 10,000 cells per T175 flask. This process was repeated twice such that P4 BMSCs were obtained for use in the indirect cytocompatibility assay.

Bone marrow stromal cells were plated in 96 well plates at a density of 500 cells/well in 100ul of BMSC growth medium. After the cells were allowed to attach and proliferate for 24h, the growth medium was aspirated and the scaffold extraction medium and extraction medium dilutions

were added (n=6 per extract). The cells were cultured for an additional six days with the extraction medium aspirated and replenished on day 3.

A Vybrant MTT assay (Life Technologies #V13154) was performed according to manufacturer's instructions on day 6 after aspirating the extraction medium and washing all wells with PBS. 100ul of the MTT reagent in phenol red-free alpha-MEM was added to each well of the 96 well plate and incubated at 37degC for 4h. Then 100ul of SDS-HCl solution was mixed into each well and allowed to incubate at 37degC for an additional 14h. Finally, the absorbance of all wells at 570nm was read using a standard plate reader (Molecular Devices Spectramax 190, Sunnyvale, CA). The absorbances for the Mg/PLGA scaffold extract groups were each normalized to the absorbances for the PLGA Only scaffold extract groups.

A one-way ANOVA with Dunnett's post-hocs was performed on the MTT absorbance data to assess statistical differences in proliferation between the Mg/PLGA and PLGA Only scaffold groups.

2.3 RESULTS

2.3.1 Porous Magnesium-PLGA Composite Scaffolds were Successfully Synthesized

The solvent casting salt leaching method for synthesizing Mg/PLGA scaffolds was found to be successful. Following the solvent casting step, the scaffolds weighed on average 10±6% less than expected based on masses in Table 5 suggesting that nearly the entirety of the Mg/NaCl was bound by nearly the entirety of PLGA added to each scaffold. Following salt washout, the scaffolds were

found to weigh on average 1±8% less than expected based on Table 5 suggesting that all of the NaCl was removed using our salt washout protocol.

Gross examination of the scaffolds was performed using a digital camera and stereo microscope both before and after salt-washout. As seen in Figure 5, the Mg/PLGA scaffolds exhibited both a larger length and diameter than the PLGA Only scaffolds after the completion of synthesis. Interestingly, the Mg/PLGA scaffolds exhibited roughly equal length and diameter compared to the PLGA Only scaffolds prior to salt washout.

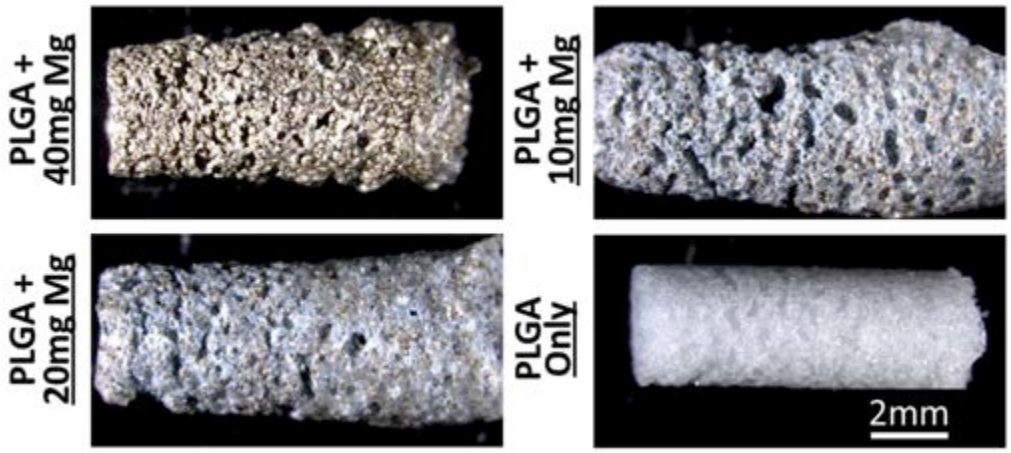

Figure 5 Mg/PLGA composite scaffolds were successfully synthesized. Stereo microscope images of representative samples for the four scaffold compositions after completion of solvent casting, salt leaching and lyophilization (Scale bar = 2mm for all images).

2.3.2 PLGA + 40mg Magnesium Scaffolds Exhibited Increased Maximum Strength and Modulus compared to PLGA Only Scaffolds

Six medium sized scaffolds per group underwent compressive failure until catastrophic cracking occurred or 0.30 strain was reached. The maximum stress reached by the PLGA + 40mg Mg

scaffolds (241±84kPa) was significantly higher ($p<0.001$) than the PLGA Only scaffolds (79±7kPa) (Figure 6A). There was no significant difference between PLGA + 20mg Mg (30±6kPa) or PLGA + 10mg Mg (26±6kPa) and PLGA Only scaffolds. PLGA + 40mg Mg scaffolds (2.9±0.7MPa) also exhibited a significant increase ($p<0.001$) in compressive modulus compared to PLGA Only scaffolds (0.7±0.1MPa) (Figure 6B). Again, PLGA + 20mg Mg (0.9±0.3MPa) and PLGA + 10mg Mg (0.7±0.2MPa) did not exhibit significant differences in compressive modulus compared to PLGA Only scaffolds. The Mg/PLGA scaffolds failed through cracking in all cases, while the PLGA Only scaffolds experienced barreling until 0.30 strain was reached.

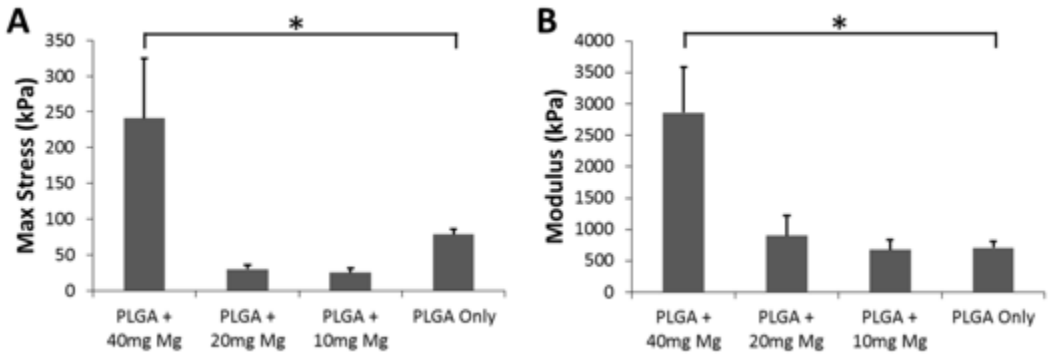

Figure 6 PLGA + 40mg Mg scaffolds exhibit increased maximum strength and modulus compared to PLGA only scaffolds. Mg/PLGA scaffolds were subjected to compressive testing in order to determine A) maximum stress and B) compressive modulus. The bars represent means + standard deviations (* $p < 0.001$, n=5, ANOVA with Dunnett's post-hoc).

2.3.3 Magnesium/PLGA Scaffolds are Highly Porous and Contain Macropores

The porosities of the PLGA + 40mg Mg (55±5%), PLGA + 20mg Mg (69±6%) and PLGA + 10mg Mg (72±9%) scaffolds were not significantly different compared to the PLGA Only scaffolds

(69±15%) (Figure 7A). The true densities measured for the four scaffold groups ranged from 1.4g/cc for the PLGA Only group to 1.6g/cc for the PLGA + 20mg Mg group (data not shown).

The pore size distribution as measured with mercury intrusion porosity was found to be similar between the four scaffold groups with minor differences seen in the overall porosities (Figure 7B). Median pore sizes were 48um, 41um, 46um and 37um for the PLGA + 40mg Mg, PLGA + 20mg Mg, PLGA + 10mg Mg and PLGA Only scaffolds, respectively. All scaffolds exhibited a negligible pore volume derived from pore sizes less than 5um. Additionally, all scaffolds exhibited a large pore volume derived from pores greater than 50um, particularly the PLGA + 10mg Mg and PLGA + 20mg Mg groups.

Scanning electron micrographs of the four scaffold groups provided qualitative data as to the porosity and pore size distribution. PLGA + 40mg Mg scaffolds were comprised of Mg particles densely glued together with PLGA resulting in pores as a result of particle packing limitations of the Mg particles (Figure 7C). PLGA + 20mg Mg and PLGA + 10mg Mg scaffolds exhibited similar morphologies to each other with more pores and larger pores derived from the empty space remaining from NaCl crystals that were washed out (Figure 7D-E). Additionally, The PLGA + 20mg Mg and PLGA + 10mg Mg scaffolds showed a more disrupted Mg matrix when compared to the PLGA + 40mg Mg scaffolds. Finally, the PLGA Only scaffolds exhibited a PLGA matrix with cubic pores derived from the washed out salt and a more densely packed appearance than the PLGA + 10mg Mg and PLGA + 20mg Mg scaffolds (Figure 7F).

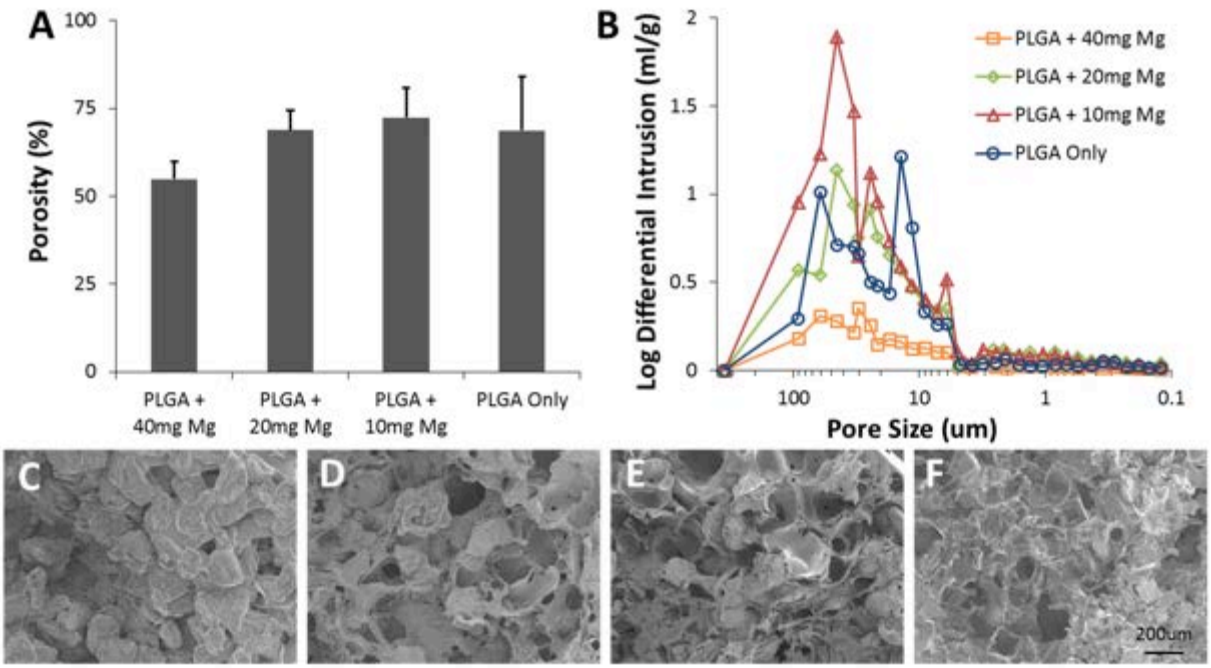

Figure 7 Mg/PLGA scaffolds are highly porous and contain macropores suitable for cell infiltration. A) Mg/PLGA scaffolds subjected to mercury intrusion porosimetry contained a large proportion of pores > 50um (n=1). B) Overall porosity of Mg/PLGA scaffolds were not significantly different from PLGA Only scaffolds as measured by true and apparent densities ($p > 0.05$, n=3, ANOVA). Representative SEM micrographs of C) PLGA + 40mg Mg, D) PLGA + 20mg Mg, E) PLGA + 10mg Mg and F) PLGA Only scaffold cross sections show an increasingly complex microstructure as Mg content decreases (Scale Bar = 200um for Figure 7C-F).

2.3.4 Addition of Magnesium Particles to PLGA Scaffolds Buffers the Acidic Byproducts Produced throughout PLGA Degradation

Measurement of the degradation medium pH yielded a significant decrease in pH for the PLGA Only scaffold group relative to all other groups as expected (Figure 8A). The PLGA Only degradation medium pH also exhibited a much larger standard deviation among samples than all other scaffold groups. The degradation medium of the Mg/PLGA scaffold groups exhibited a

small, but rapid increase in pH from the 1h timepoint to the 1d timepoint and then plateaued. After media refreshment began at 1wk, the pH of the PLGA + 10mg Mg group decreased until 4 weeks when there was no longer a significant difference between PLGA Only and PLGA + 10mg Mg groups ($p > 0.01$). The same trend occurred more slowly for the pH of the PLGA + 20mg Mg group which was no longer significantly different from the PLGA Only group at 7 weeks. The PLGA + 40mg Mg group exhibited a significantly increased pH compared to the PLGA Only group throughout the full 10 week experiment ($p < 0.01$). While the Mg/PLGA scaffold groups exhibited slightly elevated pH compared to the No Scaffold group, they did not experience the significant decrease in pH exhibited by the PLGA Only scaffold group.

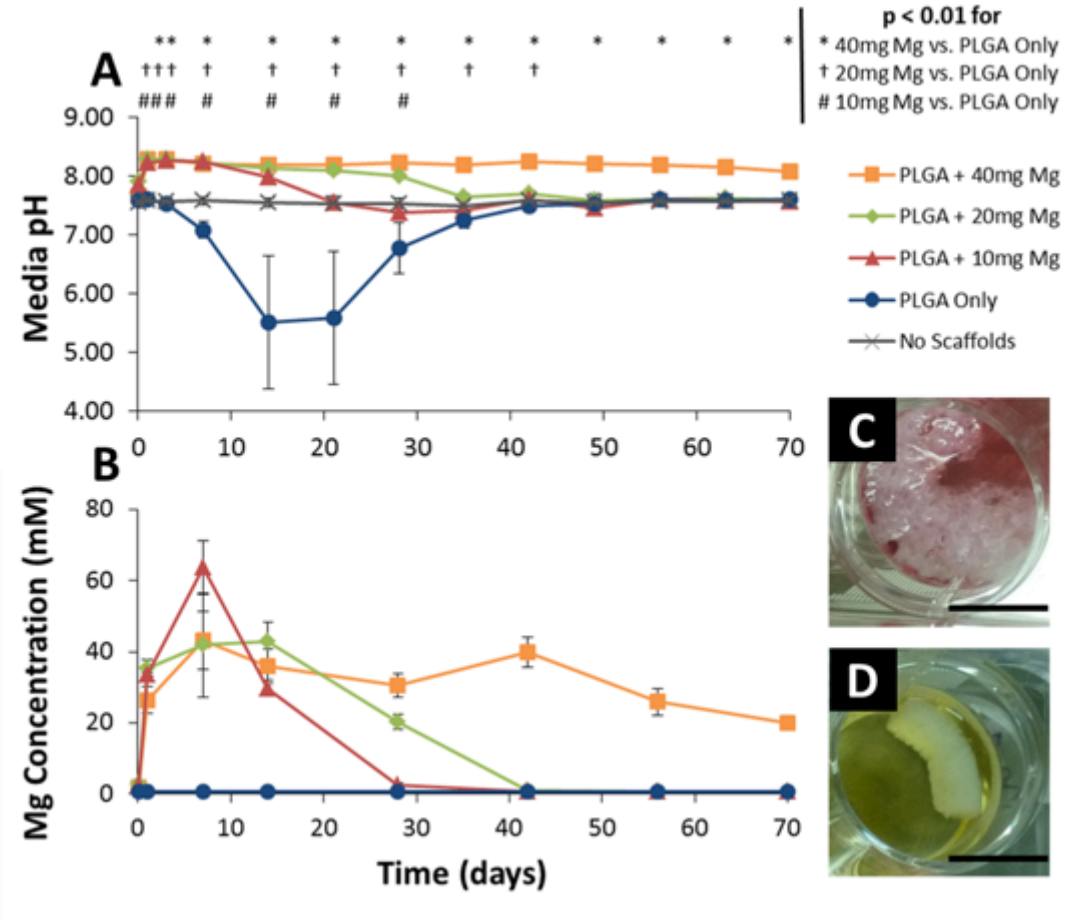

Figure 8 The addition of Mg particles to PLGA scaffolds buffers the acidic byproducts produced throughout PLGA degradation while increasing amounts of Mg powder results in longer release times into the medium. Mg/PLGA scaffolds were placed in medium with FBS, which was replaced weekly, for 10 weeks. Media was sampled at 1h, 1d, 3d and weekly thereafter. A) The pH of the medium was measured immediately upon sampling (n=4, ANOVA with Dunnett's post-hocs). Error bars are displayed on all data points; however, some are not clearly visible due to very small standard deviations. B) Media samples were diluted 20X in HBSS prior to Mg concentration measurement using ICP-AES. C) Representative PLGA + 20mg Mg and D) PLGA Only scaffolds prior to the 2w media sampling (Scale bar = 10mm for Figure 8C, D).

2.3.5 Increasing Amounts of Magnesium Particles in PLGA Scaffolds Result in Longer Magnesium Release Times

Measurement of degradation medium magnesium concentration yielded similar trends to those observed in degradation medium pH. Magnesium was rapidly released into the medium over the first week (Figure 8B). Magnesium concentrations were similar among the Mg/PLGA scaffold groups at 2 weeks and then returned to baseline (0.8mM Mg in alpha-MEM) at timepoints corresponding to their return to baseline for pH measurement. The PLGA + 10mg Mg scaffolds returned to baseline at 4 weeks and the PLGA + 20mg Mg scaffolds returned to baseline at 6 weeks. The PLGA + 40mg Mg scaffolds were still releasing Mg into the degradation medium at the end of the 10 week experiment. Interestingly, we observed an increase in size of the Mg/PLGA scaffolds (Figure 8C) throughout the degradation assay that was not observed with the PLGA Only scaffolds (Figure 8D).

2.3.6 Bone Marrow Stromal Cells Cultured in Mg/PLGA Media Extracts Exhibited Increased Proliferation Compared to BMSCs Cultured in PLGA Only Media Extracts

Cell proliferation in the indirect proliferation assay was varied among the scaffold types and the extraction dilutions (Figure 9). Culturing BMSCs in 1x extraction medium (no dilution) resulted in extensive cell death for all Mg/PLGA scaffold groups. However, the Mg/PLGA scaffold groups' 2x, 4x and 10x extraction medium dilutions did not negatively impact cell proliferation when compared to PLGA Only. Interestingly, BMSCs cultured in several of the magnesium-containing scaffold groups' extracts (PLGA + 40mg Mg 10x, PLGA + 20mg Mg 4x and 10x and all PLGA + 10mg Mg extract dilutions) exhibited increased proliferation compared to cells cultured in PLGA

Only extracts. Taken as whole, cell proliferation in each of the three Mg/PLGA scaffold groups was significantly increased ($p < 0.01$) compared to PLGA Only.

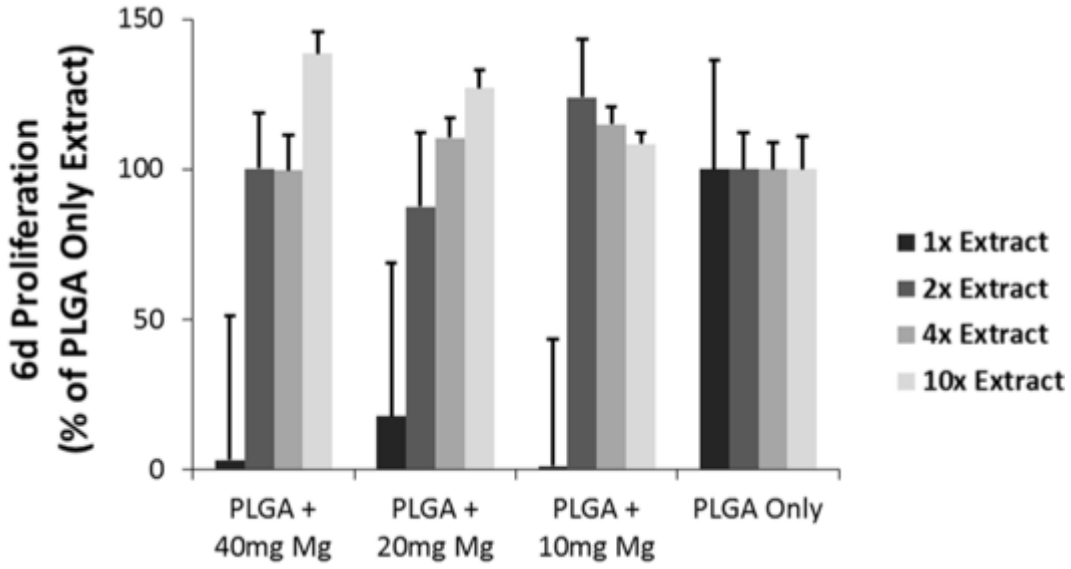

Figure 9 Bone marrow stromal cells cultured in Mg/PLGA scaffold media extracts exhibited increased proliferation compared to BMSCs cultured in PLGA Only media extracts. Scaffolds were placed in alpha-MEM + 16.5% FBS extraction medium for 72h. BMSCs were then cultured in 100%, 50%, 25% and 10% extraction medium for 6d after which an MTT assay was performed. While undiluted extracts of Mg/PLGA scaffolds inhibited proliferation, statistically significant increases in proliferation were observed for all three Mg/PLGA scaffold groups compared to PLGA Only due to proliferative effects of the 50%, 25% and 10% extracts (* $p<0.01$, n=6, ANOVA with Dunnett's post-hoc).

2.4 DISCUSSION

The objective of this aim was to develop and characterize a porous metallic magnesium particle / PLGA scaffold for bone tissue engineering. We believe this is the first report of the synthesis of a porous metallic magnesium/polymer composite, as well as the first *in vivo* assessment of a metallic

magnesium/polymer composite in the bone environment. Our Mg/PLGA scaffolds buffered the acidic byproducts of PLGA degradation and increased BMSC proliferation.

We successfully synthesized 3 different sizes of Mg/PLGA scaffolds using a solvent casting/salt-leaching method. We had optimized synthesis parameters as described in Table 5 and to provide scaffolds of similar size for the four compositions cast. Interestingly, following salt washout and lyophilization the PLGA + 10mg Mg and PLGA + 20mg Mg scaffolds exhibited a visible increase in diameter and length. This phenomenon was not observed in the PLGA Only or PLGA + 40mg Mg scaffolds. While we had minimized the salt washout time to avoid magnesium corrosion, it is likely that the saline environment within the two Mg/NaCl containing scaffold groups resulted in magnesium corrosion and subsequent hydrogen gas production within the scaffold. Increased salinity (particularly increased concentrations of Cl^-) is known to increase magnesium corrosion which could explain why this increase in size is not observed in the PLGA + 40mg Mg scaffolds (116). The evolution of hydrogen gas by the scaffolds during salt washout may have increased the pore volume of the PLGA + 10mg Mg and PLGA + 20mg Mg scaffolds resulting in the overall scaffold volume increase we observed for these two groups. However, our weight and SEM assessments of these scaffolds indicate that the overall corrosion of the magnesium particles was minor.

We hypothesized that the addition of magnesium particles to the PLGA scaffolds would increase compressive strength and modulus compared to PLGA Only scaffolds, similar to observations by Cifuentes, et al (70). In fact, only the PLGA + 40mg Mg scaffolds exhibited higher maximum stress and modulus than the PLGA Only scaffolds. We suspect that the PLGA + 20mg Mg and PLGA + 10mg Mg did not exhibit increased strength and modulus due to the lesser amounts of magnesium and the more disrupted Mg/PLGA network from the salt washout. The

Mg/PLGA scaffolds tended to fail through cracking, thus the more disruptions in the Mg/PLGA network due to washed out NaCl particles, the more nucleation points that existed for failure to occur. This theory is supported by studies of PLGA Only scaffolds that show a rapid decrease in mechanical strength as porosity and pores size are increased (117). Also, more magnesium particle corrosion may have occurred in the PLGA + 20mg Mg and PLGA + 10mg Mg scaffolds during salt washout which could have resulted in decreased mechanical properties. While the PLGA + 10mg Mg scaffold did not exhibit increased strength and modulus compared to PLGA Only scaffolds, its formability and mechanical properties proved sufficient for manipulation during *in vivo* surgical placement and still provided the necessary pH buffering properties, as well as an osteoconductive environment for bone growth.

Our second hypothesis was that the addition of magnesium particles to PLGA scaffolds would buffer the acidic byproducts of PLGA degradation. The pH of medium containing PLGA Only scaffolds decreased significantly from baseline, as is expected with degrading PLGA (104, 118, 119). We believe the larger standard deviation among samples in the PLGA Only group compared to other groups was due to small differences in the weight of PLGA in each scaffold and the lack of buffering by magnesium particles. While the medium pH of the Mg/PLGA scaffolds increased relative to baseline, this deviation was substantially smaller than the acidic deviation in the PLGA Only group. For this reason we accept our hypothesis that magnesium is capable of buffering the decreases in pH caused by PLGA degradation. Furthermore, even the PLGA + 10mg Mg scaffolds were capable of buffering the decrease in pH suggesting that small amounts of magnesium particles relative to PLGA are sufficient. Other groups have reported the use of magnesium salts as antacids to buffer pH decreases in degrading PLGA, thus improving drug release and protein stabilization (108, 109). Zhu, et al reported that in addition to directly buffering

acidic by-products of PLGA degradation, basic salts (including $Mg(OH)_2$) decrease the autocatalytic degradation rate of PLGA (108) which could be desirable for slow-to-heal bone tissue engineering applications.

Magnesium concentration in the degradation medium was also measured to determine the release rate of magnesium from the scaffold. As expected, the more magnesium particles contained in a scaffold, the longer magnesium was released from the scaffold. Higher amounts of magnesium contained in the scaffold did not result in a significantly higher concentration of magnesium in the medium at a given timepoint. One possible reason for this is that the medium volume was fixed at 3ml and only replaced on a weekly basis. This could result in the magnesium concentrations between the scaffold and the medium reaching equilibrium, thus reducing magnesium degradation in the PLGA + 40mg Mg scaffolds. Another possible explanation is an increased disruption of the PLGA coating during the salt washout on individual magnesium particles which would limit their corrosive protective abilities as suggested by Ostrowski, et al (99). Another observation was the increase in size of the magnesium containing scaffolds which was not observed with the PLGA Only scaffolds. This is likely due to the continuing evolution of hydrogen gas from the degrading magnesium. If hydrogen gas is unable to immediately diffuse away from the scaffold interior, it may enlarge the pore volume, thus resulting in an overall increase in scaffold volume. This phenomenon will likely have to be considered when optimizing scaffold geometry and magnesium content in the future. The magnesium release profiles correspond well with the pH data as we expected. Additionally, the release time of the magnesium varied depending on the initial amount of magnesium. While *in vivo* study would be necessary to confirm this phenomenon, it suggests that scaffolds could be tailored to release magnesium for longer or shorter amounts of time depending on the application or anatomical site in which they would be used.

We were able to accept our hypothesis that Mg/PLGA scaffold extracts would increase BMSC proliferation compared to PLGA Only scaffold extracts. Undiluted extracts of the Mg/PLGA scaffolds resulted in nearly complete cell death which has been reported by other groups performing indirect cytocompatibility assessments of magnesium alloys (115). This cytotoxicity is primarily related to the non-physiological degradation rate that is experienced by magnesium during the extraction process and the resulting osmotic shock experienced by the cells when exposed to the extracts. As extracts were diluted, the magnesium concentration (and overall osmotic pressure) decreased resulting in an increased BMSC proliferation which has been reported in past studies to occur at 5-20mM Mg depending on cell type (73, 107, 120). The exact mechanisms of magnesium's impact on cell proliferation are not fully understood, but support the improved bone regeneration observed with magnesium's use *in vivo*.

Analysis of the synthesized scaffolds showed that some magnesium particle corrosion may have occurred during salt washout. We plan on more fully investigating the synthesis process' effect on the oxidation state of the magnesium particles in a future study. Our *in vitro* characterization of the Mg/PLGA scaffolds was limited in its investigation of the phenomenon of magnesium's buffering of the PLGA scaffolds. Future work is planned to examine the scaffold microenvironment's pH as a result of inclusion of the PLGA. Also planned are direct cytocompatibility assessments of BMSCs on the Mg/PLGA scaffolds. Additionally, these experiments will also allow us to examine the effects of Mg/PLGA scaffolds on the osteogenic gene expression of the BMSCs.

2.5 CONCLUSIONS

Completion of this aim represented the first step towards development of a Mg/PLGA bone graft scaffold in support of this thesis' overall goal of developing degradable Mg-based guided bone regeneration devices. Promising findings related to the non-acidic degradation profile and the increased proliferation of bone marrow stromal cells encouraged us to pursue *in vivo* testing of the Mg/PLGA scaffold in two different approaches. First, to assess the ability of the Mg/PLGA scaffold to support bone regeneration in a clinically relevant socket preservation model as discussed in Specific Aim 2. Second, a shorter-term murine intramuscular implantation model to assess the angiogenic and inflammatory responses to Mg/PLGA scaffolds at shorter time periods. Successful completion of both these approaches will not only reveal more about the potential genes and proteins that are affected by degrading magnesium, but also support the case for biocompatibility of magnesium in future regulatory filings.

The work in this specific aim also formed the foundation for an invention disclosure filed with the University entitled "A composite magnesium/polymer scaffold to buffer pH changes and enhance tissue regeneration". A non-provisional patent application was filed using this specific aim as supporting data as our group performed additional business and technology development described further throughout this thesis.

2.6 ACKNOWLEDGEMENTS

This study was supported by NSF Revolutionizing Metallic Biomaterials Engineering Research Center under grant number 0812348. The authors wish to extend their gratitude to Andrew

Glowacki and Dr. Steven Little for their assistance with scaffold synthesis, as well as Dr. Michael Epperly for gamma sterilization of the scaffolds. Jesse Lowe and Dr. Alejandro Almarza's assistance with compression testing of the scaffolds is greatly appreciated. We also thank Dr. Prashant Kumta and lab members Satish Singh, Ilnar Fatykhov and Dr. Abhijit Roy for aiding in the porosity and Mg release characterization of the scaffolds. Kan Wang of the University of Pittsburgh's Statistics Consulting Center assisted with determination of appropriate statistical methods for this study. Jonathan Franks provided his expertise during our scanning electron microscopy at the Center for Biological Imaging. Finally, Nicole Myers, Andressa Pen and Sabrina Noorani were instrumental in obtaining the histological data presented in this study and their hard work is greatly appreciated.

3.0 SPECIFIC AIM 2: EVALUATE THE THERAPUTIC POTENTIAL OF MAGNESIUM/PLGA SCAFFOLDS IN A CANINE SOCKET PRESERVATION MODEL

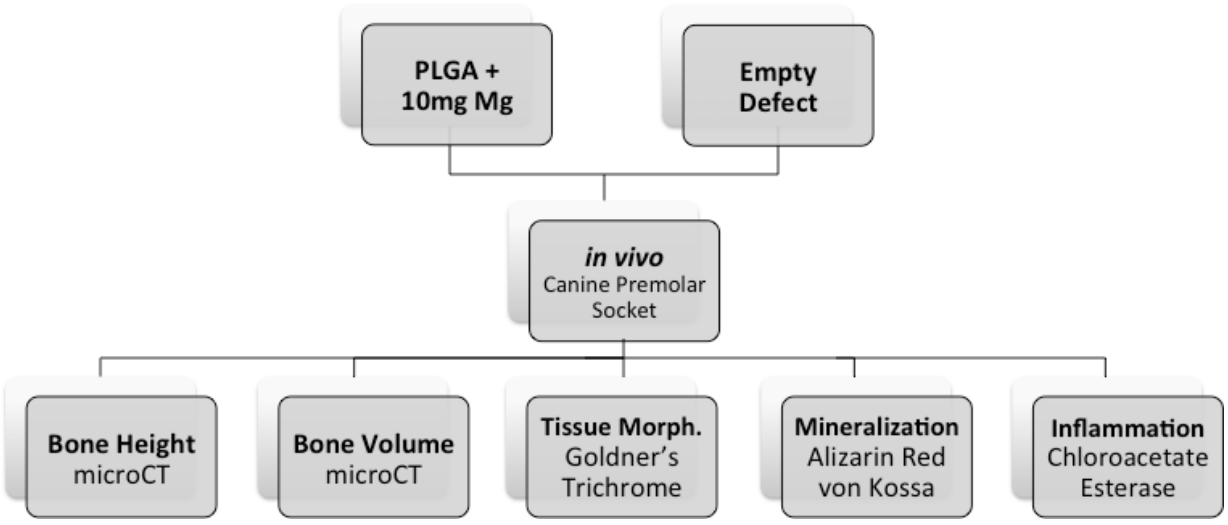

Figure 10 Experimental overview of Specific Aim 2.

Following evaluation of several Mg/polymer composite systems and selection of Mg/PLGA scaffolds and in vitro characterization of the scaffolds, an in vivo bone regeneration study was pursued (Figure 10). A canine socket preservation model was selected due to the low-risk nature of the intervention and the ability to demonstrate Mg/PLGA's support of bone regeneration. Such demonstrations would be necessary to validate Mg/PLGA's utility as a bone graft substitute for clinical use, as well as to support the development of other magnesium-based guided bone regeneration devices in the future. Finally, although not presented in this thesis, the histological samples derived from this study could be used for immunohistochemical approaches for evaluation of gene and protein activity within and surrounding the degrading Mg/PLGA scaffolds. This socket preservation model is therefore suitable for both evaluation of our novel Mg/PLGA scaffolds and elucidation of biological mechanisms affected by the presence and degradation of our Mg/PLGA

scaffolds. The in vivo evaluation of these magnesium/PLGA scaffolds was also described in: Brown A, Zaky S, Ray H, Sfeir C. Porous magnesium/PLGA composite scaffolds for enhanced bone regeneration following tooth extraction. *Acta Biomaterialia* 11(1): 543-53, 2015. Portions of the manuscript are reproduced here with permission of the publisher.

3.1 INTRODUCTION

Every year in the USA, 500,000 patients receive implant supported dental prostheses to restore functionality and cosmetic appearance of teeth extracted or lost due to poor oral hygiene, trauma and cancer. After a tooth is extracted, a blood clot is formed in the extraction socket which slowly remodels to provide a matrix suitable for bone ingrowth from the surrounding buccal bone. Unfortunately, numerous studies and clinical experience have shown that leaving this extraction socket empty, with only the blot clot formed, can lead to major bone resorption around the extraction site (121, 122). This lower quality and volume of bone is often not suitable for successful dental implant placement. Thus, sixty percent of these implant sites require some form of bone augmentation before or during implant placement to ensure sufficient bone quantity and quality for osseointegration and implant success (123-128).

Socket preservation is one type of bone augmentation typically performed immediately following tooth extraction using a bone grafting and/or a guided tissue regeneration approach (129-132). The bone grafting approach involves implantation of one of several biological or synthetic materials into the extraction socket prior to closing the gingival soft tissue. Biological materials used for this application include bone autografts (133, 134), mineralized and demineralized freeze-dried bone allografts (134-136) and bone xenografts (137, 138). While bone autografts are

considered the gold standard grafting material due to their osteoinductivity and excellent outcomes, they suffer from defect size limitations, increased surgical time and costs and cause donor site morbidity (137, 138). Allografts and xenografts are commercially available in powder, particle, gel, sponge or block form and can be found in mineralized or demineralized compositions. These allografts and xenografts address cost and size limitations of autografts, but are not vascularized, can exhibit poor mechanical properties, are less osteoconductive and carry an increased risk of infection (139, 140).

Synthetic bone grafting materials and composite materials have been developed more recently in attempts to overcome the drawbacks and limitations of autografts, allografts and xenografts. Most of these synthetic materials are calcium phosphate based in the form of hydroxyapatite and beta-tricalcium phosphate (140). These materials mimic the composition and characteristics of bone and are osteoconductive, but can inhibit full bone regeneration due to long degradation times (129, 141). Finally, several dental bone augmentation studies have used synthetic polymers, such as PLA or PLGA, as space fillers (142, 143) or barrier membranes (144, 145) in and around the defect. PLGA is a highly studied polymer and its clinical use is widespread in materials ranging from sutures to vascular stents to bone scaffolds (104, 119, 146). PLGA also has the advantage of being capable of delivering drugs, proteins and growth factors to enhance bone healing in both oral-maxillofacial and general orthopedic applications (16, 104, 143, 147). While use of these polymers resulted in good clinical outcomes for bone regeneration overall, further studies have shown that the acidic by-products produced during their degradation can lead to increased inflammation and hamper efforts at concurrent drug, protein and growth factor delivery (119).

3.2 MATERIALS AND METHODS

3.2.1 in vivo Study using a Canine Socket Preservation Model

PLGA + 10mg Mg scaffolds were selected for further study *in vivo* because they were found to be the lowest containing Mg group that still provided an enhanced proliferative effect *in vitro*. Empty tooth socket defects were chosen as a control in order to contrast any biocompatibility issues in the scaffold healing site to the native healing site. Additionally, this surgical model allows for bone regeneration to occur in the empty defect control, thus allowing comparison of bone regeneration rates between groups. The study protocol was approved by the Institutional Animal Care and Use Committee at the University of Pittsburgh. Mg/PLGA implanted defects and empty defects were randomly assigned in a split mouth design in the left or right mandibular third (P3) or fourth (P4) premolars in twelve female beagle dogs age 9-13 months old (Marshall BioResources USA). Eight week and sixteen week timepoints were assessed with 6 defects per group at each timepoint.

3.2.2 Surgery, Animal Care and Sacrifice

Animals were placed in ventral recumbency under isofluorane anesthesia. Rubber dams and dam clamps were placed on the mandibular first molar and second premolar exposing the P3 and P4 premolars (Figure 11A). The mesial and distal roots of P3 and P4 were then separated by a diamond bur under irrigation. The distal root was luxated by a periotom and extracted using #13 European style forceps (Figure 11B). The mesial root was sealed with a glass ionomer restoration to prevent bacterial contamination of the remaining root. While there was some variation between individual animals, the approximate dimensions of the resulting conically shaped tooth socket defect were

11mm in depth and 5.5mm in diameter with the diameter being larger at the alveolar crest and tapering apically. This translates to an approximate defect volume of 0.2cm^3. The empty distal sockets of P3 and P4 were filled with either 1.5 small PLGA + 10mg Mg scaffolds or left empty (Figure 11C). Buccal and lingual free gingivae were approximated for complete closure over the extraction socket with interrupted resorbable sutures (5/0 VICRYL, Ethicon, Bridgewater, NJ) (Figure 11D). Dogs were sacrificed after 8 and 16 weeks postoperative and the mandibular explants containing P3 and P4 were fixed in formalin for 48h.

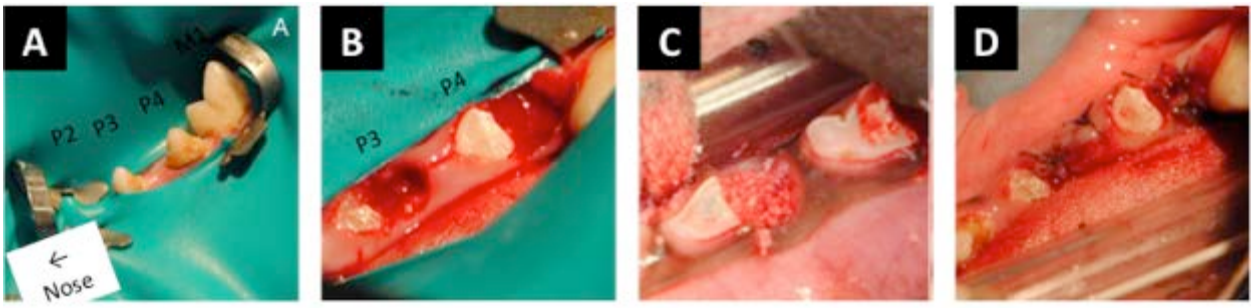

Figure 11 Implantation of magnesium/PLGA scaffolds was performed using a canine tooth extraction and socket preservation surgical model. A) Rubber dam placement on first molar and second premolar to prepare for operation on the third and fourth premolars. B) Distal roots of the third and fourth premolars were extracted (Following root canals for unrelated study). C) Mg/PLGA scaffolds were packed into empty socket defect (or no material for empty control group). D) Socket closure by interrupted sutures.

3.2.3 Micro-CT Analysis

Prior to scanning, the full mandibular explants were trimmed to separate P3 from P4 and the enamel on the crowns was ground off to reduce beam hardening artifact. The samples were scanned in an *ex vivo* uCT system (Skyscan 1172, Bruker-Skyscan, Belgium) at 10um voxel size, 60kVp beam energy, 400ms exposure, 10 frames averaged per view and 360 degrees angular range of scan. The 3D reconstruction of raw files was subsequently performed with Recon and processing and analysis was performed with CTAn (Skyscan). Preserved bone height in each socket defect was computed by connecting the plane between the alveolar crests mesial and distal to the defect (intercrestal plane) at the mid root level bucco-lingually (when the mesial root canal, including apical foramen, was wholly evident). The distance between the intercrestal plane and the preserved bone height was measured from the center of the socket defect. Bone height measurements were

averaged from 3 different sections for each defect. Defect bone volume was calculated by orienting the scans as sagittal sections (mesio-distally). The boundaries of the mesial root were set as limits of the sections to be analyzed. The upper and lower threshold levels were determined and the region of interest (ROI) was drawn around the remaining mesial root from the mesial to the distal alveolar crest. This ROI was then mirrored onto the defect space to represent the original volume of the extracted distal root. Bone volume calculation was performed using binarisation based on the defined thresholds for scan sections across the entire root thickness. This calculated bone volume in the defect was then divided by the total volume of remaining mesial root space to compute %BV/TV (Figure 12).

Differences in bone height and bone volume percent, as measured with micro-CT were analyzed using a one-way ANOVA with Bonferonni post-hocs.

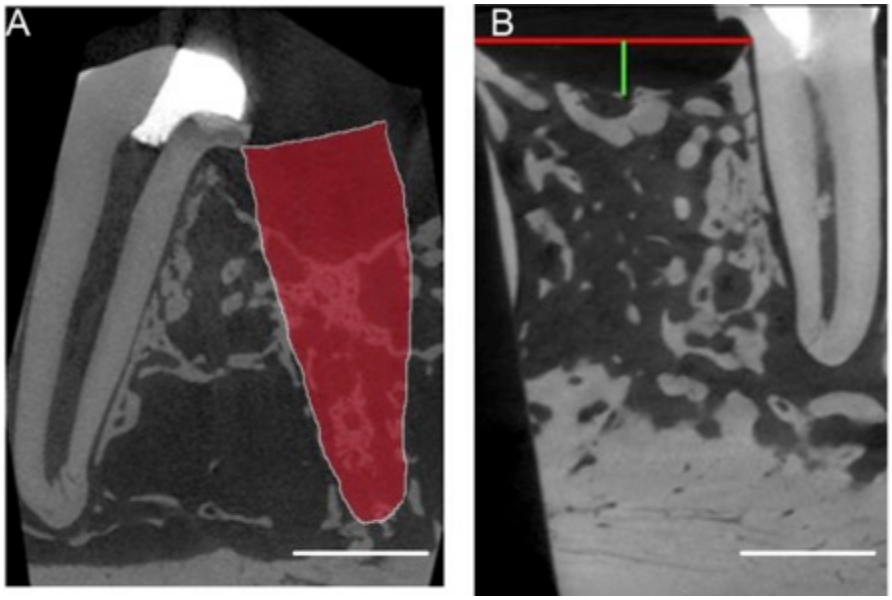

Figure 12 Schematic of bone volume and bone height determination from microCT slices of healing socket preservation defects. A) The remaining premolar tooth roots were traced and mirrored onto the defect area from which bone volume regenerated was calculated (red shaded area). B) The intercrestal plane was measured from the alveolar bone ridges (red line) and bone height was measured from the middle of the defect area (green line).

3.2.4 Histology

Following micro-CT, un-decalcified samples were embedded in Technovit 9100 New plastic according to manufacturer's protocol (Heraeus Kulzer, Hanau, Germany). Following polymerization, plastic blocks were trimmed and 5um serial sections were obtained using a microtome and tape transfer technique (Leica RM2255, Leica, Buffalo Grove, IL) with tungsten-carbide blade.

3.2.4.1 Goldner's Trichrome Staining

Goldner's Trichrome staining was performed to examine general tissue morphology and composition of the samples. Staining solutions were obtained from Electron Microscopy Sciences. Sections were deacrylated in xylene and methoxyethylacetate, cleared with a descending ethanol series and then held in distilled water. Sections were incubated with hematoxylin, Ponceau-acid, Orange G-Phospho and Light Green then dehydrated with an ascending series of ethanol prior to mounting with Eurapal mounting medium.

3.2.4.2 Von Kossa Staining

Von Kossa staining was performed to confirm the presence of mineralized tissues observed with micro-CT. Staining was performed based on manufacturer's protocol using solutions from American Master Tech (Von Kossa Stain Kit, Lodi, CA). Sections were deacrylated in xylene and methoxyethylacetate cleared with a descending ethanol series and then held in distilled water until staining commenced. Slides were incubated with 5% aqueous silver nitrate under UV light then incubated with 2% sodium thiosulphate, followed by 1% neutral red. Stained sections were then dehydrated through an ascending ethanol series and xylene prior to mounting with toluene-based mounting medium (Richard Allan Scientific, VWR, Radnor, PA).

3.2.4.3 Chloroacetate Esterase Staining

Chloroacetate esterase staining was performed to detect neutrophils as a marker of inflammation within the samples. Staining was performed based on manufacturer's protocol using solutions from Sigma Aldrich (Naphthol AS-D Chloroacetate Kit). Sections were incubated in a coplin jar containing the staining solution (sodium nitrite, fast red violet LB base, TRIZMAL 6.3 buffer

concentrate, Napthol AS-D chloroacetate, distilled water) and incubated for 30min at 37˚C. Sections were then washed in distilled water and mounted using Fluoromount (Fisher Scientific).

3.2.4.4 Microscopy

Brightfield microscopy was performed with a Nikon TE 2000 microscope (Melville, NY) equipped with a Nikon DS-Fi1 camera. Micrographs were captured and background illumination and white balance corrections were performed using Nikon NIS Elements.

3.3 RESULTS

3.3.1 Implantation of PLGA + 10mg Magnesium into Canine Pre-molar Tooth Sockets Increased the Bone Height Compared to Empty Defects

Surgeries were performed without complications and animals were extensively monitored throughout the entire experimental timeline. No post-operative infections, severe inflammation or gas bubble formations were noted around the surgical sites. All dogs returned to a normal diet and displayed no mastication difficulties and experienced no weight loss post-operatively. Additionally, no abnormal behavior indicative of pain was noted by the veterinary staff.

Defect bone height at 8 weeks post-implant was found to be 1.9mm and 2.2mm (Figure 13E) below the intercrestal plane for the PLGA + 10mg Mg (Figure 13A) and empty defects (Figure 13C), respectively. At 16 weeks post-implant, bone height in both groups had increased compared to the 8 weeks timepoint. The bone height below the intercrestal plane was found to be 0.9mm and 1.6mm for PLGA + 10mg Mg (Figure 13B) and empty defects (Figure 13D),

respectively. Overall, bone height was found to be better preserved by the Mg/PLGA scaffold compared to the empty defect ($p < 0.05$).

Bone volume as a percent of total defect volume at 8 weeks was higher for PLGA + 10mg Mg than empty defects (29% vs. 21%); however, this increase was not statistically different (Figure 13F). Similarly, at 16 weeks, bone volume as a percent of total defect volume was 39% for PLGA + 10mg Mg and 35% for empty defects which was also not a statistically significant difference.

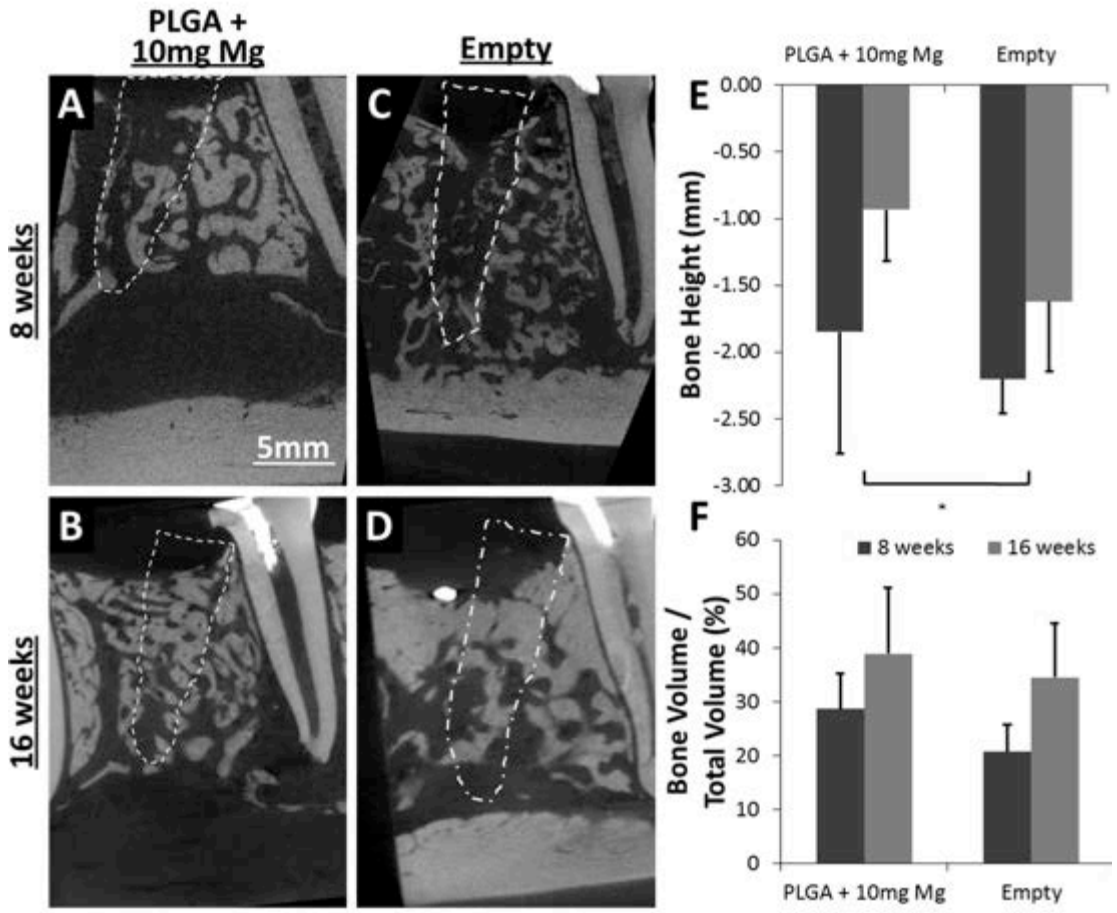

Figure 13 Implantation of PLGA + 10mg Mg scaffolds into canine pre-molar tooth sockets increased the bone height compared to empty defects. 8 week timepoint: A) PLGA + 10mg Mg, C) Empty defect. 16wk timepoint: B) PLGA + 10mg Mg and D) Empty defect. E) The bone height from the center of the defect to the intercrestal plane was measured and found to be significantly increased in the PLGA + 10mg Mg group ($p<0.05$, n=6, ANOVA). F) The remaining root outline was superimposed onto the extracted root defect and bone volume as a percentage of total volume was measured and no significant differences were found.

3.3.2 Histological Analysis of Defects Receiving PLGA + 10mg Mg Implants Confirmed Bone Ingrowth and Showed Typical Tissue Morphology

Goldner's Trichrome staining displayed similar and typical tissue morphologies for PLGA + 10mg Mg (Figure 14A) and empty defects (Figure 14B) at 8 weeks. A porous trabecular bone structure (green) was observed throughout the bone defect extending from the remaining tooth root and the adjacent tooth root. Mineralizing osteoid (purple) was identified in proximity to the mineralized bone. Healthy gingival tissue was observed overlying the bone in all samples; however, gingival soft tissue can be seen invading the bone defect space of the empty defect sample in Figure 14B. The marrow space showed normal morphology and blood vessels were observed. There were no signs of inflammation among any samples. At 16 weeks, a denser bone volume was observed in the defect space and mineralizing osteoid was again identified. All other tissue morphology appeared normal and was similar to the 8 week samples. Finally, no remnants of magnesium particles or PLGA were identified at 8 week or 16 week timepoints.

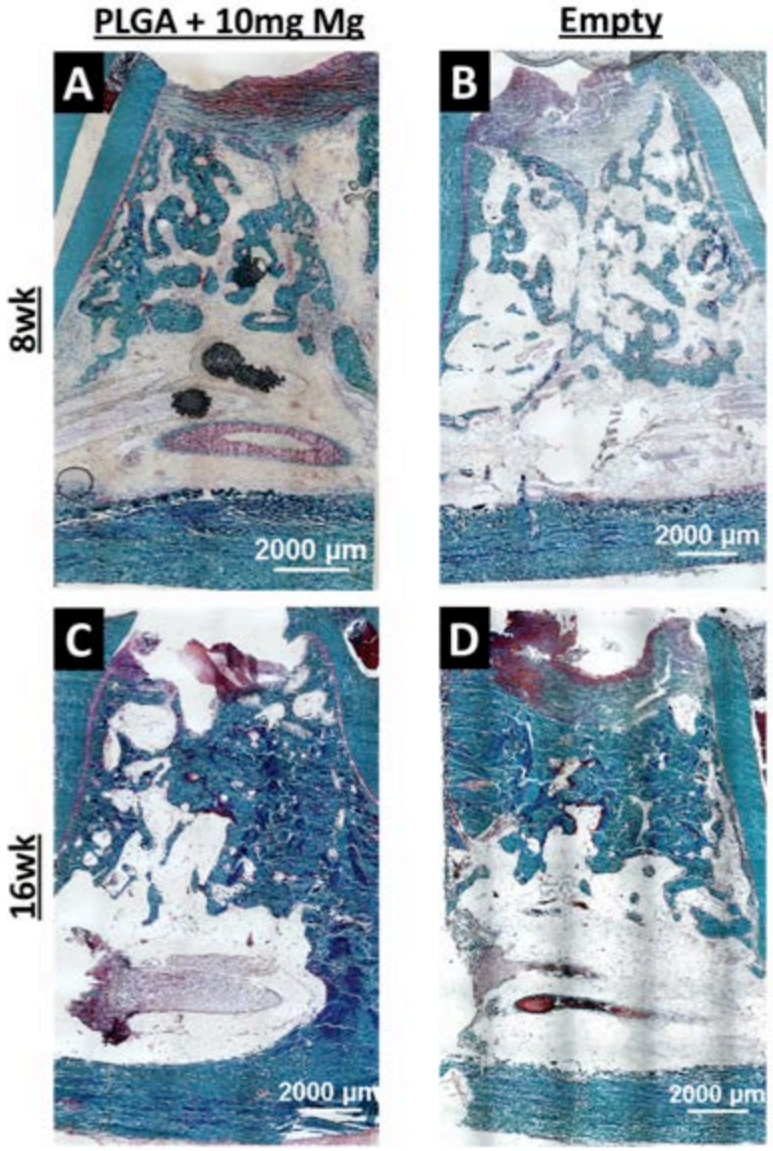

Figure 14 Bone volume in tooth root defect increased among both groups from 8wk to 16wk, but was not significantly different between groups. Goldner's Trichrome staining was performed on 5um plastic sections for the 8wk A) PLGA + 10mg Mg and B) Empty defects, as well as the 16wk C) PLGA + 10mg Mg and D) Empty defects. Green – Mineralized Bone, Purple – Osteoid, Orange – Collagen (n=6).

The Von Kossa staining confirmed the mineralized bone identified with the Goldner's Trichrome staining and micro-CT analysis (Figure 15). A more dense bone volume was observed at 16 weeks for both groups when compared to the 8 weeks timepoint.

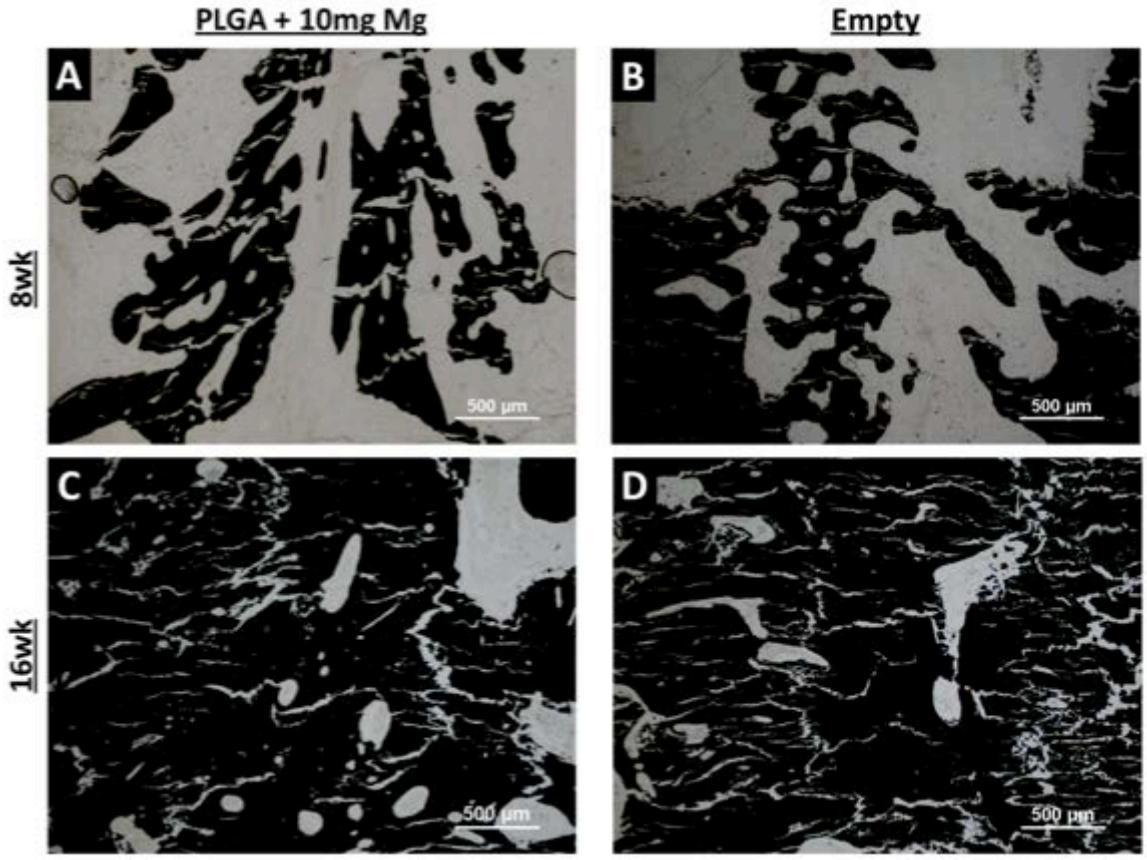

Figure 15 Bone volume in tooth root defect increased among both groups from 8wk to 16wk, but was not significantly different between groups. Von Kossa staining was performed on 5um plastic sections for the 8wk A) PLGA + 10mg Mg and B) Empty defects, as well as the 16wk C) PLGA + 10mg Mg and D) Empty defects. Black – Mineralized Bone, Red/Pink – Nuclei (n=6).

3.3.3 No Significant Chronic Inflammation was Observed in any of the Experimental Groups

Chloroacetate Esterase staining was performed to identify neutrophils, a marker of inflammation. Occasional positively stained cells were identified in the space surrounding mineralized tissue in the bone defect (Figure 16). No significant collections of positive staining were identified in any of the groups at either timepoint.

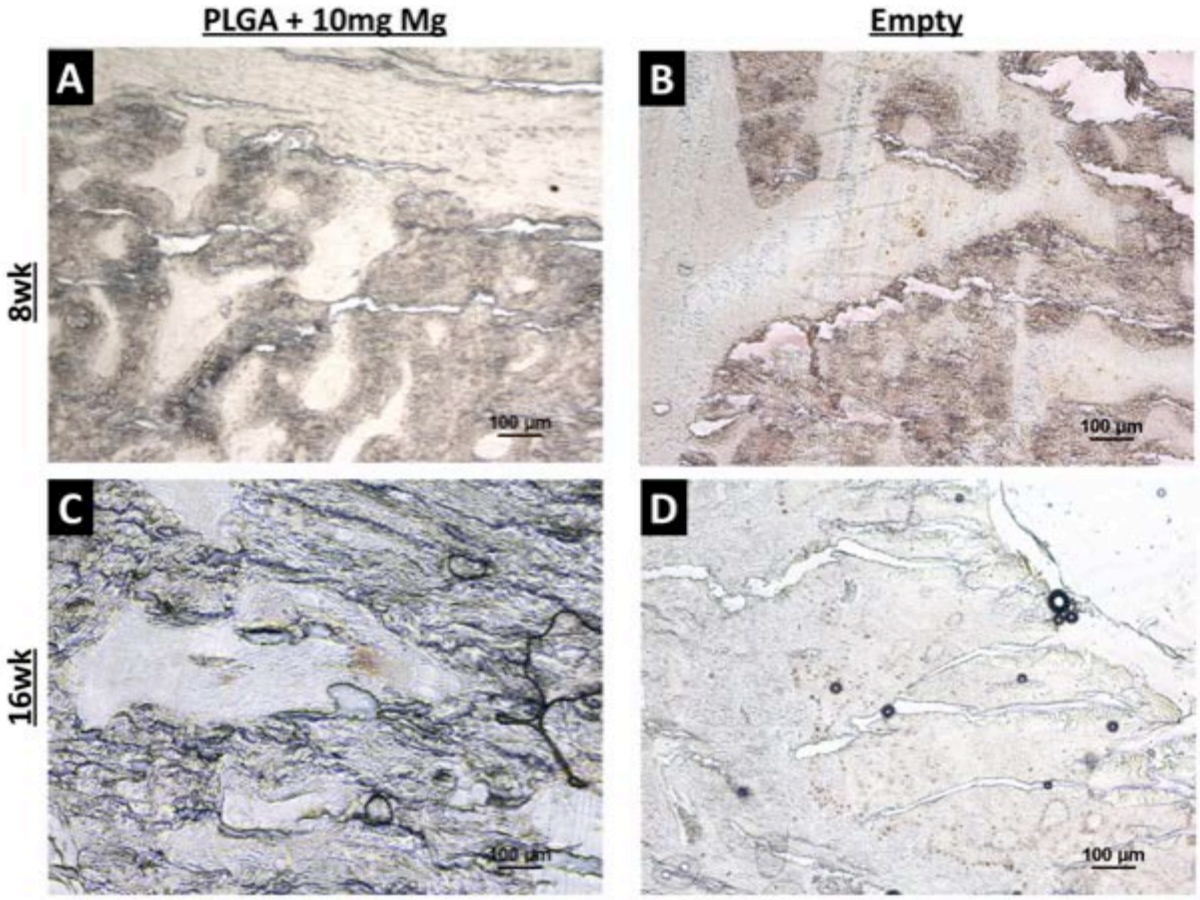

Figure 16 No significant collections of positive staining neutrophils were identified in any of the groups at either timepoint suggesting the absence of chronic inflammatory response. Chloroacetate esterase staining was performed on 5um plastic sections for the 8wk A) PLGA + 10mg Mg and B) Empty defects, as well as the 16wk C) PLGA + 10mg Mg and D) Empty defects. Neutrophils – Brown (n=6).

3.4 DISCUSSION

The objective of this aim was to evaluate the in vivo bone regeneration capabilities of our novel porous Mg/PLGA scaffolds. We believe this is the first reported in vivo evaluation of a magnesium-based dental bone grafting therapy. We successfully performed the socket preservation defect creation and repair surgeries and the Mg/PLGA scaffolds fit within the typical

clinical workflow. Qualitative feedback from our clinicians during the repair surgeries suggests that the current form of our Mg/PLGA scaffolds is suitable for clinically observed socket preservation procedures. No adverse events were observed in the immediate post-operative period nor during the 8 and 16 week healing periods. These observations are promising for the further development of the Mg/PLGA scaffold as a dental bone grafting substitute.

Our hypothesis that Mg/PLGA scaffolds would be safe and effective at regenerating bone was supported through our micro-CT and histological analyses. Defects that were treated with Mg/PLGA scaffolds had an improved bone height preservation compared to empty defects at both 8 and 16 weeks post-surgery. This effect compares well with other bone grafting materials (including polymers) that have been successfully used for socket preservation (124, 142). While the difference was not significant, defects treated with Mg/PLGA exhibited an increased bone volume compared to empty defects. Additional support for the biocompatibility of the Mg/PLGA scaffolds was provided through the lack of inflammation and presence of normal tissue morphology noted in our histological analyses. Overall, our in vivo findings suggest that Mg/PLGA scaffolds could be used to safely and effectively regenerate bone.

Limitations of this study include the lack of a PLGA Only control group and clinical gold standard control group in the in vivo socket preservation experiment. The current in vivo study focused only on establishing safety and effectiveness of the Mg/PLGA scaffold in a bone environment. Future experiments will include both a PLGA Only control group and a gold standard bone graft control group to examine the comparative effectiveness of Mg/PLGA scaffolds. Additionally, the socket preservation model is not a critical-sized defect; thus, we plan to explore the capabilities of Mg/PLGA scaffolds in orthopedic applications using a rabbit ulnae defect model. Our in vivo study was limited to 8 week and 16 week timepoints, well after any early stage

inflammation would have occurred. While the dogs implanted with this material showed no clinical issues post-implant, including the lack of gas pocket formation during our weekly observation, we plan on performing additional experiments with earlier timepoints to assess short-term tissue response to the Mg/PLGA scaffolds.

Finally, the explanted samples from this study will be used for a comprehensive immunohistochemical assessment to further elucidate the biological mechanisms affected by degrading magnesium. Work by Chaya, et. al., suggests that magnesium induces bone formation surrounding magnesium implants where there was previously not bone present (76, 148). Several other groups have found increased bone depositions and osteogenic gene and protein expression surrounding magnesium devices compared to polymeric devices (59, 60, 62, 149). These studies suggest that periosteal cells may play a major role in bone regeneration observed around degrading magnesium devices in vivo. In the future we will use these explants to assess the interface between the degrading Mg/PLGA scaffolds and the periosteum. These samples could be used to support the in vitro investigation in discussed in Specific Aim 3 by assessing in vivo the genes and proteins identified as being activated in vitro. The conclusions of this study strengthened the overall hypothesis of this thesis that a magnesium/PLGA composite guided bone regeneration platform would yield improved clinical utility over currently used devices.

3.5 CONCLUSIONS

Specific Aim 2 of this thesis established the first in vivo evidence of Mg/PLGA composites' ability to regenerate bone in a clinically relevant model. Combined with the in vitro evaluations presented in Specific Aim 1, this study was presented at the 6th Symposium on Biodegradable Metals in

Maratea, Italy (150). This work encouraged us to pursue the development of a Mg/PLGA barrier membrane and micromesh as the next pieces in our guided bone regeneration platform. Given our success at regenerating bone in a low-risk socket preservation model, we were also encouraged to explore bone regeneration capabilities in more severe bone defects. These next steps are presented in Specific Aim 4.

The in vivo findings in this specific aim, as well as increasing interest from industry, supporting converting our provisional patent application to a PCT (151). Several entrepreneurial resources within the University of Pittsburgh where engaged following the completion of the specific aim to help support additional research.

3.6 ACKNOWLEDGEMENTS

This study was supported by NSF Revolutionizing Metallic Biomaterials Engineering Research Center under grant number 0812348. The authors wish to extend their gratitude to Andrew Glowacki and Dr. Steven Little for their assistance with scaffold synthesis, as well as Dr. Michael Epperly for gamma sterilization of the scaffolds. Samer Zaky and Herbert Ray performed the defect creation and repair surgeries and provided clinical feedback on the use of the devices. The University of Pittsburgh's Division of Live Animal Research and Surgical Research aided in the execution of the animal study. We thank Kostas Verdellis for performing the microCT scanning and post-processing of the explanted samples. Finally, Nicole Myers, Andressa Pen and Sabrina Noorani were instrumental in obtaining the histological data presented in this study and their hard work is greatly appreciated.

4.0 SPECIFIC AIM 3: EVALUATE THE OSTEOGENIC, ANGIOGENIC AND INFLAMMATORY GENE EXPRESSION PROFILE OF HBMSCS EXPOSED TO MAGNESIUM

Following evaluation of our Mg/PLGA composite bone graft scaffold in both in vitro and in vivo environments, we set forth on evaluating potential biological mechanisms to explain the enhanced bone regeneration we observed. As part of this research's broader context within the Revolutionizing Metallic Biomaterials Engineering Research, we evaluated the impact of common alloying elements on cell proliferation to help better inform alloy design. However, we focused specifically on magnesium due to the cost and time necessary to examine gene and protein pathways comprehensively. Ideally, specific concentration ranges of magnesium could be identified that maximize osteogenic pathway activation and these findings could be incorporated into design criteria. While such a goal is likely not to be reached in the near future, we aimed to contribute to the growing body of evidence supporting not only magnesium's osteogenic enhancing effects, but its biocompatibility in support of future regulatory applications. Portions of this work were presented in several conference posters and compiled into a manuscript: Yoshizawa S, Brown A, Barchowsky A, Sfeir C. Magnesium ion stimulation of bone marrow stromal cells enhances osteogenic activity, simulating the effect of magnesium alloy degradation. *Acta Biomaterialia* 10(6): 2384-42, 2014.

4.1 INTRODUCTION

Every year, more than 6.2 million cases of bone fracture are reported with 56% of fractures in adults requiring internal fixation with biomedical devices such as plates and screws (152, 153). Bone fixation devices are most commonly made of non-degradable metallic alloys, such as titanium and stainless steel. Drawbacks to these traditional orthopedic alloys include stress shielding due to the mismatch in mechanical properties between the metal and the bone (154), as well as a need for secondary surgery to remove the fixation devices in some cases. Degradable polymers (e.g. poly-lactic-co-glycolic acid (PLGA), poly-L-lactic acid (PLLA), and poly-ethylene glycol (PEG)) have been employed in order to avoid the secondary removal surgery; however, their compressive strengths are not ideal for load bearing fracture repair cases (155) and foreign body reactions to the polymers have been reported (156-158). In order to address these issues, magnesium (Mg) alloys have been studied as a candidate material for bone fixation devices due to their bone-like mechanical properties, enhanced osteoconductivity when compared to polymers and ability to safely degrade *in vivo* (154).

Mg alloys were first used for biomedical applications over 200 years ago; however, their development has accelerated in the last ten years due to advances in alloy manufacturing and processing methods (50). Numerous research groups have synthesized a wide range of magnesium alloys and characterized their microstructure, corrosion properties, mechanical properties, *in vitro* cytotoxicity and *in vivo* biocompatibility. *In vivo* Mg alloy studies have involved implantation of rods into rabbit tibiae (159), ulnae (160) and femora (54, 56), rat femora (161) and guinea pig femora (73, 162). These *in vivo* studies found through micro-computed tomography, mechanical testing and histology analysis that the magnesium alloys safely degrade and allow osseointegration at the site of implantation. Additionally, comparisons of Mg alloy rods to polymer rods found that

mineralization was increased surrounding the Mg samples (162). Mg^{2+} concentrations were found to be increased in bone tissue immediately surrounding degrading Mg alloys *in vivo* (163). This finding suggests that the mechanisms underlying enhanced bone regeneration observed *in vivo* can be recapitulated using Mg^{2+} salts *in vitro*.

Most *in vitro* studies of Mg alloys have focused on cell viability and proliferation to assess cytocompatibility. Previous studies used MTT and WST-1 assays to show that Mg alloys are cytocompatible with primary human mesenchymal stem cells (160), bone derived cells (72), mouse fibroblasts (51, 56), MG-63 human osteosarcoma cells (72, 164), RAW264.7 macrophages (72) and MC3T3-E1 osteoblasts (51, 165). In addition, von Kossa and alkaline phosphatase stains were utilized to examine the effect of magnesium alloys on U2OS human osteosarcoma cell mineralization and osteogenic differentiation (74). Furthermore, immunohistochemistry and flow cytometry were employed to study the mechanisms of cell adhesion on biomaterials when stimulated by Mg (166). Overall, these in vivo studies have shown Mg-based devices to be promising for bone fracture fixation and *in vitro* studies have shown enhancement of standard osteogenic markers in bone cells. However, to the best of our knowledge, this report is the first identification of specific intracellular signaling pathways through which Mg enhances bone regeneration.

We hypothesized that treating human bone marrow stromal cells (hBMSCs) with $MgSO_4$, resulting in increased exposure of the cells to Mg^{2+}, would enhance osteogenic gene expression, matrix production and mineral deposition. We cultured hBMSCs with a large range of magnesium concentrations then used the proliferation findings to identify three concentrations of magnesium to expose hBMSCs to for more in-depth biological studies. We cultured hBMSCs with these various concentrations of $MgSO_4$, either with or without osteogenic factors. These treated cells

were then analyzed for their matrix mineralization, gene expression and protein production in order to elucidate the intracellular signaling pathways involved in bone growth around Mg alloys. In this study, we found that increased $MgSO_4$ enhanced protein expression of collagen type X (COL10A1), vascular endothelial growth factor (VEGF), hypoxia inducible factor (HIF)-1α, HIF-2α, and peroxisome proliferator-activated receptor gamma, coactivator (PGC)-1α in hBMSCs. COL10A1 is abundant in fractured bone at early stages of healing and VEGF is a major angiogenic signaling protein. This work identified specific osteogenic pathways that are affected by Mg. Identification of these pathways and the optimal Mg concentrations to enhance their activity will lead to improved Mg bone fixation device design and other possible therapeutic uses for Mg.

4.2 MATERIALS AND METHODS

4.2.1 Harvest, Expansion and Experimental Culture of Human Bone Marrow Stromal Cells (hBMSCs)

hBMSCs were harvested from surgical waste in accordance with the US NIH regulations governing the use of human subjects under protocol 94-D-0188 or OHRS Assurance No. 4165, and established from colony forming units as previously reported (167), and the osteogenic differentiation capabilities of these cells were confirmed by bone tissue formation following *in vivo* transplantation into immunocompromised mice (courtesy of Dr. Pamela Robey at National Institutes of Health). The cells were plated at 40,000 per cm^2 in Minimum Essential Medium Eagle (MEM) Alpha Modifications (α-MEM) (Life Technologies, Grand Island, NY) containing 20% fetal bovine serum (FBS; Atlanta Biologicals, Lawrenceville, GA), 1% penicillin and streptomycin

(Life Technologies) and 1% L-glutamine (Life Technologies). We used this medium formulation as "expansion medium". Cells were cultured at 37°C in an atmosphere of 5% CO_2. Non-adherent cells were washed away twenty-four hours later. For subculture, hBMSCs were detached with 0.05% of trypsin - EDTA (Life Technologies), and expanded at a 1:3 ratio. Cells were passaged three times, harvested, and then plated for experiments.

hBMSCs were cultured in either maintenance or osteogenic medium throughout experiments. "Maintenance medium" consisted of α-MEM, 5% FBS, 1% penicillin/streptomycin, 1% L-glutamine and a variable amount of $MgSO_4$ (5, 10, and 20 mM for Alizarin red staining assay, 10 and 100 mM for proliferation assay and 10 mM for gene and protein expression analysis) (Sigma Aldrich, St. Louis, MO). α-MEM, as-purchased, contains 0.8 mM of $MgSO_4$ (the 0.8mM concentration of $MgSO_4$ will be considered the control group). Osteogenic differentiation of hBMSCs was induced by culturing in "osteogenic medium" which contained α-MEM, 5% FBS, 1% penicillin/streptomycin, 1% L-glutamine, 50μM ascorbic acid, 100nM dexamethasone, and 10mM β-glycerol phosphate (Sigma-Aldrich, St. Louis, MO). Finally, a "SO_4^{2-} control medium", was formulated in the same manner as the maintenance medium, but with substituted $MgSO_4$ to Na_2SO_4 (Fisher Scientific, Pittsburgh, PA).

4.2.2 Differentiated and Undifferentiated Cell Proliferation Assay – Trypan Blue

$1X10^5$ hBMSCs were plated per well in 6 well plates in expansion medium. After twenty-four hours, the medium was switched to maintenance or osteogenic medium containing 0.8, 10 or 100 mM $MgSO_4$ with 3 biological replicates per group. Cells were detached with 0.05% of Trypsin - EDTA (Life Technologies) at 1, 3, 5 and 7 days, and the number of live cells was counted using a hemocytometer. The dead cells were excluded using the trypan blue stain.

4.2.3 Alizarin Red Staining

hBMSCs were plated in 6 well plates at a density of $1X10^5$ cells per well in expansion medium. Twenty-four hours after plating, the medium was switched to 0.8, 5, 10 or 20 mM $MgSO_4$ osteogenic medium or Na_2SO_4 (SO_4^{2-} control medium) with 3 biological replicates per group and cultured for three weeks. The cells were then fixed in 10% formalin for one hour and washed with PBS. The calcium nodules in extracellular matrix (ECM) were stained with a solution of 1% Alizarin Red (Sigma Aldrich) in 2% ethanol for 5 minutes. Following incubation, the stain was removed and washed repeatedly with ddH_2O. Finally, the amount of Alizarin Red bound to the calcium nodules was quantified by dissolving the stained ECM into 1% cetylpyridinium chloride (CPC) solution and reading the optical density at 540 nm using a plate reader (Spectramax 190, Molecular Devices, Sunnyvale, CA).

4.2.4 Assessment of Gene Expression

4.2.4.1 RNA Extraction and Purification

hBMSCs were plated in 6 well plates at a density of $1X10^5$ cells per well in maintenance or osteogenic medium (0.8 and 10 mM $MgSO_4$) with three biological replicates per group and cultured for three weeks. Total RNA was extracted and purified using RNeasy Mini Kit (Qiagen, Valencia, CA) and treated with RNase-free DNase (Qiagen) to eliminate genomic DNA according to manufacturer's instructions. The quantity and quality of RNA was measured using a Nanodrop spectrophotometer (Thermo Fisher Scientific, Waltham, MA). Total RNA samples were cleaned using RNA Clean & Concentrator™-5 (Zymo Research Corporation, Irvine, CA) until the ratio of absorbance readings at 260nm to 230nm was greater than 1.7, and 260 nm to 280 nm was between

1.8 and 2.0 according to manufacturer's instructions for quantitative PCR (qPCR) arrays (SABiosciences, Frederick, MD).

4.2.4.2 Quantitative PCR Array

500ng of purified RNA from each sample were reverse transcribed to cDNA using RT^2 First Strand Kit (SABiosciences) according to the manufacturer's instructions. qPCR array assays were performed using RT^2 Profiler^{TM} PCR Array: Osteogenesis (SABiosciences) and 7900HT Fast Real-Time PCR System (Applied Biosystems, Carlsbad, CA) according to manufacturers' instructions. Briefly, each experimental cDNA sample was mixed with RT^2 SYBR Green Master Mix and RNase-free water then plated into 96 wells of the 384 well qPCR array. The qPCR array is pre-filled with 4 replicates of 84 different primer/probe sets of osteogenesis related genes, 4 different primer/probe sets of housekeeping genes, one genomic DNA control, three reverse transcription controls and three positive PCR controls. The thermal cycler was set to incubate one time at 95°C for 10 minutes for activation of HotStart DNA *Taq* Polymerase. Amplification of DNA was performed for 40 cycles consisting of 95°C denaturing for 15 seconds and 60°C annealing for 1 minute. The fluorescence intensity for all wells was collected at the end of each cycle. The C_t values were calculated by the first cycle that the fluorescent data of each well was greater than the fixed threshold. Ct values were analyzed by $\Delta\Delta C_t$ method as previously described (168). All C_t values greater than 35 were considered negative calls. C_t values of each sample were normalized with the average C_t values of housekeeping genes (ΔC_t value). The difference of the ΔC_t value between the experimental and control wells was used as the $\Delta\Delta C_t$ value. The fold change between these two wells was calculated as $2^{(-\Delta\Delta CT)}$.

4.2.4.3 Quantitative PCR

mRNA expression of *HIF1A, HIF2A, COL10A1,* and 18S ribosomal RNA was analyzed by TaqMan ABI inventoried gene assays (Applied Biosystems) to confirm the mRNA expression data from qPCR arrays. *VEGFA* (NM_003376) was designed using Prime Express Software from ABI, Version 2.0 (Forward 5'-CATGCAGATTATGCGGATCAA-3', reverse 5'-TTTGTTGTGCTGTAGGAAGCTCAT-3', Taqman probe 5'-CCTCACCAAGGCCAGCACATAGGAGA-3'). Real time PCR reactions were conducted in 7900HT Fast Real-Time PCR system (Applied Biosystems).

4.2.5 Western Blotting

hBMSCs were plated into 6 well plates at a density of $1x10^5$ cells per well and cultured for three weeks in maintenance or osteogenic medium (0.8 and 10 mM $MgSO_4$) with 3 biological replicates per group. Proteins from cultured cells and ECM were extracted using M-PER® Mammalian Protein Extraction Reagent (Thermo Fisher Scientific). The amount of proteins was quantified by colorimetric protein assay using Pierce® 660 nm Protein Assay Reagent (Thermo Fisher Scientific). The protein samples were reduced with sample buffer containing β-mercaptoethanol at 60˚C for 10 min, and SDS-PAGE was performed with a 10% acrylamide gel. The proteins were transferred to polyvinyl difluoride (PVDF) membrane (Bio-Rad, Hercules, CA), and Western blotting was performed using primary antibodies against COL10A1 (C7974), β-actin (A5441) (Sigma-Aldrich), VEGF (NB100-648), HIF-2α (NB100−122), PGC-1α (NBΠ1−04676) (Novus Biologicals, Littleton, CO), and HIF-1α (BD Transduction Laboratories, Franklin Lakes, NJ). The secondary antibodies were HRP conjugated anti-mouse IgG or anti-rabbit IgG (R&D Systems,

Minneapolis, MN) or anti-mouse IgM (Santa Cruz Biotechnology). The blots were developed with the Western Lightning® Plus-ECL (PerkinElmer, Inc., Waltham, MA). The intensity of the bands were measured by ImageJ, and normalized by β-actin.

4.2.6 Statistical Analysis

The graphical presentations of data show the means ± standard deviations. The proliferation assay and Alizarin Red staining data were analyzed using a one-way ANOVA followed by post-hoc t-tests. The p-values from the PCR array were calculated based on Student's t-tests of the replicate $2^{-\Delta Ct}$ values for each gene in the control group and treatment groups. Student's t-tests were also performed to calculate the differences in the optical intensities of specific western blot bands obtained from cells treated with either 0.8 mM or 10 mM $MgSO_4$.

4.3 RESULTS

4.3.1 5 to 10 mM of $MgSO_4$ Induced Higher Cell Proliferation Rate and Extracellular Mineralization.

Cell proliferation rates of hBMSCs were significantly enhanced when grown in medium containing 10 mM of $MgSO_4$ in both maintenance and osteogenic medium (Figure 17), but were inhibited at 100 mM $MgSO_4$. Stronger Alizarin Red staining was observed in the wells treated with 5 and 10 mM of $MgSO_4$ (Figure 18 A and B). In comparison, Na_2SO_4 groups had fewer numbers of nodules, and lighter Alizarin Red staining of the ECM. The quantified optical density

of Alizarin Red dissolved in CPC solution was significantly higher in the 5 and 10 mM $MgSO_4$ groups when compared to Na_2SO_4 control (Figure 18 C).

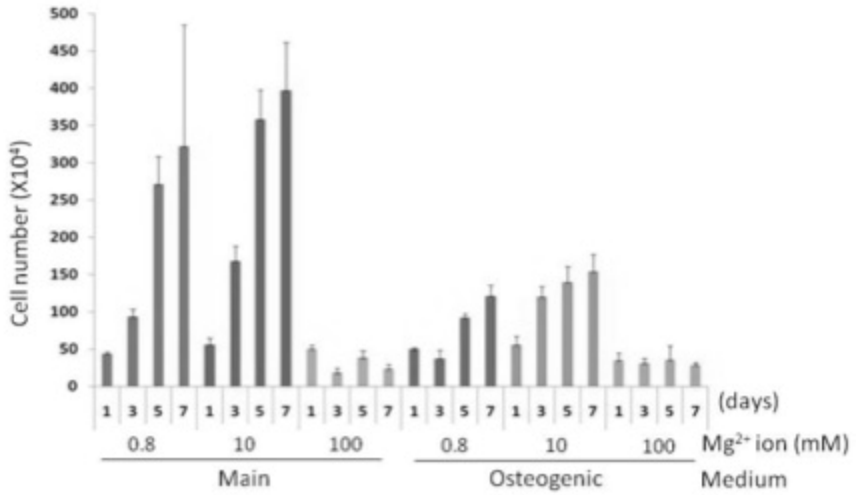

Figure 17 Result of cell count by Trypan blue assay shows proliferation rate of hBMSCs after stimulation with 0.8 mM (original concentration in the culture medium), 10 mM, and 100 mM of $MgSO_4$ contained medium. Statistical significance was observed between all three different concentration of $MgSO_4$ medium at day 3, 5, and 7. (3-way ANOVA; Media type $p<0.001$, MgSO4 concentration: $p<0.001$, Time point: $p<0.001$).

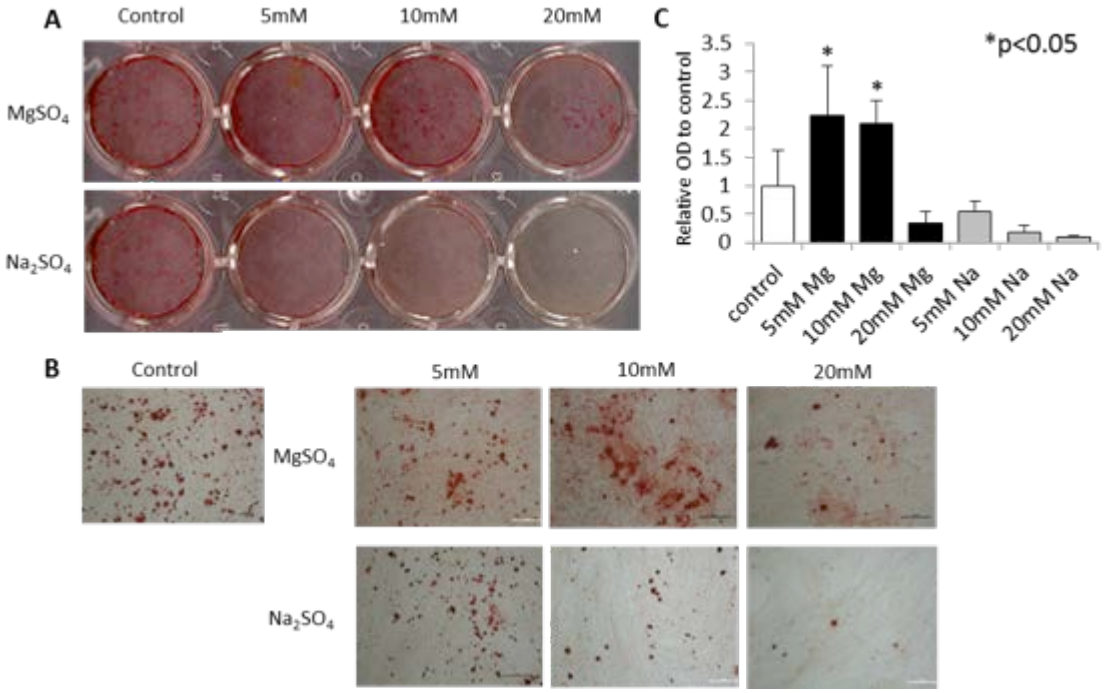

Figure 18 5 and 10 mM of $MgSO_4$ induced higher deposition of mineral into ECM. A. Alizarin red staining of ECM of hBMSCs after 3 weeks of culture in osteogenic medium containing 0.8, 5, 10 and 20mM of $MgSO_4$ or Na_2SO_4. B. 10x images of ECM stained with Alizarin red. Scale bar is 200 μm. C. The amount of Alizarin red was quantified by dissolving into 10% CPC solution. The relative OD at 562 nm to control is shown.

4.3.2 10 mM $MgSO_4$ Enhanced *COL10A1* and *IGF2* Expression and Decreased *ITGA3* Expression

The qPCR array assays yielded 14 out of 81 genes up or downregulated by greater than 2.0 fold when cultured in 10 mM $MgSO_4$ compared to 0.8 MgSO4. The expression levels of all the genes are listed in Supplemental Table 1. Among them, collagen type X (*COL10A1*), insulin like growth factor 2 (*IGF2)*, and integrin α3 (*ITGA3*) showed statistically significant difference of up/downregulation. hBMSCs treated with 10 mM of $MgSO_4$ expressed significantly higher

amounts of *COL10A1* when cultured in both maintenance and osteogenic medium compared to 0.8 mM $MgSO_4$. The expression of *COL10A1* was increased by 2.5 and 4.0 folds, respectively, in maintenance and osteogenic medium (Figure 19A and B). In addition, the expression of *IGF2* was increased by 2.4 fold when cultured in 10 mM $MgSO_4$ maintenance medium compared to 0.8 mM $MgSO_4$ maintenance medium. Furthermore, the expression of *ITGA3* in the osteogenic medium with 10 mM $MgSO_4$ was decreased by 0.42 fold compared to cells cultured in 0.8 mM $MgSO_4$ (Figure 19 A and B). The other genes upregulated in 10 mM MgSO4 were collagen type III (*COL3A1*), matrix metalloprotease (*MMP)*-8, growth differentiation factor-1 (*GDF1*), cartilage oligomeric matrix protein (*COMP*), collagen type XI (*COL11A1*), *MMP2*, cathepsin K (*CTSK*), and Twist-related protein 1 (*TWIST1*) (more than 2.0 fold). The genes downregulated were alkaline phosphatase (*ALPL*), vascular cell-adhesion molecule-1 (*VCAM1*), and collagen type XII (*COL12A1*) (less than 0.5 fold) (Figure 19A and B).

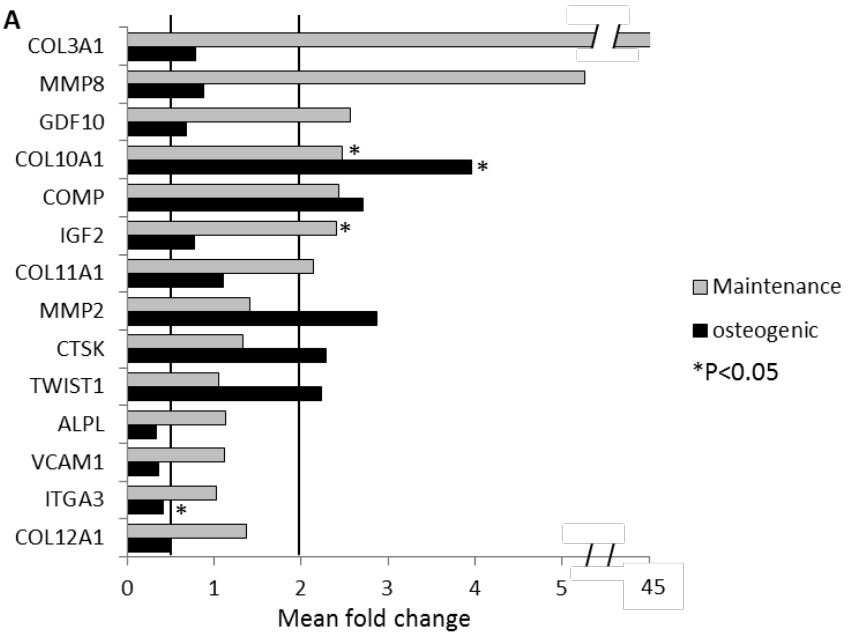

B

10mM / 0.8mM Mg (Main. Medium)

Gene (*P<0.05)	Fold Change	P-value
COL3A1	45.8	0.119
MMP8	5.26	0.145
GDF10	2.56	0.060
COL10A1*	**2.47**	**0.018**
COMP	2.43	0.102
IGF2*	**2.40**	**0.015**
COL11A1	2.14	0.063
COL2A1	1.35	0.061

10mM / 0.8mM Mg (Osteogenic Medium)

Gene (*P<0.05)	Fold Change	P-value
COL10A1*	**3.96**	**0.046**
MMP2	2.87	0.126
COMP	2.72	0.084
CTSK	2.28	0.195
TWIST1	2.23	0.275
ALPL	0.341	0.070
VCAM1	0.356	0.100
ITGA3*	**0.416**	**0.017**
COL12A1	0.476	0.106
COL2A1	1.17	0.271

Figure 19 10 mM Mg ion enhanced COL10A1 and IGF2 expression and decreased ITGA3 expression. hBMSCs were cultured in maintenance or osteogenic medium with 0.8 mM (control) or 10 mM $MgSO_4$ for three weeks. The osteogenic mRNA expression was analyzed by quantitative PCR arrays. The genes listed were fold change >2 or <0.5 and Ct value was <30. COL2A1 data is shown to prove that hBMSCs did not differentiated towards chondrogenic cells. n=3. A) mean fold change of 10 mM Mg ion groups compared to 0.8 mM Mg ion (control) groups, B) mean fold change and p-value.

4.3.3 qPCR Validation of *COL10A1* and *VEGF* and Expression Levels of *HIF2A*

The mRNA expression of *COL10A1* and *VEGF* was confirmed by qPCR showing significantly increased mRNA expression levels in the 10 mM $MgSO_4$ groups in both maintenance (1.3 fold) and osteogenic (2.6 fold) medium when compared to 0.8 mM (Figure 20). However, there was no significant change in VEGF expression by 10 mM $MgSO_4$ (Figure 20). In addition, we examined the *HIF1A* and *HIF2A* mRNA expression, since they were reported as the most potent transcriptional activators of *COL10A1* expression (169). However, we did not observe a change in mRNA expression of *HIF1A* and *HIF2A* in 10 mM $MgSO_4$. As discussed below, upon literature examination (170), it was shown that *HIF1A* and *HIF2A* are modulated at the protein level. Thus, we performed Western blot analysis to determine protein expression levels following the treatment with $MgSO_4$.

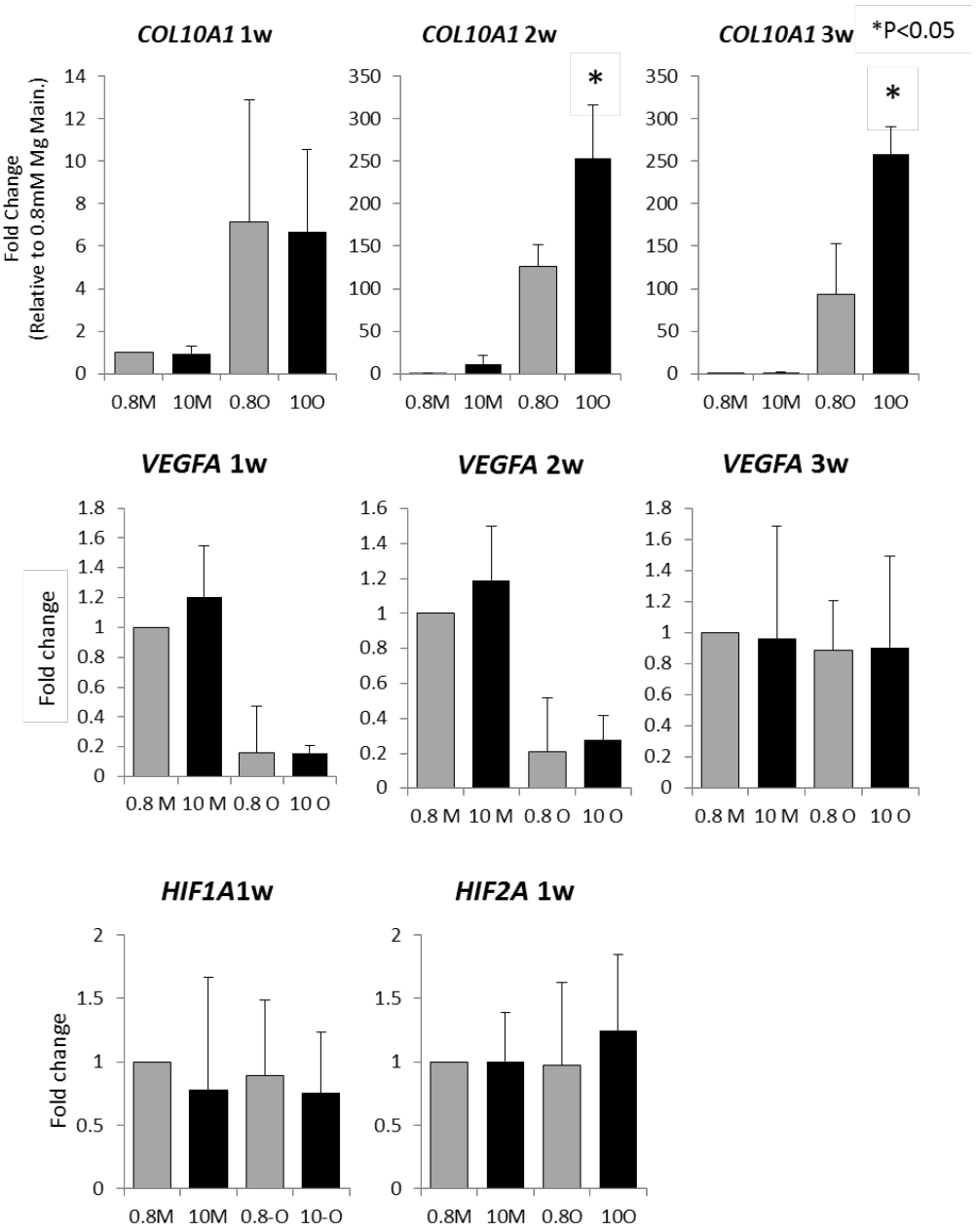

Figure 20 10 mM $MgSO_4$ changed *COL10A1* but not *VEGFA*, *HIF1A* and *HIF2A* mRNA expression. hBMSCs were cultured in maintenance or osteogenic medium with 0.8 mM (control) or 10 mM Mg ion for 1, 2 and 3 weeks. The mRNA expression of *COL10A1*, *VEGFA*, *HIF1A*, and *HIF2A* was analyzed by the quantitative PCR. 0.8 M: 0.8mM $MgSO_4$ contained maintenance medium, 10 M: 10 mM $MgSO_4$ contained maintenance medium, 0.8 O: 0.8mM $MgSO_4$ contained osteogenic medium, 10 O: 10 mM $MgSO_4$ contained osteogenic medium. n=3. *p<0.05 with Student's t-test between two samples indicated with a bar.

4.3.4 10 mM $MgSO_4$ Enhanced COL10A1, VEGF, HIF-1α, HIF-2α, and PGC-1α Protein Expression

The protein expression of hBMSCs cultured in $MgSO_4$ for three weeks was analyzed by Western blotting. Although statistically significant change was observed only in maintenance medium group, expression of COL10A1 was enhanced 1.5 to 1.9 fold in cells cultured with 10 mM $MgSO_4$ in maintenance medium, relative to control (Figure 21A and B), confirming that Mg enhances osteogenic differentiation. VEGF (an important osteogenic factor) expression was also increased by 10 mM $MgSO_4$ under both culture conditions. Since both COL10A1 and VEGF are transcriptionally activated by HIF-1α and HIF-2 α, we examined their protein expression and found that only HIF-2 α levels were increased by 10 mM $MgSO_4$ in maintenance medium, however the increase was not statistically significant (Figure 21A and B). In contrast, protein levels of PGC-1 α, another important transcriptional activator of VEGF, increase in osteogenic medium with 10 mM $MgSO_4$ (Figure 21A and B).

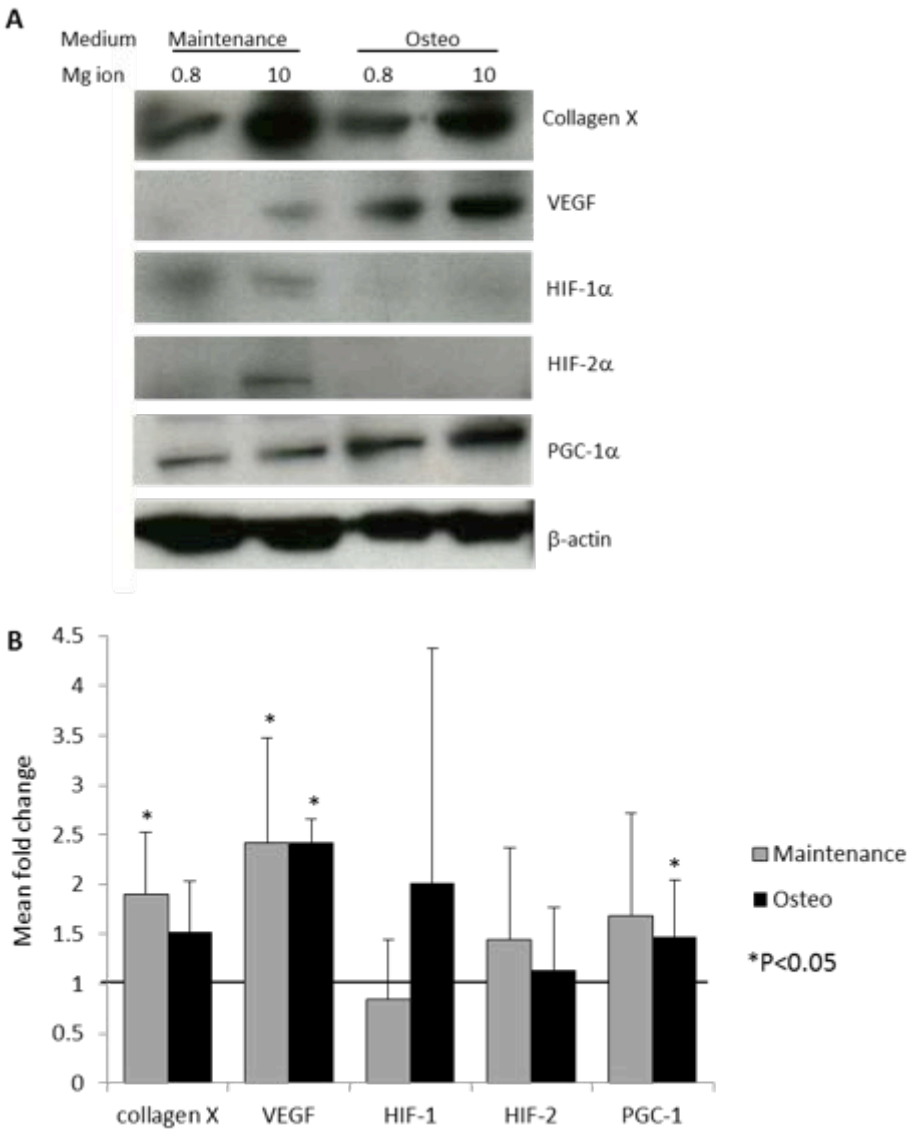

Figure 21 10 mM Mg ion enahnced collagen type X, VEGF, PGC-1α, HIF-1α, and HIF-2α protein expression. hBMSCs were cultured in maintenance or osteogenic medium with 0.8 mM (control) or 10 mM $MgSO_4$ for three weeks. The protein expression level was analyzed by Western blotting, and quantified by ImageJ. Bar graph represent the ratio of expression level of 10 mM MgSO4 samples compared to 0.8 mM MgSO4 samples in the same kind of medium (maintenance or osteogenic). n=3. *p<0.05 with Student's t-test compared to 0.8 mM MgSO4 samples in the same kind of medium (maintenance or osteogenic).

4.4 DISCUSSION

The data show that hBMSCs proliferate faster, and their extracellular matrix mineralized more *in vitro* when 10mM of $MgSO_4$ was added. Using the time points and Mg concentrations of 10 mM that showed the highest Alizarin Red staining, we then performed quantitative PCR arrays to analyze osteogenic gene expression and determined that *COL10A1* (ECM component of healing bone) gene expression was increased in both undifferentiated (2.5 fold) and osteogenic-differentiated (4.0 fold) human bone marrow stromal cells. The data obtained in these studies support the hypothesis that increasing Mg^{2+} enhances hBMSCs, osteogenic gene expression, matrix production, and mineral deposition.

In this study, hBMSCs proliferated 1.2 times more in 10 mM $MgSO_4$ medium, relative to medium with 0.8 mM $MgSO_4$. This finding is consistent with a previous report that the proliferation rate of human articular chondrocytes (73), and microvascular endothelial cells (171) was enhanced at 5 to 10 mM of $MgSO_4$. The proliferation is inhibited at higher concentration (>20 mM) of MgSO4 in this study. We speculate that this is because of the cytotoxicity of Mg ion, as various kinds of metal ion (Na, Cr, Mo, Al, Ta, Co, Ni, Fe, Cu, Mn, and V) are reported to have cytotoxic effects on osteoblasts at certain concentrations as well (172). As shown in the Alizarin Red staining data, 10 mM $MgSO_4$ stimulation resulted in the largest increase in ECM mineralization compared to control medium. Previous reports have shown the addition of 5 to 10 mM $MgSO_4$ to tissue culture medium enhanced glycosaminoglycan production, and redifferentiation (upregulation of collagen type I and melanoma inhibitory activity: MIA) of human articular chondrocytes (73). These findings are consistent with our data showing that 5 to 10mM of $MgSO_4$ were the most effective concentrations for stimulating ECM mineralization. In addition, Liu, et. al. have also shown increased alkaline phosphatase activity in MG63 when Mg

doped hydroxyapatite cement (173) was added. Furthermore, Mg^{2+} containing fluoridated hydroxyapatite (HA) coating also enhanced osteocalcin expression in MG63 cells (174). These results support our findings of osteogenic marker enhancement by $MgSO_4$ stimulation.

Summarizing our qPCR array data, chondrogenesis of hBMSCs by $MgSO_4$ stimulation was suggested because the upregulated genes included chondrocyte markers, such as *COL3A1*, *COL10A1*, *COL11A1* (175), and *COMP* (176). However, since the mRNA expression of collagen type II (*COL2A1*) was not significantly increased (data not shown), and mineral nodule formation was observed, we speculate that hBMSCs might have not differentiated to chondrocyte at this time point. Moreover, it is reported that the *COL2A1* expression is upregulated in human mesenchymal stem cells 10 - 21 days after cultured in chondrogenic condition (177), which indicates that hBMSCs in $MgSO_4$ containing medium did not differentiate into chondrocyte due to lack of *COL2A1* upregulation. Moreover, upregulation of *MMP2* suggests the enhancement of cell migration through ECM (178).

Other genes upregulated by $MgSO_4$ stimulation are *IGF2* (insulin-like growth factor 2), *GDF10* (growth differentiation factor 10), *CTSK*, and *TWIST1*. IGF2 plays an important role in the growth of long bone, and upregulation of this gene may indicate that osteoblasts stimulated with Mg ion may promote bone growth by secreting IGF2. *GDF10* (also known as BMP-3b) is reported to be associated with osteogenic differentiation of primary osteogenic cells (179) and is also suggested to increase the osteogenic inducing activity of BMP-2 (180). Cathepsin K is known as a osteoclast enzyme and is reported to accelerate trabecular bone turnover (181). Twist1 is essential for osteoblast differentiation, but overexpression may inhibit osteogenesis (182). These changes may explain the enhanced osteogenesis of hBMSCs when stimulated with $MgSO_4$. *VEGFA* expression did not change significantly in qPCR arrays (Fig 3) or confirmatory qPCR,

including at earlier time points. On the other hand, some genes were downregulated (0.34 to 0.48 fold) when assessed by qPCR. Integrin alpha 3 (*ITGA3*) expression is significantly decreased in the osteogenic medium. ITGA3 is reported to be an important receptor for osteoblast to bind to Protein kinase C-binding protein NELL1 (osteoinductive protein) in ECM (183). Decreased expression of ITGA3 may indicate enhanced migration of cells rather than adhesion, which could explain the enhanced bone regeneration in surrounding tissue of the Mg alloys in previous report(162). *VCAM1*, related to osteoclast activity, is upregulated via NFκB (184) and its expression was suppressed in the present study. This may indicate the de-activation of osteoclastic activity.

Since *COL10A1* gene expression was significantly increased in both maintenance and osteogenic medium, the intracellular signaling pathway related to *COL10A1* upregulation was further investigated in this study. The Western blotting results indicate the different pathways of COL10A1 and VEGF expression under $MgSO_4$ stimulation depending on the differentiation status of hBMSCs. In the maintenance medium, 10mM MgSO may have increased COL10A1 and VEGF levels by increasing the stability of HIF-2α protein. On the other hand, the production of HIF-2α was very low in the osteogenic medium; thus, the increase in PGC-1α expression in osteogenic medium may have contributed to increased transcription of *COL10A1* and *VEGF*.

Our data showing the mechanisms involved in Mg^{2+} signaling are schematically represented in (Figure 22). HIF-1α and HIF-2α are transcription factors that are known to be stabilized in the cytosol under hypoxia (185) and in response to various metals (186, 187) activate genes including VEGF and glycolytic genes. They are important transcription factors for bone development and regeneration (188, 189), as well as for inducing tissue remodeling (VEGF) and metabolic genes (e.g. glycolytic). Potier, et. al. reported that hypoxia induced osteogenic

differentiation and angiogenic factor expression in human mesenchymal stem cells (190), and Grayson, et. al. reported that hypoxia induced proliferation and ECM production in mesenchymal stem cells (191). In fact, nickel and cobalt are known to enhance HIF expression (186), however, to the best of our knowledge, this is the first report of upregulation of HIFs by Mg^{2+}. Since Mg deficiency causes loss of response to hypoxia in paraganglion cells (192), it may be related to the regulation of reactive oxygen species (ROS) response by Mg^{2+} intake via Ca^{2+} channels. PGC-1α is a HIF-independent transcriptional coactivator of VEGF (193) and is also known to regulate chondrogenesis in human mesenchymal stem cells (194). However, the activation of PGC-1α by Mg^{2+} has not been reported. PGC-1α expression is increased in response to Ca^{2+} activation of a calcineurin/calmodulin signaling complex (195). Mg^{2+} also binds to calcineurin (196) and thus may act through a similar activation cascade to induce PGC-1α in hBMSC in osteogenic medium via activation of specific transcription factor (Figure 22).

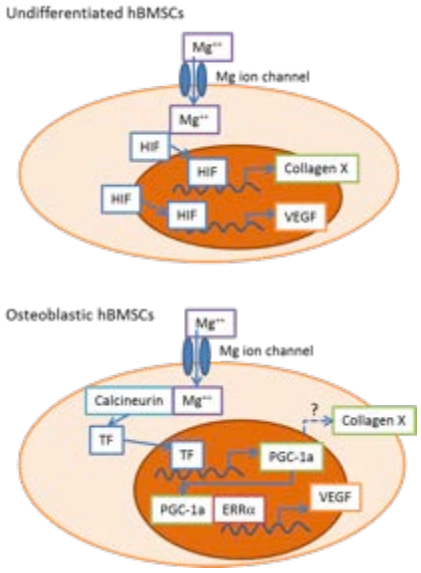

Figure 22 Hypothetical scheme of different intracellular signaling cascades via Mg ion stimulation in hBMSCs. We hypothesized that 10 mM $MgSO_4$ cause an increase of concentration of intracellular Mg ion. And in undifferentiated BMSCs, HIFs are translocated into nucleus, and induce production of COL10A1 and VEGF. On the other hand, in the osteoblastic BMSCs, the Mg ion activate transcription factor (TF), which activate PGC-1α production, and PGC-1α induce production of VEGF.

To our best knowledge, this is the first report to show a possible Mg^{2+} stimulated intracellular signaling pathway in hBMSCs that may lead to the enhanced ECM mineralization observed *in vitro* and the enhanced bone regeneration observed *in vivo* (162). Our findings, supported by those in the literature, suggest that an adequate concentration of Mg^{2+} should be maintained in healing bone tissue by adjusting the corrosion rate of Mg-based bone fixation devices. Also, the excessive deposition of COL10A1 by Mg^{2+} could be applied to treating defective bone diseases such as Schmid type metaphyseal chondrodysplasia, osteogenesis imperfecta and osteoarthritis.

4.5 CONCLUSIONS

Completion of this aim laid the groundwork for much of our research group's ongoing investigation into the biological effects of degrading magnesium. The findings of this research will support our device development efforts as they add to the body of evidence suggesting degrading magnesium is biocompatible. However, equal investigation should be performed on the alloying elements of magnesium incorporated into future medical devices. One of the limitations to the approach we used in this aim is the wide net that must be cast to investigate any and all pathways affected by magnesium. This approach is neither time nor cost-effective in the long run and requires a more targeted approach. Observations of bone regeneration phenomenon surrounding magnesium in vivo can better shape hypotheses for more mechanistic investigation in vitro. For example, work by our group showing new bone formation above magnesium plates and screws and underlying the periosteum suggests that magnesium may be affecting genes and proteins expressed more predominantly in periosteal cells. More focused hypotheses will be necessary in the future to continue the generation of high-impact biological findings that can better inform device design.

4.6 ACKNOWLEDGEMENTS

This study is supported by NSF Revolutionizing Metallic Biomaterials Engineering Research Center under grant number 0812348. We thank Dr. Pamela Robey for providing the human bone marrow stromal cells. The work of Sayuri Yoshizawa who performed much of the gene and protein

experiments is greatly appreciated. Additionally, Aaron Barchowsky provided help in drawing conclusions from preliminary data and helping to guide our experimental approach,

5.0 SPECIFIC AIM 4: SYNTHESIZE AND PERFORM A PROOF-OF-CONCEPT IN VIVO IMPLANTATION OF A COMPLETE MAGNESIUM-BASED GUIDED BONE REGENERATION PLATFORM

5.1 INTRODUCTION

Following the successes of the Mg/PLGA bone graft substitute at regenerating bone in the socket preservation model, we aimed to develop new magnesium-based dental bone graft devices to produce a full guided bone regeneration platform. The two most obvious candidates for new devices were a barrier membrane and a magnesium micromesh on which a barrier membrane of a clinician's choice could be placed. Additionally, we also planned to investigate the utility of a magnesium tenting screw serving as a bone grafting material, as is sometimes performed with titanium devices. These sorts of materials are most commonly used in more severe bone grafting settings which required development of a new surgical model. The goal of this study was not to comprehensively evaluate the magnesium/PLGA barrier membrane, magnesium micromesh and magnesium tenting screws in the same manner as the magnesium/PLGA bone graft substitutes. Rather, the goal was prototyping and manufacturing of these materials, followed by a proof-of-concept implantation to confirm bone regeneration capabilities. We believed that a successful proof-of-concept bone regeneration study would provide the preliminary data to secure funding for a large scale in vivo study and strengthen the business case for a magnesium-based guided bone regeneration platform. This work was performed as part of a larger study on degradation control and functionalization of magnesium micromeshes.

5.1.1 Sixty Percent of Patients Require Bone Grafting prior to Dental Implant Placement

Fifty percent of adults in the United States are missing at least one permanent tooth (excluding third molars) with 19% of adults aged 65 and over missing all permanent teeth (4). These teeth are commonly lost following trauma, radiotherapy or cancer resections of underlying bone, as well as poor dental hygiene resulting in tooth decay and periodontal disease. Nine percent of adults in the United States have some form of periodontitis which degrades the alveolar bone around teeth and can lead to loss of teeth in severe cases (4). Implant supported dental prostheses are becoming an increasingly prevalent method for restoring function and aesthetics following tooth loss. Unfortunately, chronic disease states frequently cause the bone resorption that underlies the original tooth loss and continues to occur following tooth loss. The lack of an adequate bony foundation (in terms of both bone quantity and quality) for implant placement results in half of patients requiring bone grafting to maximize the probability of implant survival (1).

The extent of pre-implant bone grafting required is dependent on both the degree of bone resorption that took place prior to grafting, as well as patient-specific anatomical constraints. In cases where bone grafting is performed immediately following tooth extraction, a socket preservation approach can be pursued wherein bone grafting material is placed into the extracted tooth socket and left to regenerate (123, 124, 130, 131, 133, 142). However, in cases where there is a more significant lack of bone suitable for implant placement, vertical ridge augmentation is commonly pursued to increase alveolar bone height (19, 127, 197-199). In these more advanced cases of vertical ridge augmentation, a guided bone regeneration approach is commonly pursued (21, 22, 33, 83, 145, 197, 199). Guided bone regeneration, also referred to as guided tissue regeneration, is also commonly performed in the case of severe periodontal bone loss (20, 21, 25, 33).

5.1.2 Guided Bone Regeneration Approaches Combine Bone Grafting Material and an Occlusive Barrier Membrane to Promote Growth

Guided bone regeneration approaches to vertical ridge augmentation involve the placement of bone grafting material in the region to be regenerated encompassed by an occlusive barrier membrane. The use of an occlusive barrier membrane serves to maintain the bone defect space, thus separating slowly-regenerating osteogenic cells from fast-migrating epithelial gingival cells. Commonly used non-resorbable barrier membranes are ePTFE, Ti-reinforced ePTFE and Ti mesh which provide excellent defect space maintenance, but require a removal surgery following bone regeneration (130, 197, 200). These non-degradable barrier membranes carry up to a 5% risk of membrane exposure (up to 44% risk in canine models) requiring early removal, thus jeopardizing full bone regeneration. Degradable barrier membranes, such as PLGA, allogenic dermal matrix or xenogenic collagen, reduce the exposure risk and eliminate the need for a removal surgery, but do not provide sufficient defect space preservation (25, 26, 29, 83) (Table 2). In cases where a degradable barrier membrane is used, the underlying bone graft provides a limited degree of mechanical support.

Several animal studies and clinical studies have been performed to assess the utility of implanting titanium tenting screws or titanium dental implants as a means to tent the overlying barrier membrane and provide additional mechanical integrity to the healing defect site (201-210). While the use of these tenting devices was shown to encourage vertical ridge height regeneration, in the case of titanium screws, they must be removed during re-entry for implant placement. Thus, a guided bone regeneration therapy that provides mechanical strength sufficient for protecting the healing defect site while remaining fully degradable would be highly desirable.

5.1.3 Vertical Ridge Augmentation is Challenging to Obtain and Requires Long Healing Times

As the volume of bone desired to be regenerated increases, more aggressive bone grafting techniques are required which result in longer healing times, increased probability of revision surgeries and decreasing likelihood of success. Patients requiring significant regeneration of vertical ridge height often require approximately a year of healing in order to regenerate up to only 5mm of bone height (198). This is additional time spent with impeded masticatory function and, frequently, poor aesthetic appearance. More significant pre-existing bone loss, female gender, more advanced age, tobacco use and exposure to radiotherapy can contribute to longer bone regeneration times and lower likelihood of bone grafting success. While numerous bone grafting technologies and approaches exist to enhance the speed and probability of success of vertical ridge augmentation there remains substantial room for improvement.

5.1.4 Vertical Ridge Augmentation Animal Models are Expensive and Time Consuming

There are numerous animal models used for dental bone regeneration biomaterial evaluation reported in the literature. These dental bone regeneration studies are often cost and time intensive due to the lengthy healing periods required for large bone defect repairs. The most common animals used for these surgical models is the beagle or mongrel dog (200, 211-215) with some studies reported in rabbits (216, 217). The canine animal model permits the creation of defects on the scale of those observed in humans and allows the repair to be performed using the same scale materials and the same surgical techniques used in humans. The rabbit animal model typically

requires smaller defect creation and scaling down of biomaterials and repair procedures compared to those used in humans.

Vertical ridge augmentation models are commonly pursued in the canine with both defect creation and surgical repair occurring in various manners. The most common model involves the extraction of bilateral mandibular premolars, often with extraction of molars as well, followed by 8-12 weeks of healing time prior to a defect size standardization and repair surgery (211-215). In most cases, the maxillary premolars are either extracted or amputated at the crowns and capped to prevent trauma to the now edentulous mandible. This model most accurately represents the bone resorption processes that occur in humans and allows for highly standardized defects to be created. However, the initial tooth extraction surgery and additional 8-12 weeks of housing and animal care substantially increase the cost of the study. Several studies have further simulated the human disease process by creating periodontal disease prior to the tooth extraction and repair procedures (218, 219).

Other groups have developed surgical models to perform repair procedures in the same surgery as defect creation (220, 221). While this approach reduces the cost and time associated with the experiment, defect standardization is often limited by anatomical differences between animals and between different defect sites within an animal. Common among all of these approaches though are the experimental approaches to assessing bone regeneration following the explantation of defects. All studies performed radiographic or microCT analyses of common bone measurements to provide clinically relevant outcome measures. Most also perform histological, and occasionally histomorphometric, analyses to provide more insight into device/treatment biocompatibility and biological process surrounding the bone regeneration. The choice of each

animal model, surgical model and endpoint assessments is entirely dependent on the aims of each individual study.

5.1.5 Degradable Magnesium Devices have been shown to Enhance Bone Formation

Metallic magnesium has recently emerged as an attractive material for developing orthopedic and craniomaxillofacial devices. Magnesium exhibits strength and density similar to that of bone while remaining fully degradable when exposed to body fluid. Thus, magnesium and magnesium alloys have been manufactured into plates, screws, pins and rods and exhibited excellent biocompatibility when implanted in multiple *in vivo* models (50, 51, 54, 58, 59, 61, 62, 64, 106, 222). Witte, et. al., implanted magnesium alloy rods and PLA rods into rabbit femora and monitored the osteogenic response as the rods degraded. Significantly more bone was regenerated surround the degrading magnesium rods compared to PLA controls (59). Additionally, previous work by our group demonstrated that magnesium plates and screws successfully fixated a rabbit ulnae fracture throughout a 16wk healing duration. In addition to fixating the fracture, we observed bone formation above and around the fixation plates and screws were bone had not previously existed (76, 148). This led us to investigate potential applications for magnesium's osteogenic properties in a dental defect.

As discussed in Brown, et. al., our group synthesized novel a porous Mg/PLGA composite bone graft scaffold. This composite enabled us to harness the versatility of PLGA and the osteogenic enhancement imparted by degrading magnesium. Our characterization of these Mg/PLGA scaffolds showed that they increased proliferation of bone marrow stromal cells *in vitro* and increased bone height regenerated in a canine socket preservation model (223). These findings from our group and others in the field suggest that metallic magnesium holds promise for not only

the manufacturing of degradable devices, but for imparting enhanced osteogenic activity around regenerating bone defects.

5.1.6 Could Magnesium's Osteoconductive Capabilities be Harnessed in a Novel Guided Bone Regeneration Therapy?

We hypothesized that metallic magnesium could be incorporated into devices for two GBR therapeutic approaches and that the magnesium-based GBR approach would show enhanced bone volume and bone height regenerated compared to titanium and allograft standard-of-care. To our knowledge, this is the first investigation of the manufacture and implantation of magnesium GBR devices.

Our objectives were to first modify a standard canine vertical ridge saddle defect model to allow for faster and less resource intensive evaluation of GBR devices. Then, we aimed to show that magnesium screws, micromeshes and Mg/PLGA membranes could be successfully manufactured and implanted *in vivo* using standard clinical techniques. Using the magnesium screws as tenting devices covered by Mg/PLGA barrier membranes or micromeshes, we aimed to evaluate the osteogenic response upon implantation in a canine vertical ridge augmentation model. Finally, evaluation of the explanted canine mandibles using microCT and histological techniques was performed to answer questions regarding bone regeneration, device degradation and biocompatibility to better guide device design and manufacturing as we prepare for a large scale in vivo study.

5.2 MATERIALS AND METHODS

5.2.1 GBR Materials Synthesized and Obtained for Implantation

Three types of magnesium GBR devices were manufactured for implantation in the vertical ridge augmentation model using commercially available stock material and customized manufacturing methods. These novel materials were compared to commercially available titanium micromesh and fixation screws with human allograft as described in detail below (Table 6).

Table 6 Experimental and control GBR groups and their associated materials.

	Mg Barrier Membrane	Mg Mesh	Standard of Care
Grafting Material	Mg Tenting Screws	Mg Tenting Screws	Human Allograft
Barrier Material	Mg/PLGA Barrier Membrane	Mg Micromesh	Ti Micromesh

5.2.1.1 Synthesis of Magnesium / PLGA Barrier Membranes

Magnesium/PLGA barrier membranes were synthesized using a three layer solvent casting approach (224, 225). This approach followed a similar strategy and was aimed to provide a similar device to the Mg/PLGA bone graft scaffolds described in Specific Aim 1 of this thesis (223). PLGA (50:50, M_w 7,000-17,000, Sigma Aldrich) was dissolved into dichloromethane (DCM, Sigma Aldrich) at a concentration of 20% (w/v) and briefly sonicated at room temperature. 600ul of the PLGA/DCM mixture was then added to a custom Teflon mold (30mm x 20mm x 1mm) at 4degC and the DCM was allowed to evaporate for 2h. A second layer was synthesized by adding

40mg of pure metallic magnesium particles (>99% purity, <300um particle size, Sigma Aldrich, St. Louis, MO) into the PLGA/DCM mixture and then pipetting the 600ul Mg/PLGA/DCM mixture on top of the 1st PLGA/DCM layer. An additional 2h was allowed for DCM evaporation at 4degC. Finally, a 3rd layer of PLGA was added to the mold in the same manner as layer 1. The final Mg/PLGA membrane was left at 4degC overnight to allow controlled DCM evaporation, thus minimizing bubble formation. The membranes were then removed from the molds and left in a fume hood to continue to dry for 72h (Figure 23A).

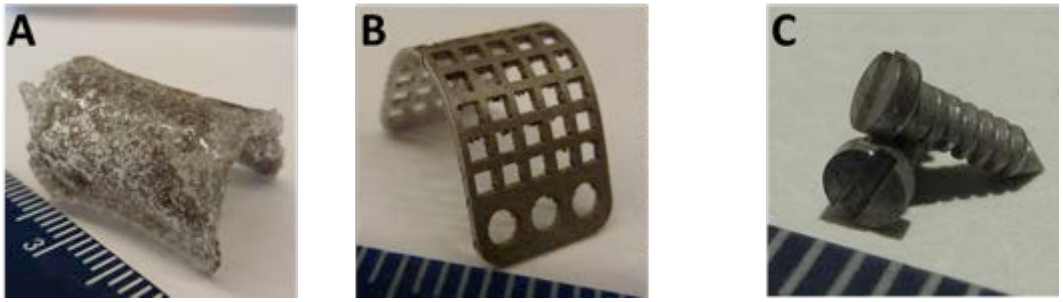

Figure 23 Experimental magnesium materials evaluated in a canine vertical ridge augmentation model. A) Mg/PLGA barrier membrane synthesized using solvent casting. B) Magnesium micromesh manufactured using laser cutting. C) Magnesium screws for periosteal tenting and mesh fixation manufacturing using CNC machining.

5.2.1.2 Manufacturing of Magnesium Micromeshes

Magnesium meshes were manufactured from commercially available magnesium foil stock subjected to laser cutting to obtain a customized design. Custom mesh geometries were designed in SOLIDWORKS (Waltham, MA) to emulate commercially available titanium micromeshes, provide geometric consistency with defects created in the *in* vivo study and optimize screw fixation. Magnesium foil (99.9% purity, 0.5mm thickness, Goodfellow, Coraopolis, PA) was laser

cut to the specified designs using a 150W laser (Kern HSE, Kern Laser Systems, Wadena, MN) at the Swanson Center for Product Innovation at the University of Pittsburgh. Magnesium meshes were deburred, polished with 1200 grit silicon carbide abrasive discs and etched in a glycerol, nitric acid, acetic acid solution for 60 seconds to provide uniform corrosion layers (Figure 23B). Meshes were then heat treated at 200degC for 1h in an argon furnace to allow for strain relief.

5.2.1.3 Manufacturing of Magnesium Tenting and Mesh Fixation Screws

Magnesium screws were manufactured from commercially available magnesium rod stock subjected to computerized numerical control machining. Screw geometries were designed in SOLIDWORKS to emulate commercially available titanium microfixation screws. The same design was used for the tenting and mesh fixation screws. Magnesium rods (99.9% purity, 3.2mm diameter, Goodfellow) were machined at the Swanson Center for Product Innovation at the University of Pittsburgh and then alkyl treated to provide uniform corrosion layers as discussed above (Figure 23C). Screws were then heat treated at 200degC for 1h in an argon furnace to allow for strain relief.

5.2.1.4 Procurement of Clinical Standard-of-Care Materials

Human allograft bone putty (RegenerOss Power Putty, Biomet 3i, Palm Beach Gardens, FL) was used as the clinical standard-of-care grafting material for this study. Titanium micromesh (0.2mm thickness, Stryker, Kalamzaoo, MI) was used as the clinical standard-of-care barrier material and was secured with titanium microfixation screws (1.2mm diameter, 3mm length, Stryker).

5.2.2 Surgical Implantation, Animal Care and Euthanasia

5.2.2.1 Surgical Study Design and Preparation

Magnesium meshes and screws, along with the Mg/PLGA barrier membranes were sterilized using gamma irradiation with a dose of 20,000Gy at a dose rate of 23.5Gy/min (Mark I 68, JL Shepherd and Associates, San Fernando, CA). Titanium micromesh, fixation screws and surgical tools were sterilized using a steam autoclave.

The *in vivo* study protocol was approved by the Institutional Animal Care and Use Committee at the University of Pittsburgh. Defects were created and repairs were performed in a split mouth design in the left or right mandibular second (P2) or fourth (P4) premolar region in three female beagle dogs aged 12 months old (Marshall BioResources USA).

5.2.2.2 Surgical Procedure

Dogs were sedated with acepromazine and placed in ventral recumbency under isofluorane anesthesia. The skin surrounding the muzzle was prepped with betadine and sterile techniques were used throughout the surgery. The gingival tissue and underlying periosteum were released following the creation of an incision from behind the first molar (M1) to in front of the second premolar. The second (P2) and fourth (P4) premolars were then extracted (Figure 24A). A reciprocating saw was then used to remove the remaining intercrestal bone and create a normalized defect 10mm in mesiodistal length, 8mm in height and the full lingual/buccal thickness (Figure 24B). For the magnesium experimental groups, pilot holes were predrilled into the remaining alveolar bone and 2 tenting screws were placed (Figure 24C). The tenting screws were then covered with either a magnesium mesh tucked into the lingual gingival flap and secured on the

buccal alveolar bone with 2 magnesium screws, or were covered with a Mg/PLGA membrane that was sutured into place with 4-0 Vicryl sutures (Figure 24D).

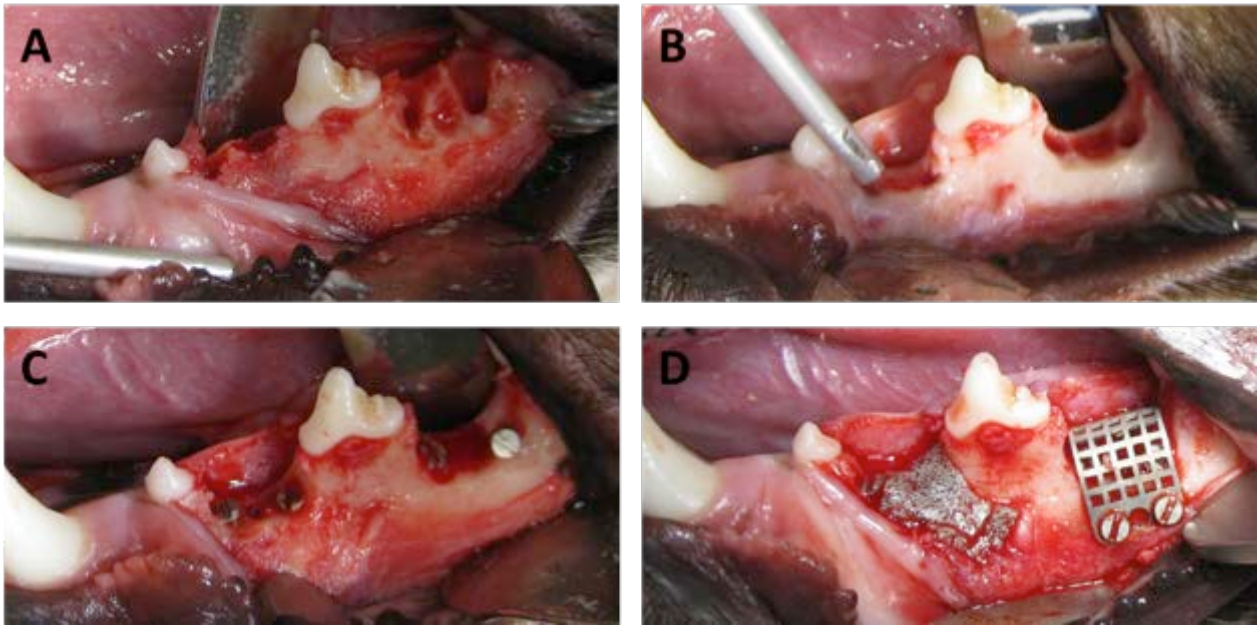

Figure 24 Proof of concept implantation of Mg/PLGA barrier membranes and Mg meshes with Mg tenting screws was performed using a canine vertical ridge augmentation surgical model. A) The second and fourth premolars were extracted and B) the standardized 10mm wide, full-thickness bone defect was created. For the magnesium experimental groups, C) 2 tenting screws were placed and D) were covered with either a magnesium mesh or Mg/PLGA membrane.

5.2.2.3 Post-Surgical Animal Care and Endpoints

Dogs received 0.2mg/kg meloxicam once a day for analgesia and 20mg/kg meloxicam twice a day for 3d post-op for antibacterial therapies. Dogs were allowed standard enrichment, but remained on a soft diet for the entire study period. Euthanasia was performed under sedation with 1ml/4.5kg beuthanasia 12 weeks post-surgical implantation. Photographs were taken of the healed defect sites to assess soft tissue healing. Left and right mandibular segments were explanted and trimmed to

separate the two defect sites on each side. The surrounding soft tissue was dissected and the samples were fixed in formalin for 3d.

5.2.3 Micro-CT Analysis

Prior to implantation, all magnesium meshes and screws were scanned in an *ex vivo* uCT system (Skyscan 1172, Bruker-Skyscan, Belgium) at 6um voxel size, 79kVp source voltage, 125uA source current 800ms exposure, 10 frames averaged per view and 360 degrees angular range of scan. Each device was individually tracked to enable 1:1 comparisons of device volume before and after implantation to provide highly specific degradation measurements. Following pre-implantation microCTs, the raw scans were reconstructed using Recon, reoriented using Dataviewer (Skyscan) and analyzed using CTAn as described below.

Following explantation of mandibular section and prior to scanning, the enamel on the P3 crown was ground off and the 1st premolar and 1st molar crowns were removed to reduce beam hardening artifact. Individual defects were then separated by trimming through the third premolar. The samples were scanned and reconstructed as described above. The post-explantation scans were analyzed using CTAn (Skyscan) following truncation to separate each defect into an individual scan. Post-implant magnesium device volume, defect bone height and defect bone volume were then calculated for each site.

5.2.3.1 Magnesium Device Degradation Measurement

Truncated pre-implantation microCT reconstructions were segmented and binarsed to allow calculation of device volume for each individual magnesium screw and mesh. For post-explantation device volume measurement, reconstructions were reoriented and output as new scans

using DataViewer such that each magnesium fixation screws or the magnesium tenting screws was oriented axially. The screws were manually segmented using circular regions of interest and then binarized using thresholds to capture only the non-corroded volume of the magnesium screws (Figure 25). Device degradation was calculated as the percentage change in device volume from pre-implantation to post-explantation (76).

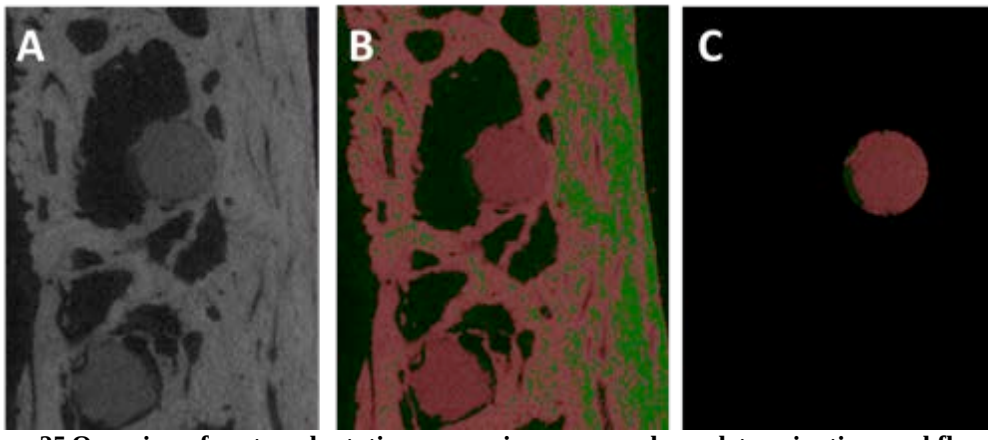

Figure 25 Overview of post-explantation magnesium screw volume determination workflow. Following microCT scanning, reconstruction and truncation, scans were A) reoriented to provide an axial view of each screw. B) Each screw was then defined with a circular region of interest across the full length of the screw and subjected to binarisation to yield C) the non-corroded screw volume absent of surrounding bone volume of similar density.

5.2.3.2 Defect Bone Height Measurements

Bone height in each defect area was computed by first connecting the plane between the alveolar crests mesial and distal to the defect (intercrestal plane) using ImageJ (NIH, Bethesda, MD) (223, 226). Then, the distance between the intercrestal plane and the bone height in the middle (mesiodistal axis) of the defect was measured from the center of the socket defect. Bone height measurements were averaged from 3 different sections for each defect (Figure 26).

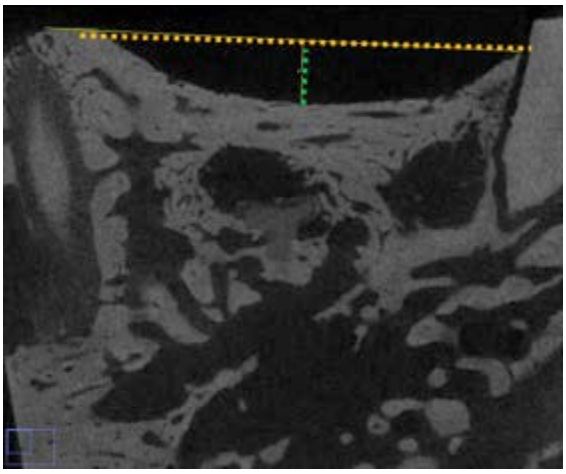

Figure 26 Schematic of bone height determination for a representative magnesium tenting screw sample. Three microCT cross-section images from each defect were imported into ImageJ. A line was drawn between the intercrestal alveolar bone borders next to the two teeth mesial and lateral to the defect (yellow dashed line). Next, a line was drawn from the intercrestal alveolar bone line to the mid-defect bone height (green dash line) and that height was measured and output from ImageJ and averaged amongst the three images from each sample.

5.2.3.3 Defect Bone Volume Measurements

Defect bone volume was calculated by orienting the scans as buccolingual sections. The boundaries of the remaining mesial and distal roots of the teeth on either side of the defect were set as the bounds of the original defect volume to be analyzed across the full buccolingual thickness. Regenerated bone volume calculation was performed using binarisation based on the defined thresholds for scan sections across the entire defect thickness with optimization to exclude remaining magnesium hardware. This calculated bone volume in the defect was then divided by the regenerated total volume of tissue space encapsulated by the outermost bone tissue to compute %BV/TV (Figure 27).

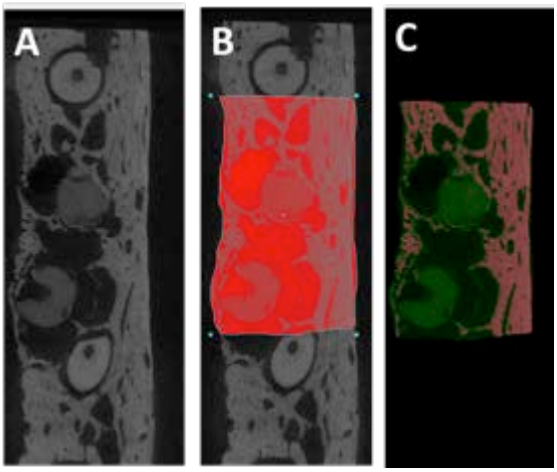

Figure 27 Overview of bone volume determination for a representative magnesium tenting screw sample. A) Cross sections of the microCT scans were taken and B) regions of interests were defined with the mesial and lateral teeth and the full buccal and lingual bone volume defining the borders to the distal root of the two tooth roots. C) The regions of interests were then binarised to threshold both the soft tissue and magnesium devices out of the final bone volume determinations.

5.2.4 Histology

Following micro-CT, un-decalcified samples were dehydrated and embedded in Osteo Bed Plus Bone Embedding solution (Polysciences, Warrington, PA) according to manufacturer's protocol. Following polymerization, plastic blocks were trimmed using a band saw and low speed diamond saw. Serial sections were then obtained at 5um thickness using a microtome with tungsten-carbide blade and tape transfer technique (Leica RM2255, Leica, Buffalo Grove, IL).

5.2.4.1 Goldner's Trichrome Staining

Goldner's Trichrome staining was performed to examine general tissue morphology and composition of the samples. Staining solutions were obtained from Electron Microscopy Sciences.

Sections were deacrylated in xylene and methoxyethylacetate, cleared with a descending ethanol series and then held in distilled water. Sections were incubated with hematoxylin, Ponceau-acid, Orange G-Phospho and Light Green then dehydrated with and ascending series of ethanol prior to mounting with Eurapal mounting medium.

5.2.4.2 Microscopy

Brightfield microscopy was performed with a Nikon TE 2000 microscope (Melville, NY) equipped with a Nikon DS-Fi1 camera. Micrographs were captured and background illumination and white balance corrections were performed using Nikon NIS Elements.

5.3 RESULTS

5.3.1 Magnesium Devices were Successfully Implanted and fit into Standard Clinical Workflow

The Mg/PLGA barrier membrane, Mg micromesh and Mg tenting screws fit into the standard clinical workflow throughout the implantation surgeries. The Mg tenting screws were placed into the remaining alveolar bone following pre-drilling with one failure of a tenting screw, at the runout, during driving. The dimensions of the screw resulted in approximately 3mm of the device remaining above the defect border. The Mg/PLGA barrier membrane could be easily trimmed with scissors, was pliable enough to be custom fit to individual defect borders and retained sutures during implantation and closure. The magnesium micromesh could be easily trimmed with scissors, if necessary due to anatomical constraints, and was pliable enough to be custom fit to

individual defect borders. There was no noticeable micromotion following mesh fixation with the Mg screws. Implantation of devices allowed for full, tension-free closure of the overlying periosteum and gingival tissue.

5.3.2 Magnesium GBR Devices caused no Detectable Adverse Events during 12 week Study Period

Following 12wks of healing post-implantation surgery, no adverse events related to the magnesium device implantation were detected. However, both titanium meshes became increasingly re-exposed throughout the duration of the study; however, no intervention was made. No significant gas bubble formation was noted on gross examination surrounding the magnesium devices as has been reported in other studies. While the titanium meshes became re-exposed, the progression of soft tissue healing surrounding the magnesium-repaired defect sites was unremarkable (Figure 28). There were no signs of infection or dehiscence surrounding the magnesium-repaired defect sites.

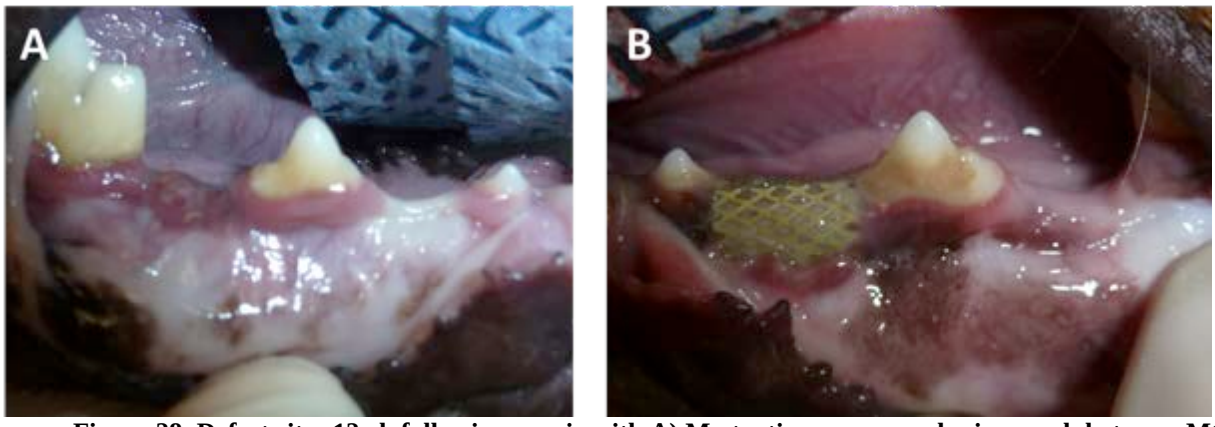

Figure 28. Defect sites 12wk following repair with A) Mg tenting screws and micromesh between M1 and P3, Mg tenting screws with Mg/PLGA barrier membrane between P3 and P1 and B) titanium micromesh with human allograft between P3 and P1.

5.3.3 Magnesium Screw Degradation Successfully Measured

All twelve magnesium screws placed in this study were subjected to pre-implantation microCT scanning. Pre-implantation screw volume was 8.4±0.2mm^3. Following the 12wk study period and explantation, six screws placed in the tenting position were found to have average screw volume of 6.3 ± 0.5mm^3. One tenting screw broke during implantation leaving only the shaft placed in the tenting positions. Another tenting screw volume could not be determined in the post-explantation scans due to a microCT scanning technical error. Four screws placed in the mesh fixation position were found to have average screw volume of 5.0 ± 0.7mm^3. These pre-implant and post-explantation screw volumes translated to 26 ± 5.3% and 41 ± 7.6% device degradation for the tenting and fixation screws, respectively (Figure 29).

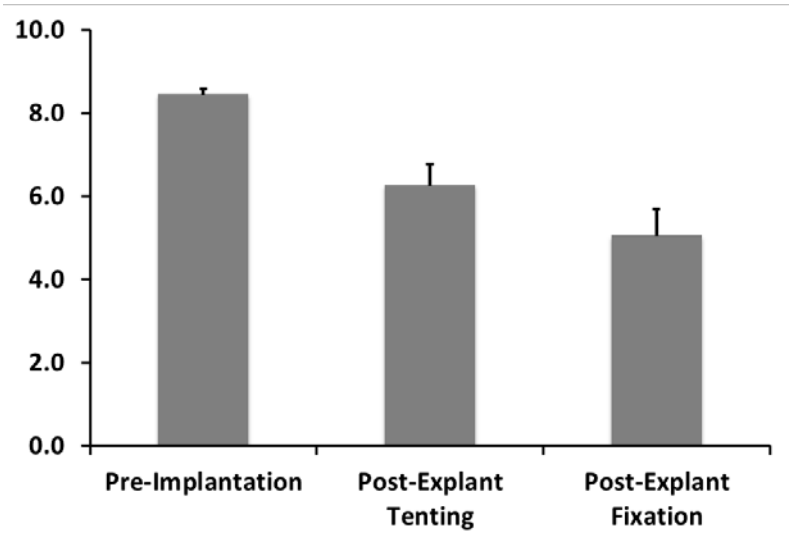

Figure 29 Screw volumes were computed using microCT analysis both before implantation and after implantation. Screws placed as tenting screws (n=6) had 74% volume remaining while mesh fixation screws (n=4) had 59% volume remaining after a 12wk implantation.

5.3.4 Magnesium GBR Groups Exhibited Increased Bone Height Relative to Titanium Mesh and Allograft groups

Bone height was successfully measured for all six defect sites included in this study. Intraobserver reliability of measurements on a single slice was found to be 6.6% RSD while intraobserver reliability of 3 full measurements on one sample was found to be 11.2% RSD. Defect sites receiving Mg tenting screws with Mg/PLGA barrier membranes had bone height 1.5 ± 0.4mm below the intercrestal plane. Mg tenting screws + Mg mesh defects had bone height 2.4 ± 0.1mm below intercrestal plane while human allograft + Ti micromesh defects had bone height 2.6 ± 0.3mm below intercrestal plane (Figure 30).

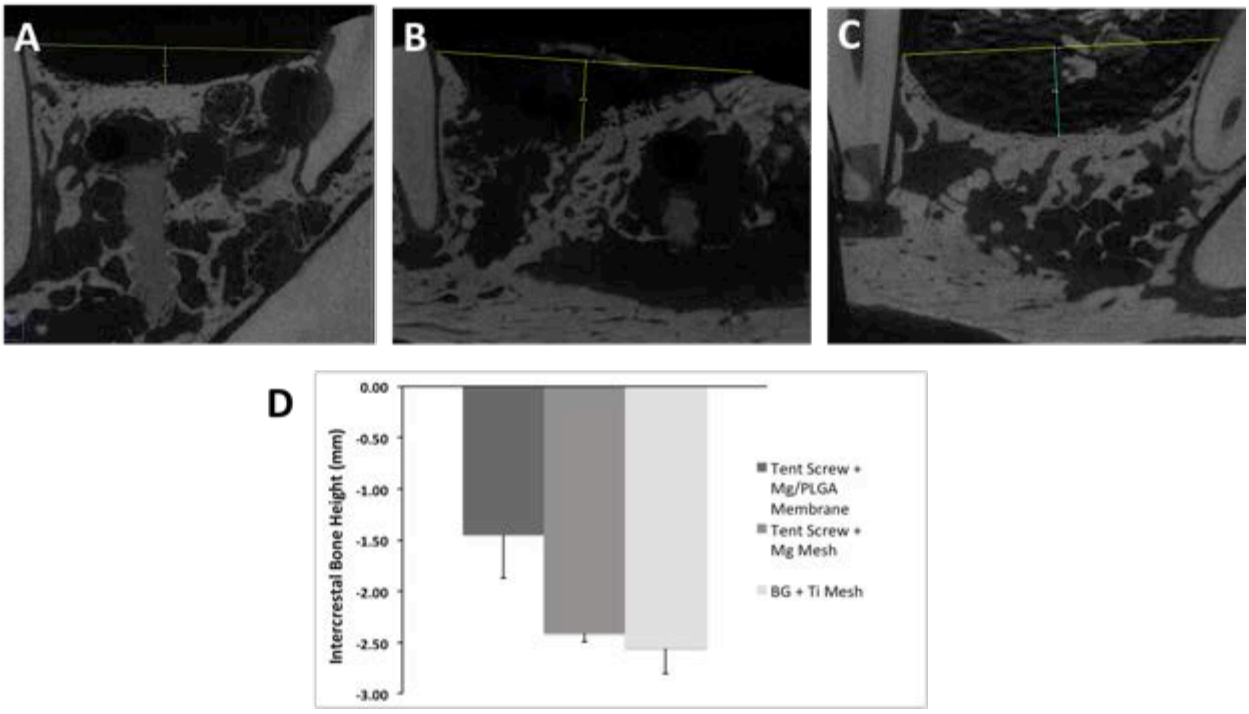

Figure 30 Representative bone heights of a A) Mg tenting screw + Mg/PLGA membrane defect, B) Mg tenting screw + Mg mesh defect, C) human allograft + titanium mesh defect. D) Bone heights were averaged from 2 samples for each group.

5.3.5 Bone Regeneration in Defect Area was Calculated using microCT

Qualitative analysis of the microCTs revealed differences in regenerated bone morphology and device/bone integration within the areas of the defect (Figure 31A-C). Bone was found to be in contact with Mg tenting (*) and fixation screws throughout some areas of interest, while areas of poor bone contact and possible bone resorption were noted in others. Additionally, possible gas bubbles were noted throughout the tissue surrounding the magnesium devices (^). Mg tenting screw + Mg/PLGA membrane samples exhibited bone thickness regeneration across the full buccolingual axis (Figure 31A). Mg tenting screw + Mg mesh samples exhibited greater buccolingual bone thickness regeneration due to bone overgrowth around the Mg mesh () on the lingual side of the defect (Figure 31B). Human allograft + Ti mesh (%) samples showed limited buccolingual thickness regeneration with a significant amount of allograft (white arrows) remaining at 12 weeks (Figure 31C).

Regenerated defect tissue volumes were measured for the Mg tenting screw + Mg/PLGA membrane (n=2), Mg tenting screw + Mg mesh (n=2) and human allograft + Ti mesh groups (n=2) as 198 ± 37, 329 ± 216 and 142 ± 12mm^3, respectively (Figure 31D). Regenerated defect bone volumes within the regenerated defect tissue volumes were determined through thresholding to be 94 ± 16, 85 ± 28 and 82 ± 3mm^3 for the Mg tenting screw + Mg/PLGA membrane, Mg tenting screw + Mg mesh and human allograft + Ti mesh groups, respectively (Figure 31D). These measurements were used to calculate regenerated defect bone volume / tissue volume percent as 47 ± 0.8, 29 ± 11 and 56 ± 3% for Mg tenting screw + Mg/PLGA membrane, Mg tenting screw + Mg mesh and human allograft + Ti mesh groups, respectively (Figure 31).

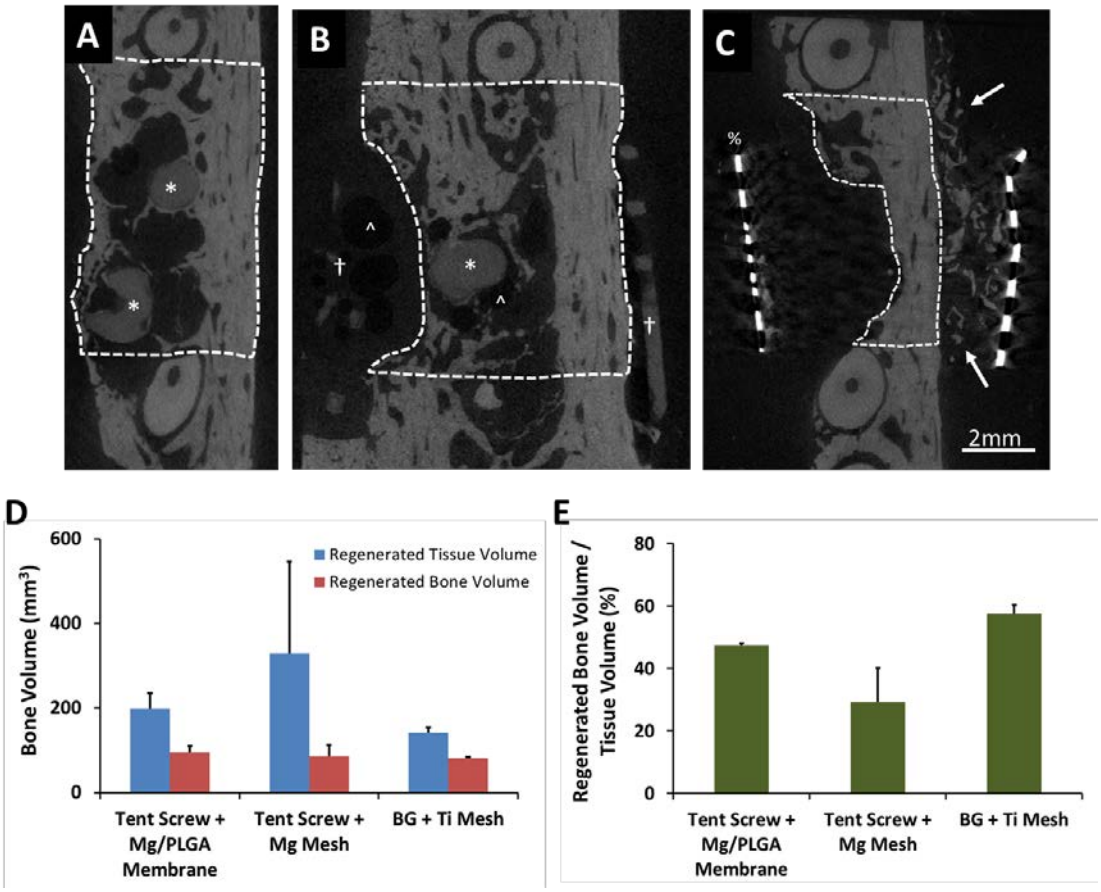

Figure 31 A-C) Regenerated defect tissue volume was identified as the region of interest (dashed white lines) for each sample. The regenerated defect tissue volume was measured from the apical root level to the highest level of intercrestal bone regeneration through the full buccolingual thickness. Also identified are Mg tenting screws (*), Mg mesh (), potential gas bubbles (^), titanium mesh (%) and remaining human allograft (white arrow) D) The regenerated bone volume was identified through thresholding of the region of interest to exclude soft tissue and magnesium devices and E) regenerated defect tissue volume / regenerated defect bone volume was calculated.

5.3.6 Magnesium GBR Groups Exhibited Good Biocompatibility when Examined with Histological Methods

Goldner's trichrome staining of full section explants revealed several differences between our experimental groups beyond microCT findings. Mg tenting screw + Mg/PLGA membrane samples showed new bone formation above the screws with active osteoid still visible. Interestingly, in some areas surrounding the screws no device remnants, bone or soft tissue was visible (Figure 32A,C). Similar results were observed around the Mg tenting screws covered by the Mg micromesh. However, areas around the mesh fixation screws where there previously was bone showed empty spaces with neither active bone resorption nor soft tissue (Figure 32B,E). Finally, histological analysis of the human allograft + Ti micromesh samples revealed active bone resorption in the defect area with substantial accumulations of inflammatory cells. The Ti mesh fixation screw that had been placed in sound alveolar bone was now surrounded entirely in nonmineralized tissue (Figure 32C,F).

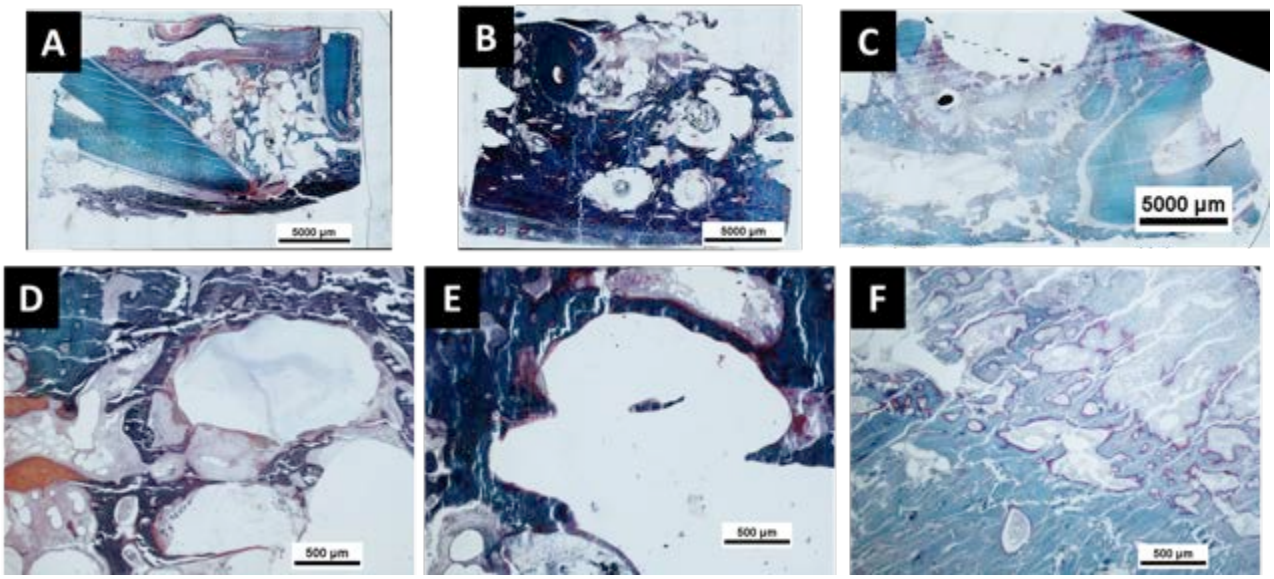

Figure 32 Goldner's trichrome staining of full section explants of A) Mg tenting screw + Mg/PLGA membrane, B) Mg tenting screw + Mg micromesh and C) human allograft + Ti micromesh samples. Higher magnification images were taken within the defect area showing D-E) new bone with active osteoid above Mg tenting screws in both Mg/PLGA membrane and Mg micromesh samples and F) bone resorption processes around human allograft + Ti micromesh samples.

5.4 DISCUSSION

The primary goal of this study was to evaluate the usability and biocompatibility of a Mg tenting screw, Mg/PLGA barrier membrane and Mg micromesh in a proof-of-concept canine vertical ridge augmentation model. We hypothesized that the novel devices would show enhanced bone volume and bone height regenerated compared to standard-of-care controls. We modified a canine vertical ridge saddle defect surgical model to allow defect creation and repair in a single surgery to reduce cost and experimental time. The Mg tenting screw, Mg/PLGA barrier membrane and Mg micromesh all fit into the standard clinical workflow and were successfully implanted with only one failure of a tenting screw during driving. The defect sites receiving Mg-based repairs exhibited

regeneration of bone, as measured with microCT, within the defects and provided better restoration of bone than the human allograft and Ti micromesh defect sites. Finally, histological analyses revealed good biocompatibility for the defect sites receiving Mg-based repairs, while the sites receiving human allograft and Ti micromesh exhibited substantial inflammation due to mesh re-exposure. Overall, we believe these findings support further investigation of the Mg tenting screw, Mg/PLGA barrier membrane and Mg micromesh in a larger scale and experimentally refined animal study.

The novel magnesium bone grafting devices were successfully synthesized using laboratory-scale manufacturing methods. The Mg tenting screws were manufactured to a high degree of precision (2.5% relative standard deviation of screw volume) and successfully implanted with 1 of 12 screws failing during driving. Magnesium alloys could be investigated as alternative materials for these tenting screws to improve mechanical properties and reduce failure during driving (51, 58, 159, 222). However, substitution of an alloy system in place of pure Mg would also alter the degradation rate and potentially the biocompatibility of our devices, requiring additional testing. The Mg/PLGA barrier membranes were successfully synthesized, but will require substantial refinement prior to clinical use. The multi-layer solvent casting method provided sub-optimal homogeneity with respect to Mg particle distribution throughout the membrane. Going forward, advancement of the Mg/PLGA barrier membrane will require new manufacturing methods to improve homogeneity and eliminate the use of chlorinated solvents which could cause toxicity issues. The Mg micromeshes were manufactured using similar process to those used for larger-scale medical mesh fabrication and would require the least refinement prior to clinical use. However, design work will be required to create a geometric pattern amenable to

trimming prior to use to provide defect-specific devices, rather than the one-size-fits-all approach we used for this study.

Our research group successfully performed an alveolar ridge saddle defect creation and repair procedure in a single surgery; however, further refinement of this surgical model is required prior to a larger scale study. We successfully validated the implantation procedures for our devices and found a lack of adverse events associated with their use. However, our standard-of-care control groups (human allograft + Ti micromesh) exhibited mesh re-exposure which likely led to subsequent infection and bone resorption / lack of regeneration. While exposure of meshes and membranes is observed clinically, it prevents appropriate comparisons between our Mg therapies and such control groups (130, 200). More care could be taken to remove sharp edges on the Ti mesh which may lead to soft tissue injury. Additionally, more screws could be used to provide additional fixation and prevent micromotion which could lead to bone resorption and mesh migration. Another limitation of this surgical model was the difficulty to standardize defect geometries due to the presence of the third premolar and anatomical difference between the bony defect site previously holding the second and fourth premolars. This could be improved by removing all premolars and allowing a healing period similar to other surgical models; however, differences in buccolingual thickness and alveolar bone height are likely to remain as confounding factors in geometrical defect standardization (200, 211-215).

Device degradation was successfully measured for the magnesium tenting screws and mesh fixation screws. There was a difference in degradation between the two different screw positions (26% volume lost for tenting screws vs. 41% volume lost for fixation screws). This may have been due to differences in the microenvironments the screws were placed in or could have been related to differences in device loading patterns. These data compare well with results published by Chaya,

et. al., which measured approximately 30% volume loss of pure Mg screws in a rabbit ulnae fracture model following 8 weeks of implantation (76). Henderson, et. al. measured volume loss of 70% following 12 weeks of implantation of pure Mg screws in a mandibular implantation model (222). These differences in degradation rates are also likely heavily dependent on the tissue environments where the magnesium devices are implanted. Magnesium micromesh degradation measurements could not be performed using standard microCT methodologies due to the complex and non-continuous geometry of the device. Alternative methods of measurement are currently under investigation.

Bone height measurements were performed to identify the intercrestal bone height deficit in the defect region as this is a common clinical measurement. The Mg tenting screw + Mg/PLGA barrier membrane group was found to have regenerated the most bone height with Mg tenting screw + Mg micromesh and human allograft + Ti micromesh groups having similar bone height regenerated. New bone was identified superior to the Mg tenting screws which is similar to observations around other implanted magnesium screws (76, 148). Bone height measurements were limited by the lack of definition of the original defect boundaries. The measurements are currently performed using the remaining intercrestal alveolar bone as the landmark for standardization. However, this intercrestal alveolar bone at the borders of the defect could resorb or regenerate as well, thus skewing bone height measurements. The more relevant measurement would be bone height regenerated, i.e. the height of new bone as measured from the apical defect border. In future studies we will pursue methods of defining the lower defect border through implantation of radiopaque markers.

Bone volume regeneration in the defect area was calculated and revealed a number of differences between the three experimental groups other than those obvious through bone height

measurements alone. Mg tenting screw + Mg micromesh samples had a larger defect tissue volume regenerated due to increased buccolingual thickness regenerated and bone overgrowth around the micromesh. This bone overgrowth, where bone had not previously been found, has been reported by others (76, 148). However, because this overgrowth left large areas of soft tissue encapsulated by bone, this group's regenerated bone volume was not larger than the other two experimental groups. Human allograft + titanium micromesh samples had a lower regenerated total volume due to a lower bone height and buccolingual width regenerated. No difference was measured in regenerated bone volume among the three groups surprisingly. This could be due to differences in anatomy at the defect sites and difficulty standardizing defect size, as previously discussed. Improved methods of defect border identification will be required for higher fidelity analysis of bone volume regenerated. Additional work is planned to better define the defect borders and newly regenerated bone through the use of toluidine blue staining and polarized light microscopy (227). A histomorphometric approach to determining bone volume regeneration may yield stronger support of bone regeneration enhancement. Potential gas bubbles were identified around the Mg devices which may have prevented additional bone regeneration and osseointegration of the Mg tenting screws throughout their full length. Immunohistochemical methods will be performed in the future to identify possible mechanisms underlying the variability in device/bone integration.

Histological assessment confirmed the overall positive osteogenic response to the implanted magnesium devices. New bone was identified surrounding the Mg micromesh and superior to the Mg tenting screws. Active osteoid was identified throughout these magnesium samples as well, suggesting that bone regeneration and remodeling was ongoing. Significant inflammatory tissue was visible throughout the human allograft + titanium micromesh samples which likely severely comprised the bone regeneration process. Bone resorption surrounding the

titanium mesh fixation screws was also noted. Further work is planned on evaluating the response to the implanted devices through tartrate resistant acid phosphatase (TRAP) staining. This procedure will enable comparison of bone formation vs. resorption around the degrading devices and could shed light on the mechanisms of osseointegration variability observed. Chloroacetate esterase staining will also be performed to assess inflammation surrounding the implanted devices. This comprehensive histological assessment will strengthen the body of evidence regarding magnesium's biocompatibility.

5.5 CONCLUSIONS

Completion of this aim demonstrated that Mg-based GBR devices could be successfully manufactured and implanted. Our primary objective was to perform this study to better guide device design, manufacturing and evaluation going forward. This objective was met. The Mg tenting screw concept, as well as the Mg/PLGA barrier membrane and Mg micromesh performed in a manner that deserves further development and evaluation. Unfortunately, endpoint assessments revealed several shortcomings in our proof-of-concept surgical model that impeded our ability to draw less descriptive and more quantitative conclusions from our data. Research on regulatory processes for these GBR devices revealed that a vertical ridge augmentation model is the most likely surgical model to be performed for approval or clearance of these devices. Thus, future efforts will be directed towards improving this surgical model for further use by our research group. Our finding of new bone growth around degrading magnesium devices where it did not previously exist supports our research group's consistent findings of enhanced osteoconductivity around magnesium. An improved vertical ridge augmentation surgical model could allow more

mechanistic biological investigations, using immunohistochemical techniques, into the potential role of the periosteum in this phenomenon. This study was successful in confirming the utility of these novel devices, but much work remains to validate their clinical and commercial potential and understand the observed variability in device osseointegration and bone regeneration.

5.6 ACKNOWLEDGEMENTS

The contributions of Avinash Patil and Elia Beniash surrounding study design, magnesium mesh polishing and alkyl treatment steps are greatly appreciated. J. Andrew Holmes of the Swanson Center for Product Innovation and Haoyuan Mu and Brian Webler of the Department of Materials Science at Carnegie Mellon University assisted with magnesium mesh and screw manufacturing and processing. Michael Epperly of the University of Pittsburgh Cancer Institute kindly provided gamma sterilization of our implanted devices. Andrew Glowacki and Steven Little provided assistance with Mg/PLGA membrane synthesis. The University of Pittsburgh's Division of Live Animal Research and Surgical Research provided husbandry care and excellent surgical support services. Christian Moore, James Omlie, Herbert Ray Jr. and Qahtan Al-Qahtani performed the surgeries with the guidance of BJ Costello and Samer Zaky. Kostas Verdelis and Rong Chong were instrumental in obtaining and processing microCT scans. Nicole Myers and Michele Mulkeen are greatly acknowledged for their work on histological assessments. Finally, the funding support of the Center for Medical Innovation, Innovation Institute, Commonwealth of Pennsylvania, McGowan Institute for Regenerative Medicine, Innovation Works and the Revolutionizing Metallic Biomaterials Engineering Research Center is greatly appreciated.

6.0 SUMMARY OF THESIS WORK

The overall goal of this thesis was to design, manufacture and evaluate Mg-based guided bone regeneration devices and to expand our knowledge of the biological effects of these Mg devices, (both directly and indirectly) on osteogenesis, angiogenesis and inflammatory processes. Our primary hypothesis was that characterization of a magnesium-based bone grafting platform would demonstrate enhanced osteogenicity over currently used materials. We designed four studies to test this overall hypothesis and work towards meeting our primary objective.

First, we successfully synthesized and performed material characterizations on a Mg/PLGA composite bone graft substitute. We confirmed our hypotheses that these Mg/PLGA bone graft scaffolds could ameliorate the acidic degradation profile observed in PLGA only devices, release magnesium throughout their degradation, increase compressive strength of PLGA only scaffolds and increase cell proliferation in vitro. More in-depth evaluation of the mechanisms of the pH buffering effect could enable us to pursue new applications for this technology in drug or biologic delivery. Additionally, various other polymer systems could be developed for other applications, such as soft tissue healing.

Next, we evaluated the bone regeneration capabilities of these Mg/PLGA composite bone graft substitutes in a clinically relevant socket preservation model. We confirmed our hypotheses that the Mg/PLGA scaffolds could be successfully implanted in the socket defects and would prove safe and effective at regenerating bone in a socket preservation model. Both the bone height and bone volume of the defects receiving Mg/PLGA scaffolds exhibited increases compared to defects left empty. While this experiment confirmed the ability of the scaffold to support bone regeneration in vivo, little is known about the mechanisms why. Future work is planned to examine the

biological response to implantation of these materials at shorter timepoints. Additionally, immunohistochemical evaluation of the interface between the devices and the periosteum could provide insight into magnesium's osteogenesis enhancement.

We expanded our knowledge on the biological mechanisms affected by magnesium by designing an in vitro study to measure osteogenesis related gene expression and protein production changes following exposure to increased concentrations of magnesium ion. We determined that 10mM $MgSO_4$ added to tissue culture medium increased hBMSC proliferation, matrix mineralization and expression of osteogenic genes and proteins. A more scalable approach is needed for future investigations of magnesium's effects on biological mechanisms. This can likely be done by leveraging already obtained in vivo explants for use in immunohistochemical examinations around possible regions of initial increased bone regeneration (periosteum, bone marrow, perivascular) and then combining those data with more focused in vitro experiments.

Finally, we designed a Mg/PLGA barrier membrane, Mg micromesh and Mg tenting screw and combined them into a new approach to dental bone grafting. We used these new devices to refine a new surgical model for our research group and hypothesized that the devices could be successfully implanted in a vertical ridge augmentation model and support bone regeneration. We showed that all devices could be manufactured and successfully implanted; however, further work is needed to develop a more reliable surgical model. The vertical ridge augmentation model will likely prove useful in the future for combination with in vitro mechanistic studies as discussed above. Elucidation of the dynamics of hydrogen gas evolution and gas exchange surrounding these magnesium implants is also greatly needed. As observed in the vertical ridge augmentation model, this buildup of gas may inhibit osseointegration and bone regeneration and may even cause bone resorption.

Overall, this work advanced the field of magnesium in terms of novel material development, medical device development and biological understanding. As more magnesium devices move towards the clinic, deeper understanding of biocompatibility issues surrounding various magnesium device compositions and applications will be required to ensure patient safety. Additionally, this deeper understanding can be harnessed to optimize device design to provide a wound or defect environment most suitable for tissue regeneration.

BIBLIOGRAPHY

1. iDataResearch. U.S. Market for Dental Bone Graft Substitutes, Barrier Membranes and Other Biomaterials. 2015. Document No.: iDATA_USDBGS15_RPT.

2. Haug RH, Foss J. Maxillofacial injuries in the pediatric patient. Oral surgery, oral medicine, oral pathology, oral radiology, and endodontics. 2000;90(2):126-34. Epub 2000/08/11. doi: 10.1067/moe.2000.107974. PubMed PMID: 10936829.

3. Gassner R, Tuli T, Hächl O, Rudisch A, Ulmer H. Cranio-maxillofacial trauma: a 10 year review of 9543 cases with 21067 injuries. Journal of Cranio-Maxillofacial Surgery. 2003;31(1):51-61. doi: 10.1016/s1010-5182(02)00168-3.

4. National Institute of Dental and Craniofacial Research - National Institutes of Health. National Health and Nutrition Examination Survey. 1999-2004.

5. Chiapasco M, Biglioli F, Autelitano L, Romeo E, Brusati R. Clinical outcome of dental implants placed in fibula-free flaps used for the reconstruction of maxillo-mandibular defects following ablation for tumors or osteoradionecrosis. Clinical Oral Implants Research. 2006;17(2):220-8. doi: Doi 10.1111/J.1600-0501.2005.01212.X. PubMed PMID: WOS:000235891700015.

6. Garrett N, Roumanas ED, Blackwell KE, Freymiller E, Abemayor E, Wong WK, Gerratt B, Berke G, Beumer J, 3rd, Kapur KK. Efficacy of conventional and implant-supported mandibular resection prostheses: study overview and treatment outcomes. The Journal of prosthetic dentistry. 2006;96(1):13-24. Epub 2006/07/29. doi: 10.1016/j.prosdent.2006.05.010. PubMed PMID: 16872926.

7. Vissink A. Oral sequelae of head and neck radiotherapy. Critical reviews in oral biology and medicine : an official publication of the American Association of Oral Biologists. 2003;14(3):199-212. Epub 2003/06/12. PubMed PMID: 12799323.

8. Anglen J. Nonunion with Bone Loss. 2006.

9. Finkemeier CG. Bone-grafting and bone-graft substitutes. Journal of Bone and Joint Surgery - American. 84A(3): 454-64. PubMED PMID: 11886919.

10. Khan SN, Cammisa FP, Sandhu HS, Diwan AD, Girardi FP, Lane JM. The Biology of Bone Grafting. Journal of the American Academy of Orthopaedic Surgeons. 2005;13(1):77-86.

11. Sotereanos N, DeMeo P, Hughes T, Bargiotas K, Wohlrab D. Autogenous osteochondral transfer in the femoral head after osteonecrosis. Orthopedics. 2008;31(2):177.

12. McAllister BS, Haghighat K. Bone Augmentation Techniques. Journal of Periodontology. 2007;78(3):377-96. doi: 10.1902/jop.2007.060048.

13. Nkenke E, Stelzle F. Clinical outcomes of sinus floor augmentation for implant placement using autogenous bone or bone substitutes: A systematic review. Clinical Oral Implants Research. 2009;20(SUPPL. 4):124-33.

14. Misch CE, Dietsh F. Bone-grafting materials in implant dentistry. Implant dentistry. 1993;2(3):158-67.

15. Mankin H. Long-term results of allograft replacement in the management of bone tumors. Clinical orthopaedics and related research. 2004;324:86-97.

16. McKay W, Peckham S, Badura J. A comprehensive clinical review of recombinant human bone morphogenetic protein-2 (INFUSE Bone Graft). International Orthopaedics. 2007;31:729-34.

17. Yaremchuk K, Toma M, Somers M, Peterson E. Acute Airway Obstruction in Cervical Spine Procedures with Bone Morphogenetic Proteins. The Laryngoscope. 2010;120:1954-7.

18. Boraiah S, Paul O, Hawkes D, Wickham M, Lorich D. Complications of Recombinant Human BMP-2 for Treating Complex Tibial Plateu Fractures. Clinical orthopaedics and related research. 2009;467:3257-62.

19. Aghaloo TL, Moy PK. Which hard tissue augmentation techniques are the most successful in furnishing bony support for implant placement? International Journal of Oral and Maxillofacial Implants. 2007;22(SUPPL.):49-70.

20. Garrett S. Periodontal regeneration around natural teeth. Annals of periodontology / the American Academy of Periodontology. 1996;1(1):621-66.

21. Murphy KG, Gunsolley JC. Guided tissue regeneration for the treatment of periodontal intrabony and furcation defects. A systematic review. Annals of periodontology / the American Academy of Periodontology. 2003;8(1):266-302.

22. Buser D, Brägger U, Lang NP, Nyman S. Regeneration and enlargement of jaw bone using guided tissue regeneration. Clinical oral implants research. 1990;1(1):22-32.

23. Dahlin C, Linde A, Gottlow J, Nyman S. Healing of bone defects by guided tissue regeneration. Plastic and Reconstructive Surgery. 1988;81(5):672-6.

24. Schenk RK, Buser D, Hardwick WR, Dahlin C. Healing pattern of bone regeneration in membrane-protected defects: a histologic study in the canine mandible. Int J Oral Maxillofac Implants. 1994;9(1):13-29.

25. Cortellini P, Prato GP, Tonetti MS. Periodontal regeneration of human intrabony defects with bioresorbable membranes. A controlled clinical trial. Journal of Periodontology. 1996;67(3):217-23.

26. Zitzmann NU, Naef R, Schärer P. Resorbable Versus Nonresorbable Membranes in Combination with Bio-Oss for Guided Bone Regeneration. International Journal of Oral and Maxillofacial Implants. 1997;12(6):844-52.

27. Hutmacher D, Hürzeler MB, Schliephake H. A Review of Material Properties of Biodegradable and Bioresorbable Polymers and Devices for GTR and GBR Applications. International Journal of Oral and Maxillofacial Implants. 1996;11(5):667-78.

28. Kellomäki M, Niiranen H, Puumanen K, Ashammakhi N, Waris T, Törmälä P. Bioabsorbable scaffolds for guided bone regeneration and generation. Biomaterials. 2000;21(24):2495-505.

29. Lekovic V, Camargo PM, Klokkevold PR, Weinlaender M, Kenney EB, Dimitrijevic B, Nedic M. Preservation of Alveolar Bone in Extraction Sockets Using Bioabsorbable Membranes. Journal of Periodontology. 1998;69(9):1044-9.

30. Stockmann P, Park J, Von Wilmowsky C, Nkenke E, Felszeghy E, Dehner JF, Schmitt C, Tudor C, Schlegel KA. Guided bone regeneration in pig calvarial bone defects using autologous mesenchymal stem/progenitor cells - A comparison of different tissue sources. Journal of Cranio-Maxillofacial Surgery. 2012;40(4):310-20. doi: 10.1016/j.jcms.2011.05.004.

31. Ji W, Yang F, Ma J, Bouma MJ, Boerman OC, Chen Z, van den Beucken JJJP, Jansen JA. Incorporation of stromal cell-derived factor-1α in PCL/gelatin electrospun membranes for guided bone regeneration. Biomaterials. 2013;34(3):735-45. doi: 10.1016/j.biomaterials.2012.10.016.

32. Lee YJ, Lee JH, Cho HJ, Kim HK, Yoon TR, Shin H. Electrospun fibers immobilized with bone forming peptide-1 derived from BMP7 for guided bone regeneration. Biomaterials. 2013;34(21):5059-69. doi: 10.1016/j.biomaterials.2013.03.051.

33. Bottino MC, Thomas V, Schmidt G, Vohra YK, Chu TMG, Kowolik MJ, Janowski GM. Recent advances in the development of GTR/GBR membranes for periodontal regeneration - A materials perspective. Dental Materials. 2012;28(7):703-21. doi: 10.1016/j.dental.2012.04.022.

34. Fu S, Ni P, Wang B, Chu B, Zheng L, Luo F, Luo J, Qian Z. Injectable and thermo-sensitive PEG-PCL-PEG copolymer/collagen/n-HA hydrogel composite for guided bone regeneration. Biomaterials. 2012;33(19):4801-9. doi: 10.1016/j.biomaterials.2012.03.040.

35. Vaquette C, Fan W, Xiao Y, Hamlet S, Hutmacher DW, Ivanovski S. A biphasic scaffold design combined with cell sheet technology for simultaneous regeneration of alveolar bone/periodontal ligament complex. Biomaterials. 2012;33(22):5560-73. doi: 10.1016/j.biomaterials.2012.04.038.

36. Mota J, Yu N, Caridade SG, Luz GM, Gomes ME, Reis RL, Jansen JA, Frank Walboomers X, Mano JF. Chitosan/bioactive glass nanoparticle composite membranes for periodontal regeneration. Acta Biomaterialia. 2012;8(11):4173-80. doi: 10.1016/j.actbio.2012.06.040.

37. Chen FM, Zhang J, Zhang M, An Y, Chen F, Wu ZF. A review on endogenous regenerative technology in periodontal regenerative medicine. Biomaterials. 2010;31(31):7892-927. doi: 10.1016/j.biomaterials.2010.07.019.

38. Mock C, Cherian MN. The global burden of musculoskeletal injuries: challenges and solutions. Clinical orthopaedics and related research. 2008;466(10):2306-16. Epub 2008/08/06. doi: 10.1007/s11999-008-0416-z. PubMed PMID: 18679760; PubMed Central PMCID: PMC2584305.

39. Bostrom M. Osteoinductive growth factors in preclinical fracture and long bone defects models. Orthopedic Clinics of North America. 1999;30(4):647-58.

40. Control CF. Incidence and Costs to Medicare of Fractures Amongh Medicare Beneficiaries Greater than or equal to 65 Years1996;45(41):866-83.

41. Antonova E, Le TK, Burge R, Mershon J. Tibia shaft fractures: costly burden of nonunions. BMC musculoskeletal disorders. 2013;14:42. Epub 2013/01/29. doi: 10.1186/1471-2474-14-42. PubMed PMID: 23351958; PubMed Central PMCID: PMC3573940.

42. Pike C, Birnbaum HG, Schiller M, Sharma H, Burge R, Edgell ET. Direct and indirect costs of non-vertebral fracture patients with osteoporosis in the US. Pharmacoeconomics. 2010;28(5):395-409. doi: 10.2165/11531040-000000000-00000.

43. Meling T, Harboe K, Søreide K. Incidence of traumatic long-bone fractures requiring in-hospital management: A prospective age- and gender-specific analysis of 4890 fractures. Injury. 2009;40(11):1212-9. doi: doi:10.1016/j.injury.2009.06.003.

44. Kuo K, Gitelis S, Sim F. Segmental replacement of long bones using titanium fiber metal composite following tumor resection. Clinical orthopaedics and related research. 1983;176:108-14.

45. Lalor P, Revell P, Gray A, Wright S, Railton G, Freeman M. Sensitivity to titanium. A cause of implant failure? Journal of Bone and Joint Surgery B. 1991;73(1):25-8.

46. Engh C, Bobyn J, Glassman A. Porous-coated hip replacement. The factors governing bone ingrowth, stress shielding and clinical results. Journal of Bone and Joint Surgery B. 1987;69(1):45-55.

47. Juutilainen T, Patiala H, Ruuskanen M, Rokkanen P. Comparison of costs in ankle fractures treated with absorbable or metallic fixation devices. Archives of orthopaedic and trauma surgery. 1997;116(4):204-8. Epub 1997/01/01. doi: 10.1007/bf00393710. PubMed PMID: 9128772.

48. Busam ML, Esther RJ, Obremskey WT. Hardware removal: indications and expectations. The Journal of the American Academy of Orthopaedic Surgeons. 2006;14(2):113-20. Epub 2006/02/10. PubMed PMID: 16467186.

49. Huse E. A new ligature? Chicago Medical Journal and Examiner. 1878:172.

50. Witte F. The history of biodegradable magnesium implants: A review. Acta Biomaterialia. 2010;6:1680-192.

51. Gu X, Zheng Y, Cheng Y, Zhong S, Xi T. In vitro corrosion and biocompatibility of binary magnesium alloys. Biomaterials. 2009;30(4):484-98.

52. Li L, Gao J, Wang Y. Evaluation of cyto-toxicity and corrosion behavior of alkali-heat-treated magnesium in simulated body fluid. Surface & Coatings Technology. 2004;185:92-8.

53. Wei J, Jia J, Wu F, Wei S, Zhou H, Zhang H, Shin J, Liu C. Hierarchically microporous/macroporous scaffold of magnesium-calcium phosphate for bone tissue engineering. Biomaterials. 2010;31:1260-89.

54. Witte F, Fischer J, Nellesen J, Vogt C, Vogt J, Donath T, Beckmann F. In vivo corrosion and corrosion protection of magnesium alloy LAE442. Acta Biomaterialia. 2010;6:1792-9.

55. Zhuang H, Hang Y, Fent A. Preparation, mechanical properties and in vitro biodegradation of porous magnesium scaffolds Materials Science and Engineering. 2007;28(8):1462-6.

56. Li Z, Gu X, Lou S, Zheng Y. The development of binary Mg-Ca alloys for use as biodegradable materials within bone. Biomaterials. 2008;29(10):1329-44.

57. Zhang S, Zhang X, Zhao C, Li J, Song Y, Xie C, Tao H, Zhang Y, He Y, Jiang Y, Bian Y. Research on an Mg-Zn alloy as a degradable biomaterial. Acta Biomaterialia. 2009.

58. Staiger M, Pietak A, Huadmai J, Dias G. Magnesium and its alloys as orthopedic biomaterials: A review. Biomaterials. 2006:1728-34.

59. Witte F, Kaese V, Haferkamp H, Switzer E, Meyer-Lindenberg A, Wirth C, Windhagen H. In vivo corrosion of four magnesium alloys and the associated bone response. Biomaterials. 2005;26(17):3557-63.

60. Janning C, Willbold E, Vogt C, Nellesen J, Meyer-Lindenberg A, Windhagen H, Thorey F, Witte F. Magnesium hydroxide temporarily enhancing osteoblast activity and decreasing the osteoclast number in peri-implant bone remodelling. Acta Biomaterialia. 2010;6:1861-8.

61. Witte F, Fischer J, Nellesen J, Crostack HA, Kaese V, Pisch A, Beckmann F, Windhagen H. In vitro and in vivo corrosion measurements of magnesium alloys. Biomaterials. 2006;27(7):1013-8.

62. Witte F, Ulrich H, Palm C, Willbold E. Biodegradable magnesium scaffolds: Part II: Peri-implant bone remodeling. Journal of Biomedical Materials Research Part A. 2007;81(3):757-65.

63. Lambotte A. Technique et indications de la protese perdue dans la traitement des fractures. Presse Med Belge. 1909;17:1325-34.

64. Witte F, Ulrich H, Rudert M, Willbold E. Biodegradable magnesium scaffolds: Part I: Appropriate inflammatory response. Journal of Biomedical Materials Research. 2007;81:748-56.

65. Zhuang H, Hang Y, Fent A. Preparation, mechanical properties and in vitro biodegradation of porous magnesium scaffolds. Materials Science and Engineering. 2007;28(8):1462-6.

66. Karageorgiou V, Kaplan D. Porosity of 3D biomaterial scaffolds and osteogenesis. Biomaterials. 2005;26:5474-91.

67. Wen C. Compressibility of porous magnesium foam: Dependency on porosity and pore size. Materials Letters. 2004;58(3-4):357-60.

68. Capek J, Vojtech D. Properties of porous magnesium prepared by powder metallurgy. Materials Science and Engineering C. 2013;33:564-9.

69. Seyedraoufi Z, Mirdamadi S. Synthesis, microstructure and mechanical properties of porous MgZn scaffolds. Journal of the Mechanical Behavior of Biomedical Materials. 2013;21:1-8.

70. Cifuentes S, Frutos E, Gonzalez-Carrasco J, Munoz M, Multigner M, Chao J, Benavente R, Lieblich M. Novel PLLA/magnesium composite for orthopedic applications: A proof of concept. Materials Letters. 2012;74(1):239-42.

71. Pietak A, Mahoney P, Dias G, Staiger M. Bone-linke matrix formation on magnesium and magnesium alloys. Journal of Materials Science: Materials in Medicine. 2008;19:407-15.

72. Witte F, Feyerabend F, Maier P, Fischer J, Stormer M, Blawert C, Dietzel W, Hort N. Biodegradable magnesium-hydroxyapatite metal matrix composites. Biomaterials. 2007;28:2163-74.

73. Feyerabend F, Witte F, Kammal M, Willumeit R. Unphysiologically high magnesium concentrations support chondrocyte proliferation and redifferentiation. Tissue Engineering. 2006;12(12):3545-56. PubMed PMID: ISI:000243202200024.

74. Yun Y, Dong Z, Yang D, Schulz M, VShanov V, Yarmolenko S, Xu Z, Kumta P, Sfeir C. Biodegradable Mg corrosion and osteoblast cell culture studies. Materials Science and Engineering C. 2009;29:1814-21.

75. Fischer J, Prosenc M, Wolff M, Hort N, Willumeit R, Feyerabend F. Interference of magnesium corrosion with tetrazolium-based cytotoxicity assays. Acta Biomaterialia. 2010;6(5):1813-23.

76. Chaya A, Yoshizawa S, Verdelis K, Myers N, Costello BJ, Chou DT, Pal S, Maiti S, Kumta PN, Sfeir C. In vivo study of magnesium plate and screw degradation and bone fracture healing. Acta Biomaterialia. 2015;18:262-9.

77. Hartwig A. Role of magnesium in genomic stability. Mutation research. 2001;475(1-2):113-21.

78. Zreiqat H, Howlett C, Zannettino A, Evans P, Schulze-Tanzil G, Knabe C. Mechanisms of magnesium-stimulated adhesion of osteoblastic cells to commonly used orthopaedic implants. Journal of Biomedical Materials Research. 2002;62:175-84.

79. Xue W, Deng Z, Chen R, Zhang T. Growth regularity of ceramic coatings formed by microarc oxidation on Al-Cu-Mg alloy. Thin Solid Films. 2000;372(1-2):114-7.

80. Maier J, Bernardini D, Rayssiguier Y, Mazur A. High concentrations of magnesium modulate vascular endothelial cell behaviour in vitro. Biochimica et Biophysica Acta - Molecular Basis of Disease. 2004;1689(1):6-12.

81. Woodruff MA, Hutmacher DW. The return of a forgotten polymer—Polycaprolactone in the 21st century. Progress in Polymer Science. 2010;35(10):1217-56. doi: http://dx.doi.org/10.1016/j.progpolymsci.2010.04.002.

82. Bergsma EJ, Rozema FR, Bos RR, de Bruijn WC. Foreign body reactions to resorbable poly(L-lactide) bone plates and screws used for the fixation of unstable zygomatic fractures. Journal of oral and maxillofacial surgery : official journal of the American Association of Oral and Maxillofacial Surgeons. 1993;51(6):666-70. Epub 1993/06/01. PubMed PMID: 8492205.

83. Simion M, Scarano A, Gionso L, Piattelli A. Guided bone regeneration using resorbable and nonresorbable membranes: a comparative histologic study in humans. Int J Oral Maxillofac Implants. 1996;11(6):735-42. Epub 1996/11/01. PubMed PMID: 8990634.

84. Liu X, Ma PX. Polymeric scaffolds for bone tissue engineering. Annals of biomedical engineering. 2004;32(3):477-86. Epub 2004/04/21. PubMed PMID: 15095822.

85. Hutmacher DW. Scaffolds in tissue engineering bone and cartilage. Biomaterials. 2000;21(24):2529-43. doi: http://dx.doi.org/10.1016/S0142-9612(00)00121-6.

86. Di Martino A, Sittinger M, Risbud MV. Chitosan: A versatile biopolymer for orthopaedic tissue-engineering. Biomaterials. 2005;26(30):5983-90. doi: http://dx.doi.org/10.1016/j.biomaterials.2005.03.016.

87. Ulery BD, Nair LS, Laurencin CT. Biomedical applications of biodegradable polymers. Journal of Polymer Science Part B: Polymer Physics. 2011;49(12):832-64. doi: 10.1002/polb.22259.

88. Peltoniemi H, Ashammakhi N, Kontio R, Waris T, Salo A, Lindqvist C, Grätz K, Suuronen R. The use of bioabsorbable osteofixation devices in craniomaxillofacial surgery. Oral Surgery, Oral Medicine, Oral Pathology, Oral Radiology, and Endodontology. 2002;94(1):5-14. doi: http://dx.doi.org/10.1067/moe.2002.122160.

89. Imola MJ, Hamlar DD, Shao W, Chowdhury K, Tatum S. Resorbable plate fixation in pediatric craniofacial surgery: long-term outcome. Archives of facial plastic surgery. 2001;3(2):79-90. Epub 2001/05/23. PubMed PMID: 11368657.

90. Eppley BL, Morales L, Wood R, Pensler J, Goldstein J, Havlik RJ, Habal M, Losken A, Williams JK, Burstein F, Rozzelle AA, Sadove AM. Resorbable PLLA-PGA plate and screw fixation in pediatric craniofacial surgery: clinical experience in 1883 patients. Plast Reconstr Surg. 2004;114(4):850-6; discussion 7. Epub 2004/10/07. PubMed PMID: 15468389.

91. Ignatius AA, Claes LE. In vitro biocompatibility of bioresorbable polymers: poly(L, DL-lactide) and poly(L-lactide-co-glycolide). Biomaterials. 1996;17(8):831-9. doi: http://dx.doi.org/10.1016/0142-9612(96)81421-9.

92. Eppley BL, Reilly M. Degradation characteristics of PLLA-PGA bone fixation devices. The Journal of craniofacial surgery. 1997;8(2):116-20. Epub 1997/03/01. PubMed PMID: 10332278.

93. Zhang P, Hong Z, Yu T, Chen X, Jing X. In vivo mineralization and osteogenesis of nanocomposite scaffold of poly(lactide-co-glycolide) and hydroxyapatite surface-grafted with poly(L-lactide). Biomaterials. 2009;30:58-70.

94. Taboas J, Maddox R, Krebsbach P, Hollister S. Indirect solid free form fabrication of local and global porous, biomimetic and composite 3D polymer-cermaic scaffolds. Biomaterials. 2003;24:181-94.

95. Rizzi S, Heath D, Coombes A, Bock N, Textor M, Downes S. Biodegradable polymer/hydroxyapatite composites: surface analysis and initial attachment of osteoblasts. Journal of Biomedical Materials Research. 2001;55:475-86.

96. Wei G, Ma PX. Structure and properties of nano-hydroxyapatite/polymer composite scaffolds for bone tissue engineering. Biomaterials. 2004;25(19):4749-57. doi: http://dx.doi.org/10.1016/j.biomaterials.2003.12.005.

97. Wahl D, Czernuszka J. Collagen-hydroxyapatite composites for hard tissue repair. European Cells and Materials. 2006;11:43-56.

98. Rezwan K, QZ C, JJ B, AR B. Biodegradable and bioactive porous polymer/inorganic composite scaffolds for bone tissue engineering. Biomaterials. 2006;27(18):3413-31.

99. Ostrowski N, Lee B, Roy A, Ramanathan M, Kumta P. Biodegradable poly(lactide-co-glycolide) coatings on magnesium alloys for orthopedic applications. Journal of Materials Science: Materials in Medicine. 2013;24(1):85-96.

100. Vranceanu M, Saban R, Antoniac I, Albu M, Miculescu F. Development and Characterization of Novel Porous Collagen Based Biocomposite for Bone Tissue Regeneration. UPB Science Bulletin B. 2012;74(3):145-56.

101. Kim S-S, Sun Park M, Jeon O, Yong Choi C, Kim B-S. Poly(lactide-co-glycolide)/hydroxyapatite composite scaffolds for bone tissue engineering. Biomaterials. 2006;27(8):1399-409. doi: http://dx.doi.org/10.1016/j.biomaterials.2005.08.016.

102. Shikinami Y, Okuno M. Bioresorbable devices made of forged composites of hydroxyapatite (HA) particles and poly-L-lactide (PLLA): Part I. Basic characteristics. Biomaterials. 1999;20(9):859-77. doi: http://dx.doi.org/10.1016/S0142-9612(98)00241-5.

103. Seitz H, Rieder W, Irsen S, Leukers B, Tille C. Three-dimensional printing of porous ceramic scaffolds for bone tissue engineering. Journal of Biomedical Materials Research - Part B Applied Biomaterials. 2005;74(2):782-8.

104. Makadia H, Siegel S. Poly Lactic-co-Glycolic Acid (PLGA) as a biodegradable controlled drug delivery carrier. Polymers. 2011;3(3):1377-97.

105. Sung H, Meredith C, Johnson C, Galis Z. The effect of scaffold degradation rate on three-dimensional cell growth and angiogenesis. Biomaterials. 2004;25:5735-42.

106. Witte F, Hort N, Vogt C, Cohen S, Kainer K, Willumeit R, Feyerabend F. Degradable biomaterials based on magnesium corrosion. Current Opinion in Solid State and Materials Science. 2009.

107. Yoshizawa S, Brown A, Barchowsky A, Sfeir C. Magnesium ion stimulation of bone marrow stromal cells enhances osteogenic activity, simulating the effect of magnesium alloy degradation. Acta Biomaterialia. 2014. Epub 2014 Feb 7.

108. Zhu G, Mallery S, Schwendeman S. Stabilization of proteins encapsulated in injectable poly (lactide-co-glycolide). Nature Biotechnology. 2000;18:52-7.

109. Zhu G, Schwendeman S. Stabilization of proteins encapsulated in cylindrical poly(lactide-co-glycolide) implants: mechanism of stabilization by basic additives. Pharmaceutical Research. 2000;17(3):351-7.

110. Guo M, Cao L, Lu P, Liu Y, Xu X. Anticorrosion and cytocompatibility behavior of MAO/PLLA modified magnesium alloy WE42. Journal of Materials Science: Materials in Medicine. 2011;22(7):1735-40.

111. Wong H, Yeung K, Lam K, Tam V, Chu P, Luk K, Cheung K. A biodegradable polymer-based coating to control the performance of magnesium alloy orthopaedic implants. Biomaterials. 2010;31(8):2084-96.

112. Mikos AG, Thorsen A, Czerwonka L, Bao Y, Langer R, Winslow D, Vacanti J. Preparation and characterization of poly(l-lactic acid) foams. Polymer. 1994;35(5):1068-77.

113. Colter D, Class R, DiGirolamo C, Prockop D. Rapid expansion of recycling stem cells in culture of plastic adherent cells from human bone marrow. Proceedings of the National Academy of Sciences. 2000;97:3213-8.

114. Sekiya I, Larson B, Smith J, OPochampally R, Cui J-G, Prockop D. Expansion of human adult stem cells from bone marrow stroma: conditions that maximize the yields of early progenitors and evaluate their quality. Stem Cells. 2002;20:530-41.

115. Fischer J, Profrock D, Hort N, Willumeit R, Feyerabend F. Improved cytotoxicity testing of magnesium materials. Materials Science and Engineering B. 2011;176(11):830-4.

116. Shaw B. Corrosion resistance of magnesium alloys. Stephen D, editor: ASM International; 2003.

117. Zhang J, Wu L, Jing D, Ding J. A comparative study of porous scaffolds with cubic and spherical macropores. Polymer. 2005;46(13):4979-85.

118. Lim T, Poh C, Wang W. Poly (lactic-co-glycolic acid) as a controlled release delivery device. Journal of Materials Science: Materials in Medicine. 2009;20(8):1669-75.

119. Athanasiou K, Niederauer G, Agarwal C. Sterilization, toxicity, biocompatibility and clinical applications of polylactic acid/polyglycolic acid copolymers. Biomaterials. 1996;17(2):92-102.

120. Knedler A, Ham R. Optimized medium for clonal growth of human microvascular endothelial cells with minimal serum. In Vitro Cellular and Developmental Biology. 1987;23(7):481-91.

121. Pietrokovski J, Massler M. Alveolar ridge reorption following tooth extraction. Journal of Prosthetic Dentistry. 1967;17:21-7.

122. Araujo M, Lindhe J. Dimensional ridge alterations following tooth extraction. An experimental study in the dog. Journal of Clinical Periodontology. 2005;32(2):212-8.

123. Ten Heggeler J, Slot D, Van der Weijden G. Effect of socket preservation therapies following tooth extraction in non-molar regions in humans: a systematic review. Clinical Oral Implants Research. 2011;22:779-88.

124. Fickl S, Zuhr O, Wachtel H, Bolz W, Huerzeler M. Hard tissue alterations after socket preservation: an experimental study in the beagle dog. Clinical Oral Implants Research. 2008;19:1111-8.

125. Wallace S, Froum S, Cho S, Elian N, Monteiro D, Kim B, Tarnow D. Sinus augmentation utilizing anorganic bovine bone (Bio-Oss) with absorbable and nonabsorbable membranes placed over the lateral window: histomorphometric and clinical analyses. International Journal of Periodontics and Restorative Dentistry. 2005;25(6):551-9.

126. Buser D, Dula K, Hirt H, Schenk R. Lateral ridge augmentation using autografts and barrier membranes: a clinical study with 40 partially edentulous patients. Journal of Oral and Maxillofacial Surgery. 1996;10:312-8.

127. Proussaefs P, Lozada J. The use of intraorally harvested autogenous block grafts for vertical alveolar ridge augmentation: a human study. International Journal of Periodontics and Restorative Dentistry. 2005;25:351-63.

128. McAllister B, Haghighat K. Bone augmentation techniques. Journal of Periodontology. 2007;78(3):377-96.

129. Mardas N, Chadha V, Donos N. Alveolar ridge preservation with guided bone regeneration and a synthetic bone substitute or a bovine-derived xenograft: a randomized, controlled clinical trial. Clinical Oral Implants Research. 2010;21(7):688-98.

130. Hoffmann O, Bartee B, Beaumont C, Kasaj A, Deli G, Zafiropoulos G. Alveolar bone preservation in extraction sockets using non-resorbable dPTFE membranes: a retrospective non-randomized study. Journal of Periodontology. 2008;79(8):1355-69.

131. Lekovic V, Camargo P, Klokkevold P, Weinlaender M, Kenney E, Dimitrijevic B, Nedic M. Preservation of alveolar bone in extraction sockets using bioabsorbable membranes. Journal of Periodontology. 1998;69(9):1044-9.

132. Retzepi M, Donos N. Guided bone regeneration: biological principle and therapeutic applications. Clinical Oral Implants Research. 2009;21:567-76.

133. Araujo M, Lindhe J. Socket grafting with the use of autologous bone: an experimental study in the dog. Clinical Oral Implants Research. 2011;22(1):9-13.

134. Becker W, Urist M, Becker B, Jackson W, Parry D, Bartold M, Vincenzzi G, De Georges D, Niederwanger M. Clinical and histological observations of sites implanted with intraoral autologous bone grafts or allografts. 15 human case reports. Journal of Periodontology. 1996;67(10):1025-33.

135. Zubillaga G, Von Hagen S, Simon B, Deasy M. Changes in alveolar bone height and width following post-extraction ridge augmentation using a fixed bioabsorbable membrane and demineralized freeze-dried bone osteoinductive graft. Journal of Periodontology. 2003;74:965-75.

136. Lasella J, Greenwell H, Miller R, Hill M, Drisko C, Bohra A, Scheetz J. Ridge preservation with freeze-dried bone allograft and a collagen membrane compared to extraction alone for implant site development: a clinical and histologic study in humans. Journal of Periodontology. 2003;74(7):990-9.

137. Keles G, Sumer M, Cetinkaya B, Tutkum F, Simsek S. Effect of autogenous cortical bone grafting in conjunction with guided tissue regeneration in the treatment of intraosseous periodontal defects. European Journal of Dentistry. 2010;4(4):403-11.

138. Kim C, Choi S, Cho K, Chai J, Wikesjo U, Kim C. Periodontal healing in one-wall intra-bony defects in dogs following implantation of autogenous bone or a coral-derived biomaterial. Journal of Clinical Periodontology. 2005;32(6):583-9.

139. Eppley B, Pietrzak W, Blanton M. Allograft and alloplastic bone substitutes: a review of science and technology for the craniomaxillofacial surgeon. Journal of Craniofacial Surgery. 2005;16(6):981-9.

140. LeGeros R. Properties of osteoconductive biomaterials: calcium phosphates. Clinical orthopaedics and related research. 2002;395:81-98.

141. Frenken J, Bouwman W, Bravenboer N, Zijderveld S, Schulten E, Ten Bruggenkate C. The use of Straumann Bone Cermaic in a maxillary sinus floor elevation procedure: a clinical, radiological, histological and histomorphometric evaluation with a 6-month healing period. Clinical Oral Implants Research. 2010;21(2):201-8.

142. Serino G, Rao W, Iezzi G, Piattelli A. Polylactide and polyglycolide sponge used in human extraction sockets: bone formation following 3 months after its application. Clinical Oral Implants Research. 2008;19(1):16-31.

143. Min C, Wikesjo U, Park J, Chae G, Pippig S, Bastone P, Kim C, Kim C. Wound healing/regeneration using recombinant human growth/differentiation factor-5 in an injectable poly-lactide-co-glycolide-acid composite carrier and a one-wall intra-bony defect model in dogs. Journal of Clinical Periodontology. 2011;38(3):261-8.

144. Schneider D, Weber F, Grunder U, Andreoni C, Burkhardt R, Jung R. A randomized controlled clinical multicenter trial comparing the clinical and histological performance of a new, modified polylactide-co-glycolide acid membrane to an expanded polytetrafluorethylene membrane in guided bone regeneration procedures. Clinical Oral Implants Research. 2014;25(2):150-8.

145. Jung R, Kokovic V, Jurisic M, Yaman D, Subramani K, Weber F. Guided bone regeneration with a synthetic biodegradable membrane: A comparative study in dogs. Clinical Oral Implants Research. 2011;22(8):802-7.

146. Battistella E, Varoni E, Cochis A, Palazzo B, Rimondini L. Degradable polymers may improve dental practice. Journal of Applied BIomaterials and Biomechanics. 2011;9(3):223-31.

147. Shen H, Hu X, Yang F, Bei J, Wang S. An injectable scaffold: rhBMP-2-loaded poly(lactide-co-glycolide)/hydroxyapatite composite microspheres. Acta Biomaterialia. 2010;6(2):455-65.

148. Chaya A, Yoshizawa S, Verdelis K, Noorani S, Costello BJ, Sfeir C. Fracture Healing Using Degradable Magnesium Fixation Plates and Screws. Journal of Oral and Maxillofacial Surgery. 2015;73(2):295-305. doi: 10.1016/j.joms.2014.09.007.

149. Bondarenko A, Angrisani N, Meyer-Lindenberg A, Seitz JM, Waizy H, Reifenrath J. Magnesium-based bone implants: Immunohistochemical analysis of peri-implant osteogenesis by evaluation of osteopontin and osteocalcin expression. Journal of Biomedical Materials Research Part A. 2014;102(5):1449-57. doi: 10.1002/jbm.a.34828.

150. Brown A, Zaky S, Ray H, Jr., Sfeir C, editors. Magnesium/PLGA Composite Scaffolds for Improved Bone Regeneration. 6th Symposium on Biodegradable Metals; 2014; Maratea, Italy: European Cells and Materials.

151. Brown A, Sfeir C, inventors; University of Pittsburgh - of the Commonwealth System of Higher Education, assignee. Magnesium composite-containing scaffolds to enhance tissue regeneration. United States of America2015.

152. Bostrom MP, Saleh KJ, Einhorn TA. Osteoinductive growth factors in preclinical fracture and long bone defects models. Orthop Clin North Am. 1999;30(4):647-58. Epub 1999/09/03. PubMed PMID: 10471769.

153. Meling. Incidence of traumatic long-bone fractures requiring in-hospital management: A prospective age- and gender-specific analysis of 4890 fractures. Injury. 2009;40(11):1212-9.

154. Staiger MP, Pietak AM, Huadmai J, Dias G. Magnesium and its alloys as orthopedic biomaterials: A review. Biomaterials. 2006;27(9):1728-34. PubMed PMID: ISI:000234962500007.

155. Forcino RG, Jonnalagadda S. The effect of fabrication methods on the mechanical and thermal properties of poly(lactide-co-glycolide) scaffolds. Journal of Applied Polymer Science. 2007;104(2):944-9. PubMed PMID: ISI:000244587000034.

156. Bostman O, Pihlajamaki H. Clinical biocompatibility of biodegradable orthopaedic implants for internal fixation: a review. Biomaterials. 2000;21(24):2615-21. PubMed PMID: ISI:000089861700014.

157. Bostman OM, Pihlajamaki HK. Adverse tissue reactions to bioabsorbable fixation devices. Clinical orthopaedics and related research. 2000(371):216-27. PubMed PMID: ISI:000085397700027.

158. Fraser RK, Cole WG. Osteolysis after Biodegradable Pin Fixation of Fractures in Children. Journal of Bone and Joint Surgery-British Volume. 1992;74(6):929-30. PubMed PMID: ISI:A1992JY81200028.

159. Erdmann N, Angrisani N, Reifenrath J, Lucas A, Thorey F, Bormann D, Meyer-Lindenberg A. Biomechanical testing and degradation analysis of MgCa0.8 alloy screws: A comparative study in rabbits. Acta Biomaterialia. 2011;7:1421-8.

160. Smith M, Atkinson P, White D, Piersma T, Gutierrez G, Rossini G, Desai S, Wellinghoff S, Yu H, Cheng X. Design and assessment of a wrapped cylindrical Ca-P AZ31 Mg alloy for critical-size ulna defect repair. Journal of Biomedical Materials Research Part B. 2011;100B(1):206-16.

161. Castellani C, Lindtner RA, Hausbrandt P, Tschegg E, Stanzl-Tschegg SE, Zanoni G, Beck S, Weinberg AM. Bone-implant interface strength and osseointegration: Biodegradable magnesium alloy versus standard titanium control. Acta Biomaterialia. 2011;7(1):432-40. PubMed PMID: ISI:000284795300042.

162. Witte F, Kaese V, Haferkamp H, Switzer E, Meyer-Lindenberg A, Wirth CJ, Windhagen H. In vivo corrosion of four magnesium alloys and the associated bone response. Biomaterials. 2005;26(17):3557-63. PubMed PMID: ISI:000226968200021.

163. Ghazi AM, Wataha JC, O'Dell NL, Singh BB, Simmons R, Shuttleworth S. Quantitative concentration profiling of nickel in tissues around metal implants: a new biomedical application of laser ablation sector field ICP-MS. Journal of Analytical Atomic Spectrometry. 2002;17(10):1295-9. PubMed PMID: ISI:000178313400013.

164. Witte F, Feyerabend F, Maier P, Fischer J, Stormer M, Blawert C, Dietzel W, Hort N. Biodegradable magnesium-hydroxyapatite metal matrix composites. Biomaterials. 2007;28(13):2163-74. Epub 2007/02/06. doi: S0142-9612(07)00022-1 [pii] 10.1016/j.biomaterials.2006.12.027. PubMed PMID: 17276507.

165. Bae S, Ahn JH, Park CW, Son HK, Kim KS, Lim NK, Jeon CJ, Kim H. Gene and microRNA expression signatures of human mesenchymal stromal cells in comparison to fibroblasts. Cell Tissue Res. 2009;335(3):565-73. Epub 2008/12/18. doi: 10.1007/s00441-008-0729-y. PubMed PMID: 19089456.

166. Zreiqat H, Howlett CR, Zannettino A, Evans P, Schulze-Tanzil G, Knabe C, Shakibaei M. Mechanisms of magnesium-stimulated adhesion of osteoblastic cells to commonly used orthopaedic implants. Journal of Biomedical Materials Research. 2002;62(2):175-84. PubMed PMID: ISI:000177754800004.

167. Bianco P, Kuznetsov SA, Riminucci M, Robey PG. Postnatal skeletal stem cells. Adult Stem Cells. 2006;419:117-48. PubMed PMID: ISI:000242860600006.

168. Jadlowiec J, Koch H, Zhang XY, Campbell PG, Seyedain M, Sfeir C. Phosphophoryn regulates the gene expression and differentiation of NIH3T3, MC3T3-E1, and human mesenchymal stem cells via the integrin/MAPK signaling pathway. Journal of Biological Chemistry. 2004;279(51):53323-30. PubMed PMID: ISI:000225680600064.

169. Saito T, Fukai A, Mabuchi A, Ikeda T, Yano F, Ohba S, Nishida N, Akune T, Yoshimura N, Nakagawa T, Nakamura K, Tokunaga K, Chung U, Kawaguchi H. Transcriptional regulation of endochondral ossification by HIF-2 alpha during skeletal growth and osteoarthritis development. Nature Medicine. 2010;16(6):678-U83. PubMed PMID: ISI:000278394200034.

170. Soucy NV, Klei LR, Mayka DD, Barchowsky A. Signaling pathways for arsenic-stimulated vascular endothelial growth factor-A expression in primary vascular smooth muscle cells. Chemical Research in Toxicology. 2004;17(4):555-63. PubMed PMID: ISI:000220971400012.

171. Knedler A, Ham RG. Optimized medium for clonal growth of human microvascular endothelial cells with minimal serum. In Vitro Cell Dev Biol. 1987;23(7):481-91. Epub 1987/07/01. PubMed PMID: 3301790.

172. Hallab NJ, Vermes C, Messina C, Roebuck KA, Glant TT, Jacobs JJ. Concentration- and composition-dependent effects of metal ions on human MG-63 osteoblasts. J Biomed Mater Res. 2002;60(3):420-33. PubMed PMID: 11920666.

173. Lu JX, Wei J, Yan YG, Li H, Jia JF, Wei SC, Guo H, Xiao TQ, Liu CS. Preparation and preliminary cytocompatibility of magnesium doped apatite cement with degradability for bone

regeneration. Journal of Materials Science-Materials in Medicine. 2011;22(3):607-15. PubMed PMID: ISI:000289302600019.

174. Cai YL, Zhang JJ, Zhang S, Venkatraman SS, Zeng XT, Du HJ, Mondal D. Osteoblastic cell response on fluoridated hydroxyapatite coatings: the effect of magnesium incorporation. Biomedical Materials. 2010;5(5). PubMed PMID: ISI:000282277300015.

175. Eyre D. Collagen of articular cartilage. Arthritis Research. 2002;4(1):30-5. PubMed PMID: ISI:000173864700006.

176. Zaucke F, Dinser R, Maurer P, Paulsson M. Cartilage oligomeric matrix protein (COMP) and collagen IX are sensitive markers for the differentiation state of articular primary chondrocytes. Biochemical Journal. 2001;358:17-24. PubMed PMID: ISI:000170627300003.

177. Barry F, Boynton RE, Liu BS, Murphy JM. Chondrogenic differentiation of mesenchymal stem cells from bone marrow: Differentiation-dependent gene expression of matrix components. Experimental Cell Research. 2001;268(2):189-200. PubMed PMID: ISI:000170509900008.

178. Ries C, Egea V, Karow M, Kolb H, Jochum M, Neth P. MMP-2, MTI-MMP, and TMP-2 are essential for the invasive capacity of human mesenchymal stem cells: differential regulation by inflammatory cytokines. Blood. 2007;109(9):4055-63. PubMed PMID: ISI:000246091400066.

179. Hino J, Matsuo H, Kangawa K. Bone morphogenetic protein-3b (BMP-3b) gene expression is correlated with differentiation in rat calvarial osteoblasts. Biochemical and Biophysical Research Communications. 1999;256(2):419-24. PubMed PMID: ISI:000079238200032.

180. Kaihara S, Bessho K, Okubo Y, Sonobe J, Komatsu Y, Miura M, Miyatake S, Nakao K, Iizuka T. Over expression of bone morphogenetic protein-3b (BMP-3b) using an adenoviral vector promote the osteoblastic differentiation in C2C12 cells and augment the bone formation induced by bone morphogenetic protein-2 (BMP-2) in rats. Life Sciences. 2003;72(15):1683-93. PubMed PMID: ISI:000180879500002.

181. Kiviranta R, Morko J, Uusitalo H, Aro HT, Vuorio E, Rantakokko J. Accelerated turnover of metaphyseal trabecular bone in mice overexpressing cathepsin K. Journal of Bone and Mineral Research. 2001;16(8):1444-52. PubMed PMID: ISI:000170078000008.

182. Bialek P, Kern B, Yang XL, Schrock M, Sosic D, Hong N, Wu H, Yu K, Ornitz DM, Olson EN, Justice MJ, Karsenty G. A twist code determines the onset of osteoblast differentiation. Developmental Cell. 2004;6(3):423-35. PubMed PMID: ISI:000222442900015.

183. Hasebe A, Nakamura Y, Tashima H, Takahashi K, Iijima M, Yoshimoto N, Ting K, Kuroda Si, Niimi T. The C-terminal region of NELL1 mediates osteoblastic cell adhesion through integrin α3β1. FEBS Letters. 2012;586(16):2500-6. doi: http://dx.doi.org/10.1016/j.febslet.2012.06.014.

184. Dong AL, Shen JK, Zeng MB, Campochiaro PA. Vascular cell-adhesion molecule-1 plays a central role in the proangiogenic effects of oxidative stress. Proceedings of the National Academy of Sciences of the United States of America. 2011;108(35):14614-9. PubMed PMID: ISI:000294425900051.

185. Semenza GL. Angiogenesis in ischemic and neoplastic disorders. Annual Review of Medicine-Selected Topics in the Clinical Sciences. 2003;54:17-28. PubMed PMID: ISI:000182433600002.

186. Salnikow K, Donald SP, Bruick RK, Zhitkovich A, Phang JM, Kasprzak KS. Depletion of intracellular ascorbate by the carcinogenic metals nickel and cobalt results in the induction of hypoxic stress. Journal of Biological Chemistry. 2004;279(39):40337-44. PubMed PMID: ISI:000223916800015.

187. Maxwell P, Salnikow K. HIF-1: an oxygen and metal responsive transcription factor. Cancer Biol Ther. 2004;3(1):29-35. Epub 2004/01/17. doi: 547 [pii]. PubMed PMID: 14726713.

188. Shomento SH, Wan C, Cao XM, Faugere MC, Bouxsein ML, Clemens TL, Riddle RC. Hypoxia-Inducible Factors 1 alpha and 2 alpha Exert Both Distinct and Overlapping Functions in Long Bone Development. Journal of Cellular Biochemistry. 2010;109(1):196-204. PubMed PMID: ISI:000273339200022.

189. Riddle RC, Khatri R, Schipani E, Clemens TL. Role of hypoxia-inducible factor-1 alpha in angiogenic-osteogenic coupling. Journal of Molecular Medicine-Jmm. 2009;87(6):583-90. PubMed PMID: ISI:000266475800005.

190. Potier E, Ferreira E, Andriamanalijaona R, Pujol JP, Oudina K, Logeart-Avramoglou D, Petite H. Hypoxia affects mesenchymal stromal cell osteogenic differentiation and angiogenic factor expression. Bone. 2007;40(4):1078-87. PubMed PMID: ISI:000245419800034.

191. Grayson WL, Zhao F, Bunnell B, Ma T. Hypoxia enhances proliferation and tissue formation of human mesenchymal stem cells. Biochemical and Biophysical Research Communications. 2007;358(3):948-53. PubMed PMID: ISI:000247124900047.

192. Torii S, Kobayashi K, Takahashi M, Katahira K, Goryo K, Matsushita N, Yasumoto KI, Fujii-Kuriyama Y, Sogawa K. Magnesium Deficiency Causes Loss of Response to Intermittent Hypoxia in Paraganglion Cells. Journal of Biological Chemistry. 2009;284(28):19077-89. PubMed PMID: ISI:000267711500056.

193. Arany Z, Foo SY, Ma YH, Ruas JL, Bommi-Reddy A, Girnun G, Cooper M, Laznik D, Chinsomboon J, Rangwala SM, Baek KH, Rosenzweig A, Spiegelman BM. HIF-independent regulation of VEGF and angiogenesis by the transcriptional coactivator PGC-1 alpha. Nature. 2008;451(7181):1008-U8. PubMed PMID: ISI:000253313100052.

194. Kawakami Y, Tsuda M, Takahashi S, Taniguchi N, Esteban CR, Zemmyo M, Furumatsu T, Lotz M, Belmonte JCI, Asahara H. Transcriptional coactivator PGC-1 alpha regulates chondrogenesis via association with Sox9. Proceedings of the National Academy of Sciences of the United States of America. 2005;102(7):2414-9. PubMed PMID: ISI:000227073100031.

195. Chin ER, Olson EN, Richardson JA, Yano Q, Humphries C, Shelton JM, Wu H, Zhu WG, Bassel-Duby R, Williams RS. A calcineurin-dependent transcriptional pathway controls skeletal muscle fiber type. Genes & development. 1998;12(16):2499-509. PubMed PMID: ISI:000075604900006.

196. Liu P, Zhou K, Xiang BQ, Wei Q. Effect of metal ions on the activity of the catalytic domain of calcineurin. Biometals. 2004;17(2):157-65. PubMed PMID: ISI:000189394800010.

197. Pieri F, Corinaldesi G, Fini M, Aldini NN, Giardino R, Marchetti C. Alveolar Ridge Augmentation With Titanium Mesh and a Combination of Autogenous Bone and Anorganic Bovine Bone: A 2-Year Prospective Study. Journal of Periodontology. 2008;79(11):2093-103. doi: 10.1902/jop.2008.080061.

198. Rocchietta I, Fontana F, Simion M. Clinical outcomes of vertical bone augmentation to enable dental implant placement: a systematic review. Journal of Clinical Periodontology. 2008;35:203-15. doi: 10.1111/j.1600-051X.2008.01271.x.

199. Urban IA, Jovanovic SA, Lozada JL. Vertical ridge augmentation using guided bone regeneration (GBR) in three clinical scenarios prior to implant placement: a retrospective study of 35 patients 12 to 72 months after loading. Int J Oral Maxillofac Implants. 2009;24(3):502-10. PubMed PMID: 19587874.

200. Jovanovic S, Hunt DF, Bernard GW, Spiekermann H, Wozney JM, Wikesjo UM. Bone reconstruction following implantation of rhBMP-2 and guided bone regeneration in canine alveolar ridge defects. Clinical Oral Implants Research. 2007;18(2):224-30.

201. Wang X, Zakaria O, Madi M, Hao J, Chou J, Kasugai S. Vertical bone augmentation induced by ultrathin hydroxyapatite sputtered coated mini titanium implants in a rabbit calvaria model. Journal of Biomedical Materials Research - Part B Applied Biomaterials. 2015;103(8):1700-8. doi: 10.1002/jbm.b.33347.

202. Simion M, Jovanovic SA, Tinti C, Benfenati SP. Long-term evaluation of osseointegrated implants inserted at the time or after vertical ridge augmentation: A retrospective study on I23 implants with I-5 year follow-up. Clinical Oral Implants Research. 2001;12(1):35-45.

203. Marx RE, Shellenberger T, Wimsatt J, Correa P. Severely resorbed mandible: Predictable reconstruction with soft tissue matrix expansion (tent pole) grafts. Journal of Oral and Maxillofacial Surgery. 2002;60(8 SUPPL. 1):878-88. doi: 10.1053/joms.2002.33856.

204. Le B, Burstein J, Sedghizadeh PP. Cortical tenting grafting technique in the severely atrophic alveolar ridge for implant site preparation. Implant Dentistry. 2008;17(1):40-50. doi: 10.1097/ID.0b013e318166d503.

205. Cillo Jr JE, Theodotou N, Samuels M, Krajekian J. The Tent Pole Splint: A Bone-Supported Stereolithographic Surgical Splint for the Soft Tissue Matrix Expansion Graft Procedure. Journal of Oral and Maxillofacial Surgery. 2010;68(6):1365-70. doi: 10.1016/j.joms.2009.11.004.

206. Korpi JT, Kainulainen VT, Sándor GK, Oikarinen KS. Long-term follow-up of severely resorbed mandibles reconstructed using tent pole technique without platelet-rich plasma. Journal of Oral and Maxillofacial Surgery. 2012;70(11):2543-8. doi: 10.1016/j.joms.2012.07.027.

207. Korpi JT, Kainulainen VT, Sándor GK, Oikarinen KS. Tent-pole approach to treat severely atrophic fractured mandibles using immediate or delayed protocols: Preliminary case series. Journal of Oral and Maxillofacial Surgery. 2013;71(1):83-9. doi: 10.1016/j.joms.2012.09.008.

208. Kuoppala R, Kainulainen VT, Korpi JT, Sándor GK, Oikarinen KS, Raustia A. Outcome of treatment of implant-retained overdenture in patients with extreme mandibular bone resorption treated with bone grafts using a modified tent pole technique. Journal of Oral and Maxillofacial Surgery. 2013;71(11):1843-51. doi: 10.1016/j.joms.2013.06.204.

209. Sverzut CE, Trivellato AE, Sverzut AT. Use of a titanium mesh “shelter” combined with the soft tissue matrix expansion (Tent pole) grafting in the reconstruction of a severely resorbed edentulous mandible. Technical note. Brazilian Dental Journal. 2015;26(2):193-7. doi: 10.1590/0103-6440201301957.

210. Le B, Rohrer MD, Prassad HS. Screw "Tent-Pole" Grafting Technique for Reconstruction of Large Vertical Alveolar Ridge Defects Using Human Mineralized Allograft for Implant Site Preparation. Journal of Oral and Maxillofacial Surgery. 2010;68(2):428-35. doi: 10.1016/j.joms.2009.04.059.

211. Wang S, Zhang Z, Zhao J, Zhang X, Sun X, Xia L, Chang Q, Ye D, Jiang X. Vertical alveolar ridge augmentation with β-tricalcium phosphate and autologous osteoblasts in canine mandible. Biomaterials. 2009;30(13):2489-98. doi: 10.1016/j.biomaterials.2008.12.067.

212. Carmagnola D, Berglundh T, Araújo M, Albrektsson T, Lindhe J. Bone healing around implants placed in a jaw defect augmented with Bio-Oss®. Journal of Clinical Periodontology. 2000;27(11):799-805. doi: 10.1034/j.1600-051x.2000.027011799.x.

213. Simion M, Dahlin C, Rocchietta I, Stavropoulos A, Sanchez R, Karring T. Vertical ridge augmentation with guided bone regeneration in association with dental implants: An experimental study in dogs. Clinical Oral Implants Research. 2007;18(1):86-94. doi: 10.1111/j.1600-0501.2006.01291.x.

214. Simion M, Nevins M, Rocchietta I, Fontana F, Maschera E, Schupbach P, Kim DM. Vertical ridge augmentation using an equine block infused with recombinant human platelet-derived growth factor-BB: a histologic study in a canine model. The International journal of periodontics & restorative dentistry. 2009;29(3):245-55.

215. Kawakatsu N, Oda S, Kinoshita A, Kikuchi S, Tsuchioka H, Akizuki T, Hayashi C, Kokubo S, Ishikawa I, Izumi Y. Effect of rhBMP-2 with PLGA/gelatin sponge type (PGS) carrier on alveolar ridge augmentation in dogs. Journal of Oral Rehabilitation. 2008;35(9):647-55. doi: 10.1111/j.1365-2842.2008.01850.x.

216. Tamimi F, Torres J, Gbureck U, Lopez-Cabarcos E, Bassett DC, Alkhraisat MH, Barralet JE. Craniofacial vertical bone augmentation: A comparison between 3D printed monolithic monetite blocks and autologous onlay grafts in the rabbit. Biomaterials. 2009;30(31):6318-26. doi: 10.1016/j.biomaterials.2009.07.049.

217. Kon K, Shiota M, Ozeki M, Yamashita Y, Kasugai S. Bone augmentation ability of autogenous bone graft particles with different sizes: A histological and micro-computed tomography study. Clinical Oral Implants Research. 2009;20(11):1240-6. doi: 10.1111/j.1600-0501.2009.01798.x.

218. Schliephake H, Dard M, Planck H, Hierlemann H, Stern U. Alveolar Ridge Repair Using Resorbable Membranes and Autogenous Bone Particles with Simultaneous Placement of Implants: An Experimental Pilot Study in Dogs. International Journal of Oral and Maxillofacial Implants. 2000;15(3):364-73.

219. Schliephake H, Kracht D. Vertical Ridge Augmentation Using Polylactic Membranes in Conjunction with Immediate Implants in Periodontally Compromised Extraction Sites: An Experimental Study in Dogs. International Journal of Oral and Maxillofacial Implants. 1997;12(3):325-34.

220. Wikesjö UME, Qahash M, Thomson RC, Cook AD, Rohrer MD, Wozney JM, Hardwick WR. Space-providing expanded polytetrafluoroethylene devices define alveolar augmentation at dental implants induced by recombinant human bone morphogenetic protein 2 in an absorbable collagen sponge carrier. Clinical Implant Dentistry and Related Research. 2003;5(2):112-23.

221. Susin C, Qahash M, Polimeni G, Lu PH, Prasad HS, Rohrer MD, Hall J, Wikesjö UME. Alveolar ridge augmentation using implants coated with recombinant human bone morphogenetic protein-7 (rhBMP-7/rhOP-1): Histological observations. Journal of Clinical Periodontology. 2010;37(6):574-81. doi: 10.1111/j.1600-051X.2010.01554.x.

222. Henderson SE, Verdelis K, Maiti S, Pal S, Chung WL, Chou DT, Kumta PN, Almarza AJ. Magnesium alloys as a biomaterial for degradable craniofacial screws. Acta Biomater. 2013. Epub 2014/01/05. doi: 10.1016/j.actbio.2013.12.040. PubMed PMID: 24384125.

223. Brown A, Zaky S, Ray H, Jr., Sfeir C. Porous magnesium/PLGA composite scaffolds for enhanced bone regeneration following tooth extraction. Acta Biomaterialia. 2015;11:543-53.

224. Loo SCJ, Ooi CP, Boey YCF. Radiation effects on poly(lactide-co-glycolide) (PLGA) and poly(l-lactide) (PLLA). Polymer Degradation and Stability. 2004;83(2):259-65. doi: http://dx.doi.org/10.1016/S0141-3910(03)00271-4.

225. Dorta MaJ, Santoveña A, Llabrés Ma, Fariña JB. Potential applications of PLGA film-implants in modulating in vitro drugs release. International Journal of Pharmaceutics. 2002;248(1–2):149-56. doi: http://dx.doi.org/10.1016/S0378-5173(02)00431-3.

226. Rasband W. ImageJ. Bethesda, Maryland: US National Institutes of Health; 1997-2015.

227. Bromage TG, Goldman HM, McFarlin SC, Warshaw J, Boyde A, Riggs CM. Circularly polarized light standards for investigations of collagen fiber orientation in bone. Anatomical record Part B, New anatomist. 2003;274(1):157-68. Epub 2003/09/10. doi: 10.1002/ar.b.10031. PubMed PMID: 12964206.